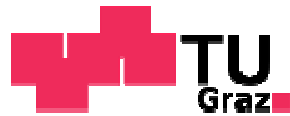


DEVELOPMENT OF A CONTINUOUS SAMPLING SYSTEM FOR MONITORING TRANSPORT ACROSS THE INTACT BLOOD- BRAIN BARRIER

DI THOMAS BIRNGRUBER



DOCTORAL THESIS

JOANNEUM RESEARCH FORSCHUNGSGESELLSCHAFT GMBH
HEALTH - INSTITUTE FOR BIOMEDICINE AND HEALTH SCIENCES
ELISABETHSTRASSE 5, 8010 GRAZ

GRAZ UNIVERSITY OF TECHNOLOGY
INSTITUTE OF MEDICAL ENGINEERING
KRONESGASSE 5/II, 8010 GRAZ, AUSTRIA

GRAZ, SEPTEMBER 2013

Preface and statutory declaration

This doctoral thesis summarizes my work on the topic of continuous monitoring of substance transport across the intact blood-brain barrier in the period of 09-2007 – 06-2013. It summarizes the peer reviewed publications, book chapters and patents which I published as a first or co-author. Parts of this thesis are submitted to peer review journals and are under review. Therefore some chapters are partly or completely taken as published or submitted and eventually adapted from the original manuscripts when it appeared to be necessary. Most chemical analytical work was conducted in the bioanalytical facility of Joanneum Research by trained and experienced personnel (stated in each chapter).

STATUTORY DECLARATION

I declare that I have authored this thesis independently, that I have not used other than the declared sources / resources, and that I have explicitly marked all material which has been quoted either literally or by content from the used sources.

Place, date

(signature)

FIRST EXAMINER: Ao.Univ.-Prof. Dipl.-Ing. Dr.techn. Scharfetter, Hermann
Graz University of Technology
INSTITUTE OF MEDICAL ENGINEERING
Kronesgasse 5/II, 8010 GRAZ, AUSTRIA
hermann.scharfetter@tugraz.at

SECOND EXAMINER: Priv.-Doz. Dr. Frank Sinner
Joanneum Research Forschungsgesellschaft GMBH
HEALTH – Institute for Biomedicine and Health Sciences
Elisabethstrasse 5, 8010 Graz, Austria
frank.sinner@medunigraz.at

FIRST ADVISOR: Priv.-Doz. Dr. Frank Sinner
Joanneum Research Forschungsgesellschaft GMBH
HEALTH – Institute for Biomedicine and Health Sciences
Elisabethstrasse 5, 8010 Graz, Austria
frank.sinner@medunigraz.at

SECOND ADVISOR: Prof. Dr. Thomas Rudolf Pieber
Medical University of Graz
Division of Endocrinology and Metabolism
Auenbruggerplatz 15, 8036 Graz, Austria
thomas.pieber@medunigraz.at

„Ich weiß, das klingt alles sehr kompliziert..“
Alfred Sinowatz

Prediction is very difficult, especially if it's about the future.
Niels Bohr

für Andi

DEVELOPMENT OF A CONTINUOUS SAMPLING SYSTEM FOR MONITORING TRANSPORT ACROSS THE INTACT BLOOD-BRAIN BARRIER

DI THOMAS BIRNGRUBER

DOCTORAL THESIS

Abstract

The blood-brain barrier (BBB) is a specialized capillary structure with tight junctions between the endothelial cells that restricts the substance exchange between blood and brain tissue. The BBB protects the brain from harmful substances in the blood but it also hinders potential neuroactive drugs from entering the brain. This presents a major challenge in the development of drugs that target the central nervous system because therapeutic agents must overcome the BBB to reach the site of action. To address this situation, there is a need for test methods to describe the efficacy of substance transporter systems to cross the BBB. This work describes a new *in vivo* technique for continuous sampling of the interstitial fluid in brain tissue, named cerebral open flow microperfusion (cOFM). cOFM was developed from sketch to proof of concept in rats within this doctoral thesis. cOFM is based on open flow microperfusion (OFM), a relatively new technique that is based on a probe with macroscopic openings in combination with a push-pull pump. Since OFM requires no membrane, it puts the perfusate into direct contact with the tissue being sampled, which means that lipophilic and high-molecular-weight substances can also be sampled, including antibodies, and even entire cells. OFM does not face problems that can arise due to protein clotting or biofouling, which can lead to membrane occlusion, as described for membrane based technologies. Like all invasive probe techniques, cOFM probe insertion causes tissue trauma, damage to capillaries, and therefore BBB disruption.

Important parts of this work address the topics of:

- (a) The determination of the time between cOFM probe insertion and BBB re-establishment
- (b) The demonstration of cOFM sampling in the interstitial cerebral fluid with intact BBB
- (c) Investigation of brain tissue changes as a reaction to cOFM probe implantation
- (d) The conduction of a proof of principle study with a pharmaceutical product in development

Keywords

cerebral open flow microperfusion
cOFM
blood-brain barrier
pharmacokinetic
pharmacodynamics
tissue specific sampling

Abbreviations

OFM	...	open flow microperfusion
cOFM	...	cerebral open flow microperfusion
dOFM	...	dermal open flow microperfusion
aOFM	...	adipose tissue open flow microperfusion
BBB	...	blood-brain barrier
MD	...	microdialysis
FEP	...	fluorinated ethylene propylene
PTFE	...	polytetrafluorethylen
EB	...	evans blue
Naf	...	sodium fluoresceine
PK	...	pharmacokinetics
PD	...	pharmacodynamics
PBS	...	phosphate buffered saline
LH	...	left brain hemisphere
RH	...	right brain hemisphere
ROI	...	region of interest
LLOQ	...	lower level of quantification
ULOQ	...	upper level of quantification
Da	...	dalton
GFAP	...	glial fibrillary acidic protein
IBA1	...	ionized calcium binding adaptor molecule 1
H&E	...	hematoxylin and eosin
LRP	...	lipoprotein receptor-related protein
GSH	...	glutathione
PEG	...	polyethylene glycol
GMP	...	good manufacturing practice
GLP	...	good laboratory practice
Na	...	sodium
ACN	...	acetonitrile
AUC	...	area under the curve
SD	...	standard deviation
SEM	...	standard error of mean

Contents

PREFACE AND STATUTORY DECLARATION.....	I
ABSTRACT	VI
KEYWORDS.....	VII
ABBREVIATIONS.....	VII
CONTENTS.....	VIII
INTRODUCTION.....	1
1. THE NEED FOR A NEW TECHNIQUE TO MEASURE SUBSTANCE TRANSPORT ACROSS THE BLOOD-BRAIN BARRIER.....	2
2. SOCIAL ECONOMIC RELEVANCE OF AN IMPROVED DEVELOPMENT PROCESS FOR NEUROACTIVE DRUGS.....	2
BACKGROUND.....	5
1. THE BLOOD-BRAIN BARRIER AS THE PROTECTIVE SHIELD OF THE BRAIN	6
1.1 <i>Structure and function of the blood-brain barrier.....</i>	6
1.2 <i>Transport across the blood-brain barrier</i>	8
2. METHODS OF STUDYING TRANSPORT ACROSS THE BBB	12
2.1 <i>Brain biopsy based techniques.....</i>	13
2.2 <i>Imaging techniques.....</i>	14
2.3 <i>Microdialysis (MD).....</i>	15
2.4 <i>In-vitro methods.....</i>	16
2.5 <i>Behavioral Tests</i>	18
GENERAL CONCEPT OF CEREBRAL OPEN FLOW MICROPERFUSION (COFM).....	19
1. OPEN FLOW MICROPERFUSION (OFM)	20
2. GENERAL CONCEPT OF CEREBRAL OPEN FLOW MICROPERFUSION (COFM)	22
3. DESIGN OF THE COFM PROBE	23
3.1 <i>cOFM probe requirements</i>	23
3.2 <i>cOFM probe.....</i>	25
3.3 <i>cOFM sampling system</i>	28
TESTING OF BBB INTACTNESS AFTER COFM PROBE IMPLANTATION	30
1. INTRODUCTION.....	31
2. MATERIAL AND METHODS.....	32
2.1 <i>Chemicals, injected or infused solutions</i>	32
2.2 <i>Animals</i>	33
2.3 <i>Surgery</i>	33
2.4 <i>Experimental design.....</i>	34
2.5 <i>Analytical methods.....</i>	37
2.6 <i>Statistical methods.....</i>	38
3. RESULTS.....	38
3.1 <i>Local BBB re-establishment after cOFM insertion (study 1).....</i>	39
3.2 <i>BBB permeability characterization by brain biopsy</i>	40
3.3 <i>BBB permeability during cOFM monitoring (study 2)</i>	40
4. DISCUSSION.....	41
5. CONCLUSION.....	43
EVALUATION OF TISSUE REACTION AS A RESULT OF COFM PROBE IMPLANTATION	45
1. INTRODUCTION.....	46
2. MATERIAL AND METHODS.....	47
2.1 <i>Animals</i>	47
2.2 <i>Implantation of cOFM probe.....</i>	47
2.3 <i>Sampling</i>	48
2.4 <i>Experimental setup</i>	48
2.5 <i>Immunohistochemistry and staining.....</i>	49

2.6	<i>Histological analysis</i>	49
2.7	<i>Statistical analysis</i>	50
3.	RESULTS.....	51
3.1	<i>H&E</i>	51
3.2	<i>GFAP</i>	51
3.3	<i>Iba-1</i>	52
4.	DISCUSSION.....	57
5.	CONCLUSION.....	59
APPLICATION OF COFM IN A PHARMACEUTICAL STUDY: ENHANCED DELIVERY OF DOXORUBICIN TO THE BRAIN BY FORMULATION IN TARGETED NANOCARRIERS.....		60
1.	INTRODUCTION.....	61
2.	MATERIAL AND METHODS.....	62
2.1	<i>Animals</i>	62
2.2	<i>Experimental set-up</i>	62
2.3	<i>Treatment</i>	63
2.4	<i>Analysis</i>	64
2.5	<i>Sodium fluorescein (Naf) as BBB integrity marker</i>	64
3.	RESULTS.....	65
4.	DISCUSSION.....	66
SUMMARY.....		69
1.	SUMMARY.....	69
2.	CONCLUSIONS.....	71
3.	OUTLOOK AND ONGOING INVESTIGATIONS:.....	71
PUBLICATIONS.....		73
1.	JOURNALS.....	73
2.	BOOK CHAPTERS.....	73
3.	PROCEEDINGS.....	74
REFERENCES.....		76
CURRICULUM VITAE.....		85
APPENDIX.....		86

CHAPTER I

Introduction

The following chapter gives a brief overview of diseases affecting the central nervous system (CNS) and their socioeconomic importance. The high complexity of the CNS impedes drug development for CNS diseases. One major obstacle for drug transport to the brain is the blood-brain barrier (BBB). A reliable method for continuous measurement of transport across the intact BBB would greatly improve and facilitate the pharmaceutical development process. The basic structure of the BBB and different transport pathways across the BBB are explained in this chapter as well as the blind spots in this area. Methods for measuring transport across the BBB are explained and benefits and drawbacks are discussed

1. The need for a new technique to measure substance transport across the blood-brain barrier.

The BBB is a special feature of the capillary system in the central nervous system (CNS), resulting in a restricted exchange between blood and brain tissue (Miller, 2002; Pardridge, 2005). The BBB's protective function excludes many harmful substances but also potentially therapeutic agents from entering the brain (F. Lai, Fadda, & Sinico, 2013). Therefore it is one of the main hurdles to overcome during the development of neuroactive drugs (Boado, 2008). An effective development of these neuroactive drugs and formulations requires a feedback system that provides information about the efficacy with which substances cross the BBB (N Joan Abbott, 2013). Existing methods show substantial drawbacks like a narrow limitation of the spectrum of substances that can be measured and in particular for imaging techniques a lack in spatial resolution that is needed to distinguish between intravascular and extravascular substance fractions (Mensch, Oyarzabal, Mackie, & Augustijns, 2009). cOFM was designed to measure substance transport across the intact BBB and shows the potential to bridge the feedback gap in neuroactive drug development.

2. Social economic relevance of an improved development process for neuroactive drugs.

The brain is what makes us human and provides the seemingly boundless possibilities of our species. However, in spite of its impressive ability to heal itself, the central nervous system (CNS) also occasionally fails. This can be due to a traumatic injury such as a car accident or because of autoimmune reactions such as multiple sclerosis or a cerebrovascular incident like stroke. Functional changes in the brain function caused by e.g. stress can lead to cognitive and behavioural deviations such as depression, anxiety or schizophrenia. Probably, the most important and fastest growing group of brain diseases are dementia and neurodegenerative diseases due to an increasing average age. The socio-economic relevance of CNS disorders is determined by the financial cost to society but also by individual suffering due to anxiety and personality loss. The following paragraph focuses on the financial cost of these diseases in Europe (Gustavsson et al., 2011).

The bottom line is alarming: the financial burden of CNS disorders on society is immense. Across Europe approx. 160 million people are affected, equivalent to about 36% of the total population. CNS diseases account for over 26% of disabilities as per disability adjusted life years, which is more than any other group of disorders (Nutt, 2011). Brain disorders

represent the top four in the list of the most burdensome diseases, namely depression, dementia, alcohol abuse related damage and stroke. This has been confirmed by a European study in 2005 (Andlin-Sobocki & Rössler, 2005). Unfortunately, more recent studies found no evidence for any change in this situation in the past five years. Moreover, they found that only a third of all individuals with a CNS disease receive appropriate treatment (Wittchen et al., 2011). A closer look at the costs reveals an alarming amount of € 798 billion in 2010; this means € 1500 for every person in Europe. The top three diseases, dementia, mood disorders and psychotic disorders cost about € 100 billion each. The next group in terms of high costs are stroke, anxiety and addiction, each with over € 60 billion. A closer look at the nature of the costs reveals that only about one third are direct healthcare costs, about 25% are non-medical associated costs and the remaining 40% are indirect costs related to loss of personal productivity (Olesen & Leonardi, 2003). Summit conferences under the auspices of the ECNP (European college of neuropsychopharmacology) (Nutt and Goodwin, 2011) listed a number of factors that play key roles:

Investment in brain research and development of neuroactive drugs is disproportionately low despite the fact that brain disorders have such a high prevalence and such disabling effects. Current data reveal that in Europe fewer funds are spent on brain research than on any other physiological systems and that research in neurosciences is fragmented and heterogeneous.

Among the many different complex reasons is the fact that in the last few years investments in the development of new drugs for brain diseases by the pharmaceutical industry have been decreasing. Major companies like Pfizer, GSK, Merck Sharp and Dohme (MSD) and Astra Zeneca have closed their European neuroscience research facilities. The Netherlands which has always been a traditional leading country in brain research, has cut back research activity on a large scale, mainly because of the long and cost intensive phase of bringing a drug to the market (Amara, Grillner, Insel, Nutt, & Tsumoto, 2011). On average it takes more than 13 years and more than € 1,000 million to develop a neuroactive drug. For comparison: a new cancer drug can be on the market within five years whereas a treatment for dementia may take four years to obtain phase 2, proof-of principal, and the following registration for phase 3 may take even longer (IMS, 2004; Innovative Medicines Initiative (IMI), 2008; Kola & Landis, 2004). Neuroactive drugs often fail in a late state of the development process which also increases financial losses (IMS Retail Monitor 2004; The Innovative Medicines Initiative (IMI) 2008; Kola & Landis 2004).

A major aspect of this problem can be attributed to the complex pharmacokinetic pathways into the brain determined by the blood-brain barrier (BBB), the brains' protection system against harmful substances in the blood. "BBB is the bottleneck in neuroactive drug development and is the single most important factor limiting the future growth of neurotherapeutics" (Pardridge, 2005). Statements like this illustrate the significance of the

BBB during the development of neurotherapeutics and also underline that the BBB does not receive sufficient attention in both the industrial development as well as in academic research. The present situation with very few effective treatments for most brain disorders is a direct result of underestimating or avoiding the BBB problem. This problematic situation can be addressed by an increased effort to build a knowledge base for the elementary transport characteristics of the BBB and by developing measurement methods that give a direct feedback on how to improve transport strategies across BBB (Fig. 1).

Cerebral open flow microperfusion (cOFM) is a sampling technique developed to enable measurement of substance transport across the intact BBB and it shows the potential to improve the critical situation in neuroactive drug development. cOFM is a probe based technique that continuously samples the interstitial fluid of the brain in-vivo and can thus be used to measure drug transport across the intact BBB. This thesis describes the main features of cOFM, explains the fundamental steps in the development of the technique, and aims to explain the possibilities of cOFM in the context of BBB and neuroactive drug development.

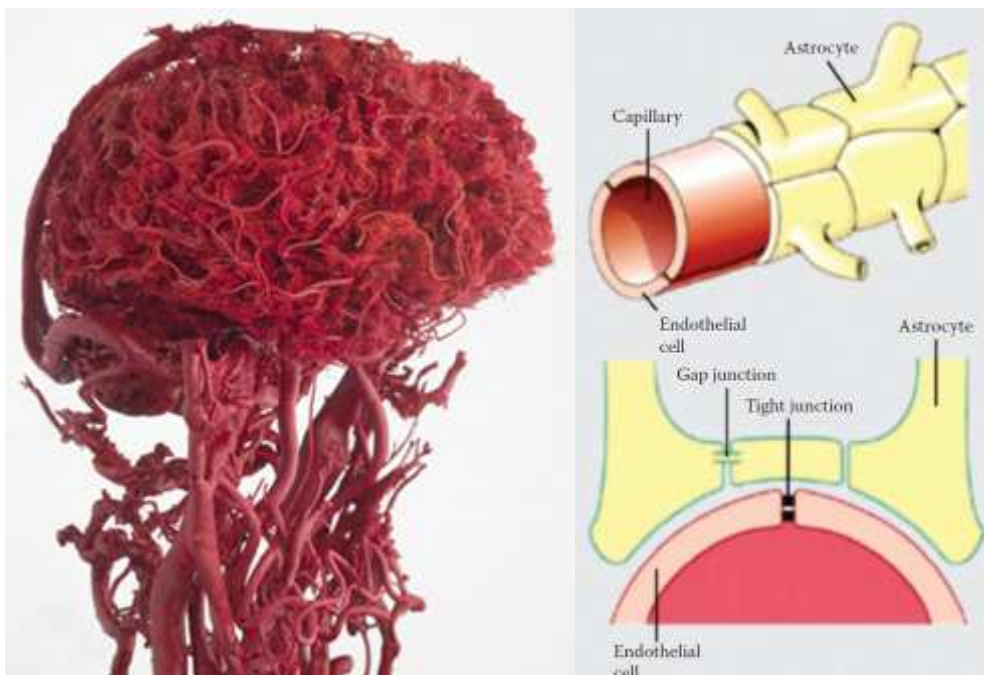


Fig. 1: BBB consists of the capillary structure that is specially sealed with tight junctions. A plastification of the capillary system of the brain (left) and a schematic drawing of a single capillary. (Reprinted with permission from Speckman, E.-J. et al., Physiologie, Urban & Fischer, Munich, 2008.)

CHAPTER II

Background

The following chapter describes the cell structure of the blood-brain barrier and transport pathways across the BBB. Methods that allow measurement across the BBB and their advantages and drawbacks are discussed.

Parts of this chapter are based on the book:

The Textbook of Nanoneuroscience and Nanoneurosurgery:

Chapter 35 "*In Vitro* and *In Vivo* Techniques to Assess Neurotoxicity of Nanoparticles"

Birngruber et al. 2013

1. The blood-brain barrier as the protective shield of the brain

The brain is of extraordinary importance and extremely sensitive. Therefore it needs to be mechanically and chemically protected against harmful influences. The skull, meninges and cerebrospinal fluid (CSF) protect the brain against mechanical damage and the blood-brain barrier and the blood-CSF barrier protect the brain from chemical and biologically harmful substances.

The blood-brain barrier (BBB) is a special property of the capillaries in the brain; the endothelial cells forming the capillaries are sealed with tight junctions. The capillaries permeate the brain tissue at an average distance of 40 μm and have a total length of about 600 km. The BBB ensures the supply of the brain with nutrients and prevents harmful xenobiotic substances present in blood from entering the brain. The choroid plexus, also referred to as blood-CSF barrier, is another barrier between blood and brain tissue, adjoins the endothelium with a dense epithelium. The arachnoid membrane represents another barrier between blood and cerebrospinal fluid. The BBB is however by far the most important separation between blood and brain tissue as it is present almost all over the brain and is mainly responsible for nutrition and substance transport in the brain (N Joan Abbott, 2013; Hawkins & Davis, 2005; Pardridge, 2005; Upton, 2007).

1.1 Structure and function of the blood-brain barrier

The blood-brain barrier (BBB) is the determining factor for brain nutritional supply and pharmacokinetics into the brain. Almost all drug application routes like oral, intravenous or even subcutaneous need blood for distribution. Blood brings substances to all tissues and the blood vessels and their specific structure influence the exchange rate between blood and tissue. The blood capillaries in the brain are especially tight and impede passive paracellular transport across capillary walls. In order to maintain tissue nutrition and metabolism a variety of transporter systems are responsible for a very selective form of transport to and from brain tissue – maintaining the delicate homeostasis inside the brain. This specialized form of capillary walls is called the blood-brain barrier (Bundgaard & Abbott, 2008; Ohtsuki, 2004; Wolf, Seehaus, Minol, & Günter Gassen, 1996).

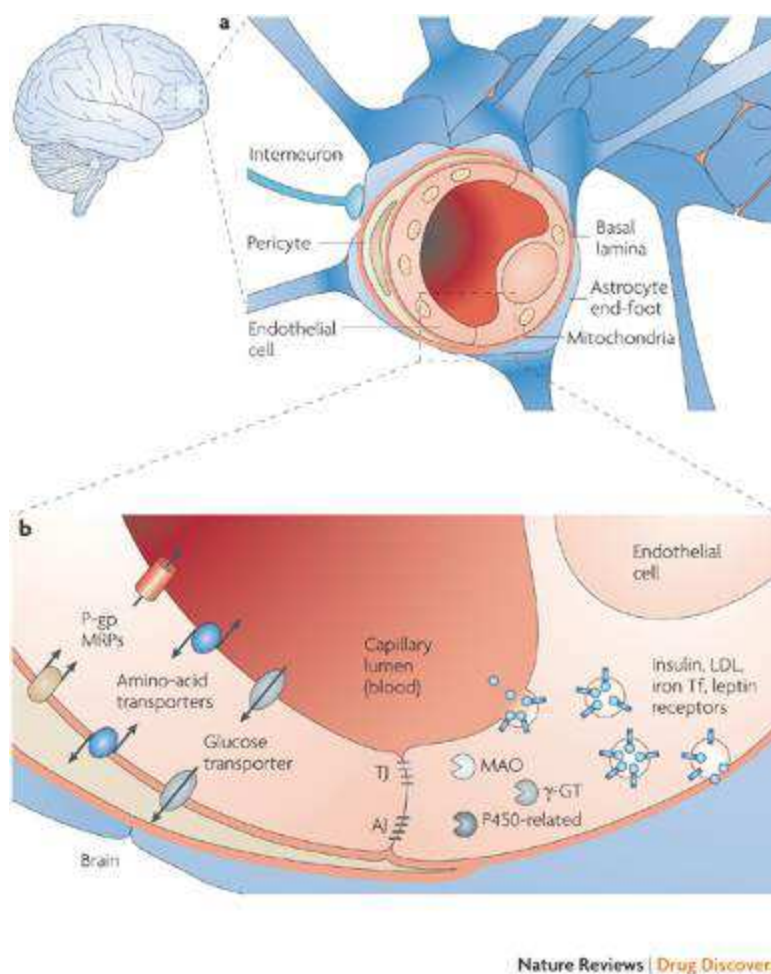


Fig. 2: Schematic representation of a brain capillary from (Cecchelli et al., 2007)

Endothelial cells form the vascular system in the body from the central aorta to the capillary system in the periphery. Endothelial cell forming capillaries are specialized to exchange water and suspended substances. Gaps of about 50 μm , so called fenestrations, allow effective exchange. Endothelial cells in the brain do not form fenestrations, not even intracellular gaps but form a continuous endothelium by sealing the intercellular gap with occlusion proteins to form tight junctions. The tight junctions restrict paracellular transport, particularly important for hydrophilic, large substances and cells. Due to the inhibited paracellular pathway almost all drugs have to cross the endothelial cell transcellularly in order to enter the brain parenchyma. (Fukuuchi, Tomita, & Koto, 2001) (Fig. 1 and Fig. 2)

Tight junctions are the cell-cell interconnectors between endothelial cells contributing significantly to the barrier function of the BBB (Claude & Goodenough, 1973; Wolburg et al., 1994). Several occlusion proteins such as occludin, claudin and the junctional adhesion molecules (JAM) link the endothelial cells in the apical region of the lateral cell walls and inhibit the substance transport between the cell membranes of two endothelial cells

(Cecchelli et al., 2007). Therefore, tight junctions cause an extremely high transendothelial resistance (TEER) of up to 2,000 Ohm/cm². TEER is used in BBB in-vitro models to test intactness of the experimental setup (Butt, Jones, & Abbott, 1990). (Fig. 1 and Fig.2)

Astrocytes belong to the glia of the CNS, the structural and functional non-neuronal cells that constitute approximately 50% of all the cells of the CNS. They contact the capillaries via foot-like extensions, the astrocytic end-feet. Astrocytic and endothelial cells are separated by the basement membrane. About 80% of the capillary surface is covered with astrocytic end-feet. The astrocytes have no significant barrier function, but most likely they have a control function on the endothelial cells. Astrocytes regulate, among other functions, the density of tight junctions and induce the expression of transport related enzymes such as g-glutamyl transferase (GGT) and transport proteins. Furthermore, astrocytes regulate the ionic environment of the extracellular space in the brain, in order to ensure neuronal and BBB function. (Dehouck, Dehouck, Fruchart, & Cecchelli, 1994; Johanson, 1980; Neuhaus, Risau, & Wolburg, 1991; Pardridge, 2005) (Fig. 1 and Fig.2)

Pericytes are arranged helically around the endothelial cells and wrapped in the basal membrane. They are separated from the endothelial cells by the basal membrane. Pericytes are responsible for the formation of tight junctions and postnatal formation of the BBB by inhibiting the effect of CNS immune cells that would attack the brain during BBB formation. Pericytes regulate the transport of large plasma proteins and play a key role in regulation the capillary blood flow due to their elasticity. Their functionality or dysfunctionality is supposed to be involved in many neurological diseases like Alzheimer, ALS, Multiple Sclerosis and different forms of CNS inflammation. The role of pericytes in the BBB is still under investigation. (N J Abbott; C.-H. Lai & Kuo, 2005; Rucker, Wynder, & Thomas, 2000; Shepro & Morel, 1993) (Fig. 2)

The basal membrane is an extracellular matrix surrounding pericytes and endothelial cells. It is about 40 to 50 nm thick and consists essentially of collagen and fibronectin. In addition to the supporting role, it is involved in the barrier function. (Fig. 2)

1.2 Transport across the blood-brain barrier

Despite of its function as a protective barrier the BBB has to ensure nutrient transport to the brain and metabolic waste transport from the brain. Water-soluble nutrients and peptides cross the BBB through specific transporters or specific channels. Lipophilic substances of low molecular weight are able to cross the BBB by transcellular passive diffusion. Unwanted

substances, the so called xenobiotics, can be eliminated from brain parenchyma back into the blood vessels by efflux pumps. (Pardridge, 2012; Saunders, Daneman, Dziegielewska, & Liddelow, 2013)

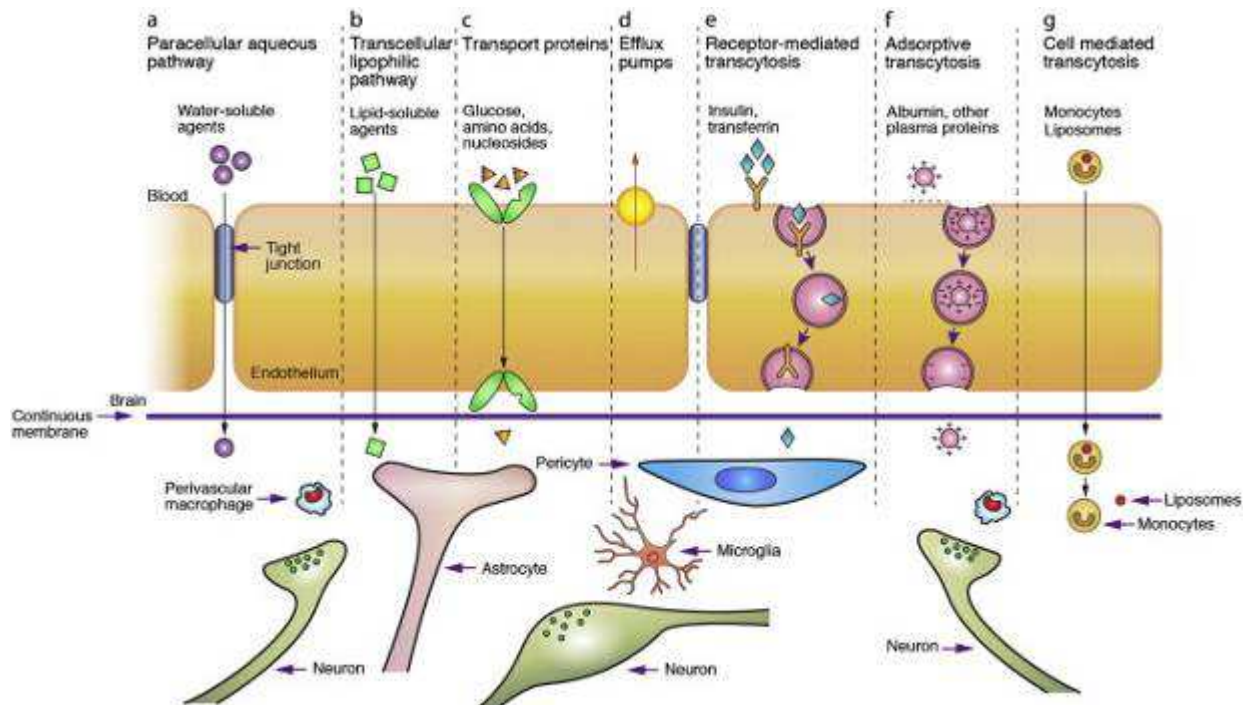


Fig. 3: Transport processes at the BBB from (Chen & Liu, 2012)

Paracellular transport

In healthy and intact cerebral capillaries endothelial cells are connected to each other with the tight junctions. Brain capillaries allow only transcellular transport which can be regulated more accurately than paracellular transport. Water, glycerine and urea, are examples of small polar compounds that can cross the tight junctions of the BBB to small extents. (Madara, 1988; Newton, 2006) (Fig.3)

Passive Diffusion

Passive diffusion is the most basic form of transport across the BBB and mainly uses transcellular pathways through endothelial cells. Diffusion is driven by a concentration gradient and does not depend on additional energy. The ability of a substance to passively diffuse across the BBB mainly depends on their physical characteristics such as molecular weight, lipophilicity and charged/uncharged state. For small, lipid-soluble, uncharged substances passive transcellular diffusion is the most effective pathway. Molecules larger than approx. 500 Da are excluded from transcellular pathway. For substances below this limit passive transport into the brain is indirectly proportional to molecular size and lipophilicity (Fig. 3 and Fig. 4). (Egleton & Davis, 2005; Kaliszan, 1996; Oldendorf, 1974)

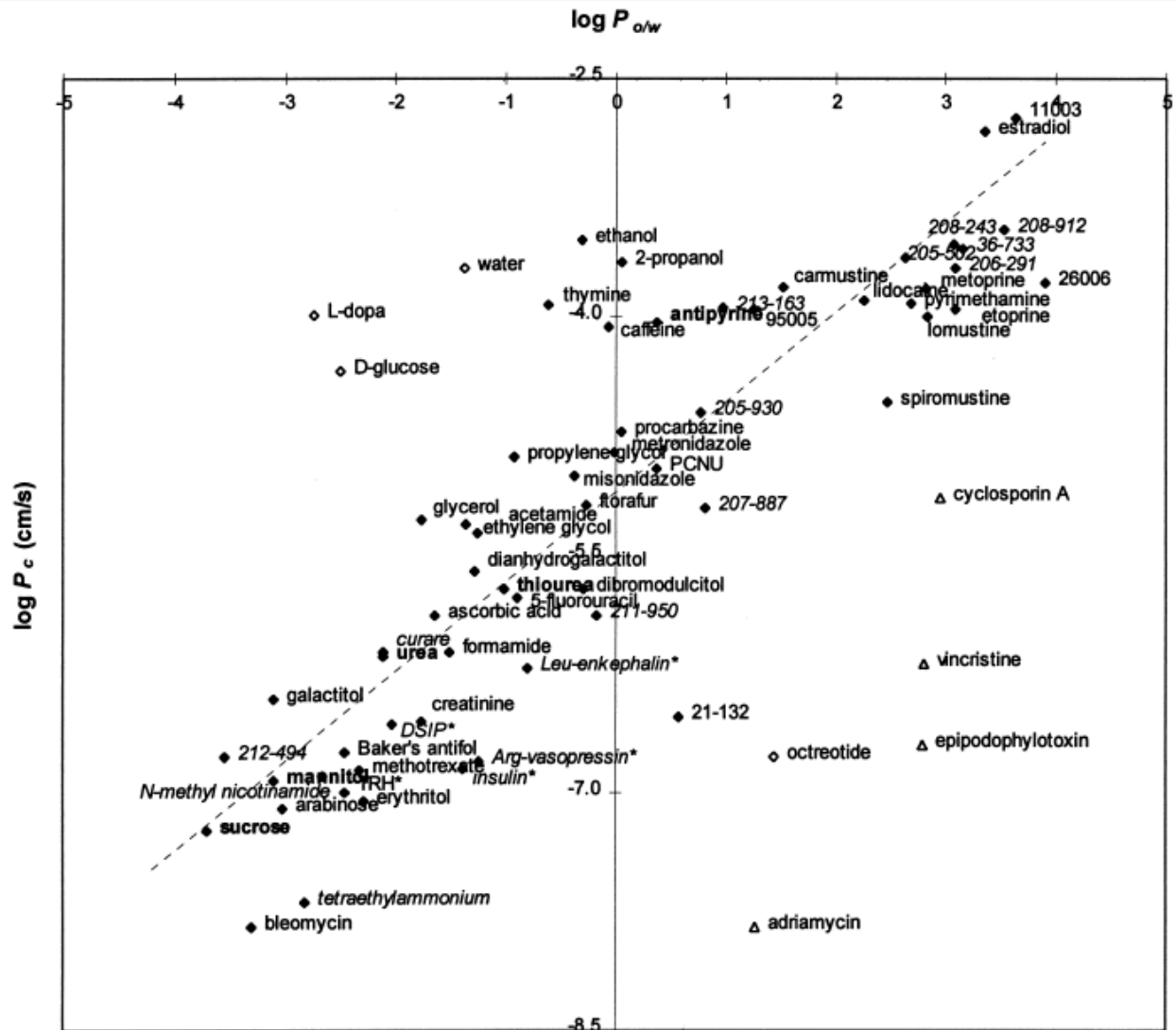


Fig. 4: The diagram shows a strong correlation between the lipophilicity ($\log P$) and $\log P_c$ (permeability coefficient of rat brain capillaries in cm per second) for range of substances and drugs. Most strong deviants below the line (triangles) are substrates for P- glycoprotein, an efflux pump that actively removes them from the brain. (Bodor & Buchwald, 1999)

Channel mediated transport

Polar molecules like water are very limited in crossing the BBB through the pathways described above but the BBB still has a very high permeability for water. Special hydrophilic proteins, the so called aquaporins facilitate passive water transport in both directions. Channel transport is a very effective pathway and faster than transporter systems. Channels can be activated and deactivated, by a mechanism called gating (Badaut, Brunet, & Regli, 2007; Bloch & Manley, 2007; Dolman, Drndarski, Abbott, & Rattray, 2005; Oldendorf, 1970; Verkman, 2005). (Fig. 3)

Facilitated diffusion

Nutrients and other endogenous substances like glucose and amino acids are polar molecules and too large for the previously described pathways. These crucial molecules use special carrier mediated transporter systems. D-glucose for example is transported by GLUT-1 into the brain. The transport is passive and therefore only dependent on concentration gradients. The Brain has high energy consumption and as glucose is the main energy source, glucose transport is crucial. Other similar transporter mechanisms are MCT-1 and MCT-2, responsible for lactate and pyruvate transport. SLC7 is responsible for the transport of amino acids. These transporters work uni- or bidirectionally. (Agus et al., 1997; Cornford & Hyman, 1999; Dahlin, Royall, Hohmann, & Wang, 2009) (Fig. 3)

Active transport

Active transport allows substance transport against concentration gradients and is therefore energy consuming. Adenosine triphosphate (ATP) provides the required energy. Active transport into the brain is called influx; the transport from the brain is called efflux. A wide variety of active influx and efflux transporters are expressed on both sides (luminal and abluminal) of the BBB, maintaining an asymmetric distribution of various molecules between blood and brain. Substance uptake into the brain is either restricted or facilitated by active transport systems depending on the affinity of the substrate to either influx or efflux transporters. (Caruso et al., 2013)

Active efflux transporters

Many different BBB transporters and transporter families have been identified. P-glycoprotein (P-gp) is among the most important and definitely the best studied efflux transporters. P-gp is a transporter for a broad spectrum of compounds and considered to play a central role in the development of multidrug resistance by impeding drug transport into the brain. P-gp is a member of the ABC (ATP-binding cassette) superfamily, consisting of about 30 subfamilies. Different hypotheses on the P-gp working principle have been developed. P-gp acts either as a substrate transporter from inside the endothelial cells back to blood circulation or as a flippase, allowing the movement of membrane lipids between the two leaflets that compose a cell's membrane in order to extract the substrates. P-gp is a very important component for the protective function of the BBB. Efflux transporters are currently subjects of investigation and every year more transporter systems are found and better understood. (Fig. 3)

Active influx transporters

Active transport of amino acids and nutrients into the brain has been well known for quite long time but the first uptake transporters have only been described very recently. The solute carrier family (SLC) contains OATP2B1 and OATP1A2 which are expressed on the luminal side of the BBB and involved in active uptake. Investigating active influx transporters at the BBB is of uttermost importance for the development of formulations to bring neuroactive pharmaceuticals to the site of action, the brain. (Fig. 3)

Transcytosis

Receptor mediated transport of large molecules is often done by vesicular transcytosis. Specialized receptors protruding from the cell membrane into capillaries recognize the payload substrate. The receptor is internalized into the cell membrane after connecting to the substrate. The substrate can traverse the BBB in a coated pit, a vesicle formed at the surface of the membrane. On the abluminal side in the brain the substrate is released. Substances like transferrin with a size of 75 kDa use this pathway as well as low density lipoproteins (LDL), insulin, cytokines and other lipid proteins. (Fig. 3)

Adsorption mediated transcytosis is a similar and but less specific pathway. Electrostatic interaction between the cell surface and the substrate replaces the function of the receptors for cationic molecules, therefore this type of transport is also called cationic transport. Due to the lower affinity between substrate and transporter the transport capacity is higher than in receptor mediated transcytosis. (Fig. 3)

2. Methods of studying transport across the BBB

Effectiveness of substance transport across the BBB and substance concentration in the brain tissue needs to be determined to give feedback in the development of neuroactive substances, since non-sufficient drug pharmacokinetics is the main cause of failure. In order to investigate the extent and the mechanism of substance transport across the BBB a variety of different techniques have been developed. Conventional methods work with animal models in-vivo but newer approaches also use in-vitro cell cultures or even computer simulations. Due to largely the same structure of the BBB in all mammals, in-vivo results are highly relevant for human applications. Other methods still have to be validated but have shown promising results in the early high-throughput phases of drug development. A detailed discussion of these methods is given below (Mensch et al., 2009).

2.1 Brain biopsy based techniques

Experiments based on brain tissue homogenates remain the gold standard for measurement of transport across the BBB and the most widespread technique in pharmacological industries. They can be classified in two categories:

- (a) Techniques based on equilibrium between blood and brain (extent of brain uptake, brain/plasma ratio, etc.)
- (b) Techniques based on pharmacokinetic parameters (rate of brain uptake, permeability \times surface product (PS) as an indicator for initial brain uptake, etc.)

An example of each technique is given below:

(a) Brain/plasma ratio (log BB):

The distribution between blood and brain in equilibrium is expressed as the logarithm of the steady state concentration of a substance in brain and plasma (log BB). Log BB depends on passive diffusion, uptake and efflux transporters, substance metabolism and protein binding in plasma and brain tissue. Multiple log BB determinations are conducted at different time-points after application (oral, i.v, i.p., etc.) conducted in order to address time dependence. The brain/plasma ratio is calculated from the AUC's in brain and plasma. Substances with a brain/plasma ratio greater than 1 freely cross the BBB freely, substances with a ratio smaller than 0.1 are usually not able to enter the CNS in an effective dose. Determination of log BB determination is an endpoint investigation and usually requires several animals per time-point and is therefore expensive, laborious and ethically delicate. Log BB does not differentiate between the bound and the free substance fraction and free substance fraction; only the free fraction is causing the pharmacological effect. Therefore, log BB values cannot be directly linked to the pharmacodynamic effect of a substance. (N. Joan Abbott, 2004; Bourasset, Bernard, Muñoz, Genissel, & Scherrmann, 2005; Doran et al., 2005; Reichel, 2006).

(b) Brain uptake index (BUI)

The brain uptake index (BUI) with carotid artery single injection and brain tissue biopsy sampling was first described in 1970 by Oldendorf. BUI is applied in anesthetized rats and involves a rapid (~0.5 s) intra-arterial carotid injection of the labeled test substance and a labeled reference compound. The reference substance can cross the BBB to a large extent and serves as an internal standard to normalize the total amount of injected material that distributes into the brain tissue. The rat is decapitated 15 s after injection. This short time span minimizes efflux effects from the brain and inhibits systemic recirculation (single pass technique). Immediately after decapitation the brain is extracted and test as well as reference

substances are measured and compared to the plasma concentration to determine the BUI. The BUI technique is a very fast method and therefore suitable for substance with a short half-life. The main limitations of this technique are a short contact time with the brain tissue, and no direct correlation with BBB permeability as the BUI is influenced by many factors such as: brain region, blood flow and exposure time. Therefore applications of the BUI technique are limited to substance with a high BBB permeability (Bonate, 1995; Oldendorf, 1970; Pardridge, 1995).

2.2 Imaging techniques

2.2.1 Positron Emission Tomography (PET)

Positron emission tomography is a noninvasive technique that can be used to measure changes in the brain metabolism of humans and animals (Brooks et al., 1984) (Josserand et al., 2006). The subject is positioned in a detector that counts gamma photon emission emitted by the tracer. A two-dimensional (2-D) or 3-D image of the brain can be generated in real time by applying computer-supported imaging techniques (Dingemans, Sollie, Breimer, & Danhof, 1988; Hilbert & Battista, 1991). Altered glucose metabolism, for instance, can be recorded by (18F) fluoro-deoxy-glucose. PET provides high sensitivity and exact time resolution; in addition, pharmacological compartment modeling can be used to assess PK. PET scans are increasingly combined with other imaging techniques such as MRI or CT to acquire both anatomic and metabolic information (Fig. 5). This combination has many potential applications for brain imaging. Limitations of PET arise from the high costs of cyclotrons necessary to produce short-lived radionuclides for PET scanning and the need for a specially adapted on-site chemical synthesis apparatus to produce radiopharmaceuticals. Parent compounds and metabolites can be differentiated and special resolution of the PET scanner does not allow differentiation between intravascular space and brain tissue. (Fig. 5)

2.2.2 Magnetic Resonance Imaging (MRI) and Magnetic Resonance Spectroscopy (MRS)

MRI is a sensitive, non-invasive technique to monitor a range of clinical pathologies such as multiple sclerosis, stroke, and brain tumors (Ewing et al., 2003; Patlak, Blasberg, & Fenstermacher, 1983). Contrast agents such as gadolinium-DTPA (Gd-DTPA) improve the identification of changes in blood perfusion and morphology and allow clinical MRI applications to detect a leaking BBB in brain tumors, multiple sclerosis and stroke. A quantitative measurement of substance transport across the BBB is performed with tracers

used as vascular markers and the application of multi-compartment pharmacokinetic models or a graphical Patlak analysis. The analysis of drug transport across the BBB is limited by the inherent low sensitivity of MRI, which requires high local concentrations to measure MR contrast.

MRS can differentiate a wide range of chemical substances within the body but has the disadvantage of poor spatial resolution compared to MRI. A combination of both technologies can provide information about the distribution of substances as well as information about PD during toxicological analyses. Similar to PET scans, MRI and MRS are very cost-intensive methods, which limit their applicability as screening methods. (Fig. 5)

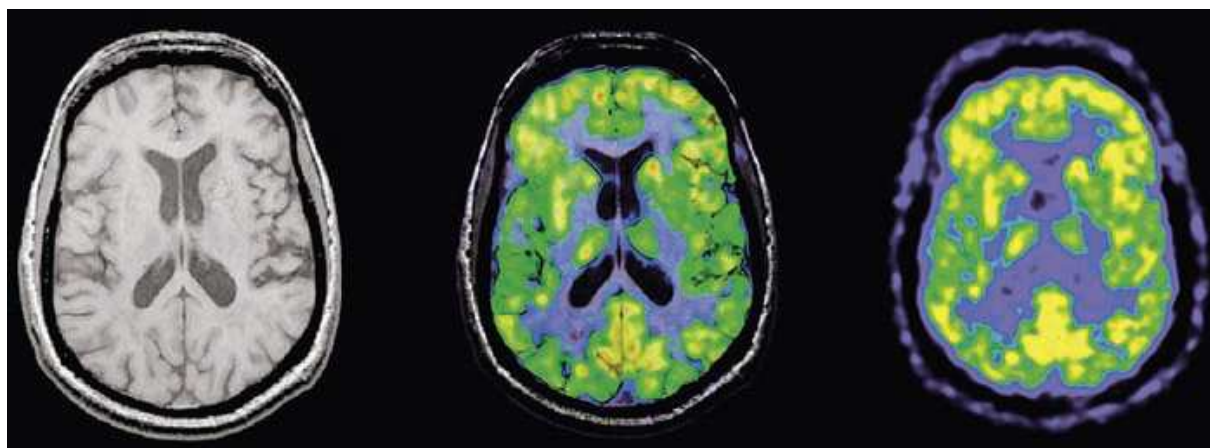


Fig.5: MR image (left) and PET image (right) and are merged to an image incorporating anatomical and metabolic information (center). Siemens Ref. Nr: somed200701-01.

2.3 Microdialysis (MD)

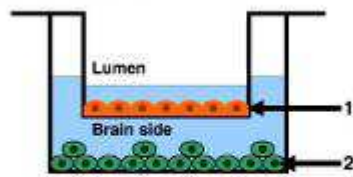
Intracerebral MD is an invasive technique to continuously sample substances in extracellular tissue space. A cylindrical, semipermeable membrane is implanted into the target area in the brain and perfused with a physiological solution, the perfusate (Elmqvist & Sawchuk, 1997). The perfusate is ideally closely matched to the ionic composition and the pH-value of the interstitial fluid (ISF) of the brain to avoid changes in brain physiology that could lead to interference with the BBB (E. C. de Lange, de Boer, & Breimer, 2000). The membrane allows substance exchange between ISF and perfusate according to concentration gradients and diffusion parameters. The perfusate inside the membrane is continuously exchanged; the standard setup consists of an active inflow, driven by a syringe pump; the outflow is passive and the perfusate (enriched with components from ISF) is collected into a vial, which is replaced periodically. A constant perfusate flow through the membrane allows continuous, parallel measurement of several markers and metabolites and a differentiation between parent compounds and metabolites. Toxicity markers such as the above-mentioned S100b and the cytokines are accessible by MD. Continuous sampling reduces the number of animals used and statistical problems such as inter-subject variability compared to a

measurement with standard brain biopsies techniques require several animals per time-point. MD allows time-resolved determination of cerebral ISF, which enables in combination with plasma sampling kinetic and dynamic monitoring of substances. To investigate a specific brain region, the MD probe can be implanted stereotactically with high local accuracy; several probes can be implanted. A drawback in the MD application is that implantation of the MD probe damages cerebral capillaries and consequently affects BBB function. Different time spans (hours up to days) until the BBB is reestablished have been reported (E. C. de Lange, Danhof, De Boer, & Breimer, 1997; Groothuis et al., 1998; Westergren, Nyström, Hamberger, & Johansson, 1995). A short time span between probe implantation and start of sampling may result in decreased local blood flow (Benveniste, Drejer, Schousboe, & Diemer, 1987). Moreover, the membrane is the limiting factor in the exchange between tissue and perfusate because substances larger than the pore size of the membrane and lipophilic substances cannot pass the membrane and are subsequently excluded from the analysis (Alan J Rosenbloom, Sipe, & Weedn, 2005). One problem of microdialysis is the combination of biofouling of the membrane surface combined with collagen deposition that occurs 5–7 days after implantation. For molecules that are replenished into the tissue space via blood capillaries, the walling-off with the collagen capsule and the biofouling layer appear to affect the supply to the dialysis probe and thus result in a lower recovery rate for different compounds. Finally, accurately determining the relationship between concentrations of the drug of interest in the solution that exits the dialysis probe and concentrations in the tissue (recovery) can be difficult. Pinpointing recovery in vitro is inaccurate because in vitro results usually exceed in vivo measurements. In particular, two methods are applied to overcome the recovery problem: no-net flux, which delivers a reliable outcome but is very time consuming, and retro dialysis, where a substance with similar diffusion behavior is added to the perfusate and the loss to the tissue of this substance is detected.

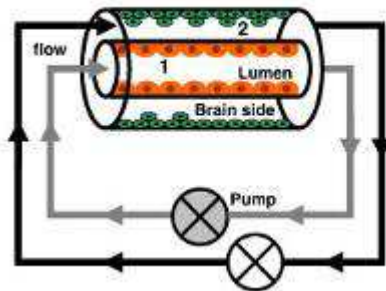
2.4 In-vitro methods

In-vitro methods are used for high-throughput scanning of substances in the initial phase of pharmaceutical development projects and should therefore be simple, reproducible and should mimic the in-vivo situation as closely as possible. Good applicability in industrial research projects led the development of different in-vitro models. (Fig. 6)

A Static BBB models



B Dynamic 3-D flow BBB model



1 Brain endothelial cells

- Primary endothelial cells:

- bovine (Cecchelli et al., 1989)
- porcine (Meyer et al., 1980)
- rat (Perrine et al., 2007)
- mouse (Cosme et al., 2005)
- human (Persidsky et al., 1997; Biernacki et al., 2005)

- Endothelial cell lines:

- bovine : SV-BEC (Dunau-Trautmann et al., 1991)
- porcine : PBMEC (Tittel M & Friedl, 1998)
- rat : RBE4 (Roux et al., 1994)
- mouse : bEnd5 (Laschinger & Engelhardt B, 2000)
- human : hCMEC/D3 (Wekator et al., 2005)

2 Co-culture or not with

- Glial cells / Astrocytes (Cecchelli et al., 1989)
- Pericytes (Zonulya et al., 2008)
- Astrocytes and Pericytes (Nakagawa et al., 2007)
- Neurons (Stanness et al., 1999)

Fig.6: Modelling the blood-brain-barrier and neurovascular unit in vitro. Static BBB models (A) use brain endothelial cells (1), primary brain endothelial cells or endothelial cell lines, grown in the upper compartment of Boyden chambers. In order to model the neurovascular system, various other cell types (glial cells, pericytes or neurons) can be co-cultured in the lower compartment (2). Recently described dynamic three-dimensional flow BBB models (B) provide an interesting model to study brain endothelial cells properties under flow conditions, based on observations that pulsatile flow induces further differentiation of cultured brain ECs to a BBB phenotype (Weiss et al. 2009).

In-vitro models based on cells of non-cerebral origin use cells originating from e.g. canine kidney and show good paracellular permeability characteristics and considerable similarities in tight junctions and transendothelial resistance (TEER). Main differences are found in transporter expression which is important for drug transport or inhibition of transport. In summary these models might be suitable to investigate specific questions but cannot be considered accurate BBB models.

In-vitro models based on cerebral endothelial cells are grown in tissue cultures and the transport can be investigated using or avoiding astrocytic co-cultures. Primary brain capillary cells are, with the exception of explanted cerebral capillaries, the in-vitro model closest to the in-vivo experiment. One major drawback of these models is the time and effort needed to isolate, seed and incubate the primary cells and the co-cultures. The lacking reproducibility of the primary cell model regarding permeability and transporter expression is a very important disadvantage.

Immortalized brain endothelial cells are the solution to most disadvantages of primary cell models. Immortalized cell lines form cell monolayers without complete tight junctions between the cells. This leakiness limits their usefulness in BBB transport studies but the immortalized cell lines have proven to be beneficial in mechanistic and biochemical studies.

Immortalized cell lines are the most widespread in-vitro model mostly due to their easy handling and acceptable reproducibility (Weiss et al., 2009).

2.5 Behavioral Tests

One aspect of brain pharmacokinetics and pharmacodynamics is the change in the behavior of animals under the influence of neuroactive substances. Two types of behavioral tests can be distinguished: stimulus-oriented and internally generated behavior tests. Stimulus-oriented behavior involves conditioned and unconditioned experimental setups in which the response to a particular stimulus is tracked. The conditioned test involves training to perform an action in order to receive a reward or avoid pain. Internally generated behavioral tests involve monitoring animal behavior in experimental situations such as social behavior, circadian behavior, and exploratory behavior. The performance of subjects treated with the test substance is compared to that of a control group. Groups must be matched in terms of age, sex, species, and housing conditions. Combined with other techniques, behavioral variations represent an integrated whole organism response that is mostly nonspecific but sensitive and can increase our understanding of the toxicological effects in the CNS. (Alavijeh, Chishti, Qaiser, & Palmer, 2005; Bricker, Jackson, Boateng, Zhu, & Ablordeppey, 2012; Eskow Jaunarajs et al., 2010; Polt, 1994)

CHAPTER III

General concept of cerebral open flow microperfusion (cOFM)

Parts of this chapter are based on the book:

Microdialysis in drug development

Chapter 15 "*Open Flow Microperfusion: An Alternative Method to Microdialysis?*"

Pieber TR, Birngruber T, Bodenlenz M, Höfferer C, Mautner S, Tiffner K, Sinner F; 2013

1. Open flow microperfusion (OFM)

OFM is an in-vivo sampling technique that is closely related to minimally invasive interstitial sampling methods such as microdialysis and push-pull perfusion (Myers, 1986). The fundamental difference between the standard microdialysis and OFM is that microdialysis uses a paper-like membrane as a tissue interface whereas OFM uses macroscopic opening to exchange substances between the interstitial fluid (ISF) of a tissue and the perfusate in the probe. The membrane-free concept of OFM avoids membrane related problems such as biofouling and protein clotting (Alan J Rosenbloom et al. 2005; A J Rosenbloom et al. 2006) or the inherent issue of molecular cut-off and the exclusion of large substances (Fig. 8). Endogenous and exogenous substances present in the ISF of targeted tissues can therefore be quantified without the risk of investigating an altered or filtered sample. So far, OFM has been used in tissues such as skin, muscle, adipose tissue and the aim of this thesis was the development of a suitable OFM application for brain tissue.

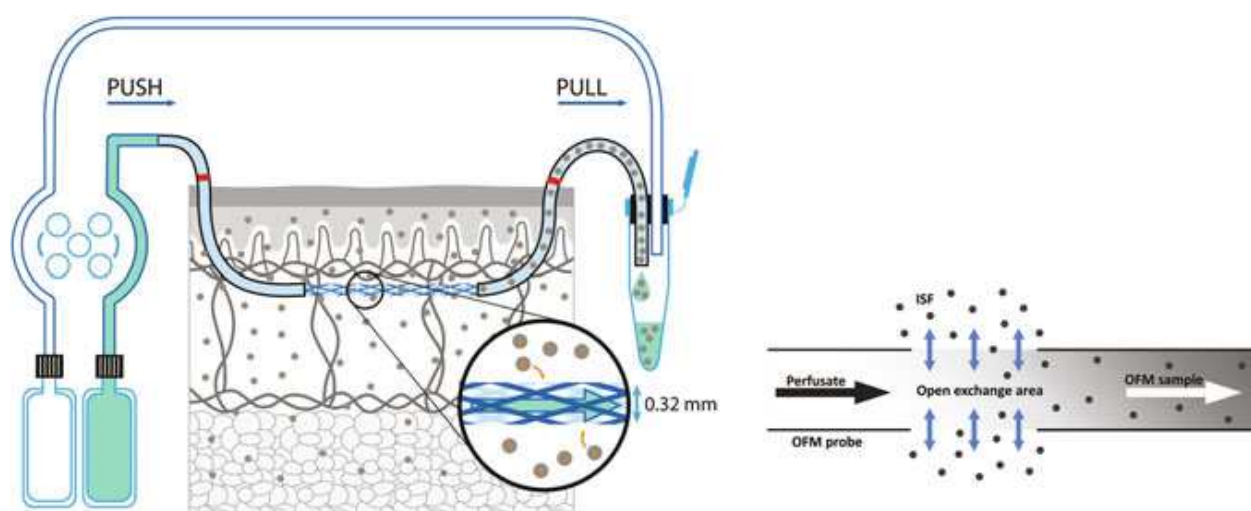


Fig. 7: Schematic figure of the OFM system in skin and adipose tissue with a linear membrane-free OFM probe. The inserted OFM probe is connected to a peristaltic pump via push-pull tubing. The OFM pump simultaneously pushes the perfusate into the OFM probe and pulls the OFM sample into an easily exchangeable vial. At the exchange area, substances are freely exchanged between the ISF and the perfusate.

The open structure of the exchange area bears the risk of fluid loss to the tissue. To avoid loss of fluid and to ensure stable sampling volumes a tightly controlled fluidic path has to be established. OFM systems actively push the perfusate into the probe lumen, and actively pull the OFM sample at the same flow-rate from the probe into a sampling vial using push-pull pumps similar to those that would be required for high molecular weight cut-off MD systems (Sjögren et al. 2002; Jensen et al. 2007) (Fig. 8). The technical implementation of the push-pull mode in OFM systems has already been shown to work effectively and to ensure stable,

drift-free recovery and sampling for at least 24 h in clinical and preclinical studies. The OFM pump was realized as a small, wearable, multi-channel, push–pull peristaltic pump which increases the mobility of study subjects and allows longer study periods. In addition, the current OFM probes have been optimized for application in different target tissues and for minimal trauma during insertion.

The OFM system facilitates reliable quantification of analytes including lipophilic and high molecular weight substances. OFM and its CE-certified devices can be used in skin and adipose tissue for basic and pharmaceutical research not only in a clinical in vivo setting but also in preclinical in vivo and ex vivo settings. Both MD and OFM are efficient sampling techniques for substances in the ISF. While OFM offers advantages regarding the range of sampled substances, it also faces challenges when analyzing the more complex OFM samples. Table 1 gives a brief summary of differences between the two sampling systems.

Table 1: Key features of OFM and MD sampling systems

Component	OFM	MD
Probe	membrane-free	semi-permeable membrane
	no nominal cutoff	molecular weight cutoff
Sample	Sample unfiltered, diluted	filtered, diluted
	long-term sampling	membrane fouling or clotting can limits sampling time
	low–high molecular weight	low–moderate molecular weight
	low–high lipophilicity	low–moderate lipophilicity
	high protein load	no–low protein load
Pump	push–pull mode	push suitable for low molecular cutoff
Tubing	no to low adsorption due to direct coupling of sampling vial to OFM probe	possible adsorption in outflow tubing
Analysis	sample pretreatment required	sample pretreatment advised

2. General concept of cerebral open flow microperfusion (cOFM)

cOFM - cerebral open flow microperfusion provides access to the interstitial brain fluid of a living organism and is the most recent development in OFM. cOFM utilizes the strengths of OFM and microdialysis to sample in the ISF of the brain and thus allows monitoring of substance transport across the BBB. As described in more detail in chapter I and II the BBB protects the brain from potential harmful chemical substances in the blood and limits therefore substance and drug transport into brain. Development of new pharmaceutical products is hampered due to the access limiting nature of the BBB. A straightforward development of neural drugs and transporter systems demands a measurement system that gives direct feedback about the effectiveness of substance transport into the brain. This illustrates the need for a method to determine the chemical and metabolic composition of fluids and tissues in the CNS without limitations in terms of:

Lipophilicity – as most natural drugs that are effective in the brain are small and lipophilic, these substances can cross the BBB via passive transport.

Molecular weight – The most promising technology to transport substances across BBB are nanocarriers that contain the substance of interest and an active transporter to cross the BBB and release the substance there. These nanocarriers form large complexes compared to the size of a single molecule of the substance to be transported.

cOFM is designed to monitor the transport of large and lipophilic substances across the BBB and shows the potential to bridge the gap in the development of neural drugs. Like all invasive sampling techniques, cOFM probe implantation causes trauma, destruction of capillaries and disruption of the BBB. But the design of the cOFM probe allows sampling after the implantation trauma has healed and BBB has been re-established. During BBB re-establishment and healing of the damaged tissue the cOFM probe stays in place and encapsulation has to be avoided. Tissue encapsulation of the cOFM probe would act as a diffusion barrier between healthy brain tissue and the probe and decrease measurement sensitivity or even impede measurement.

cOFM probe design and the used materials are chosen to meet the following requirements:

- produce minimal implantation trauma
- address different brain areas with high accuracy
- allow healing of implantation trauma and BBB re-establishment provoke minimal tissue reaction during the healing process
- provide stable exchange performance with the surrounding healthy tissue

Some of these requirements are conflicting and require a balanced design.

3. Design of the cOFM probe

3.1 cOFM probe requirements

During implantation a slim stiff rod-like structure with a sharp pointy tip would be perfect in order to navigate exactly to the brain area of interest with minimal tissue traumatization.

During the healing process a slim very flexible structure with a smooth, slick surface and a rounded design is needed to avoid repeated injuries to the brain.

Studies about tissue reaction following the implantation of cerebral fluid sampling systems observed the formation of a glial scar around the probe with a lot of brain tissue damage along the implantation track with extending tissue changes observed up to 1.4 mm from the probe (Clapp-Lilly et al., 1999; Borland et al. 2005; Hascup et al. 2009). A result like this would impair the cOFM probe at the time point when the BBB has re-established after implantation trauma, since a glial scar acts as a diffusion barrier and hampers substance exchange between healthy brain tissue and the probe

Regarding the flexibility of the implanted probe previous investigations have found considerably increased brain tissue reaction to implants anchored to the skull in comparison to the same material implanted intraparenchymally without fixation to the skull (Kim et al. 2003). Another more recent study revealed that implant stiffness affects the neuronal response and augments the degree of the glial scar (Harris et al. 2011). This has been attributed to micro-movements of the brain floating in cerebro-spinal fluid CSF. Movements cause a constant irritation on the stiff probe anchored to the bone structure of the skull. A flexible probe is supposed to cause less irritation and therefore less tissue reaction.

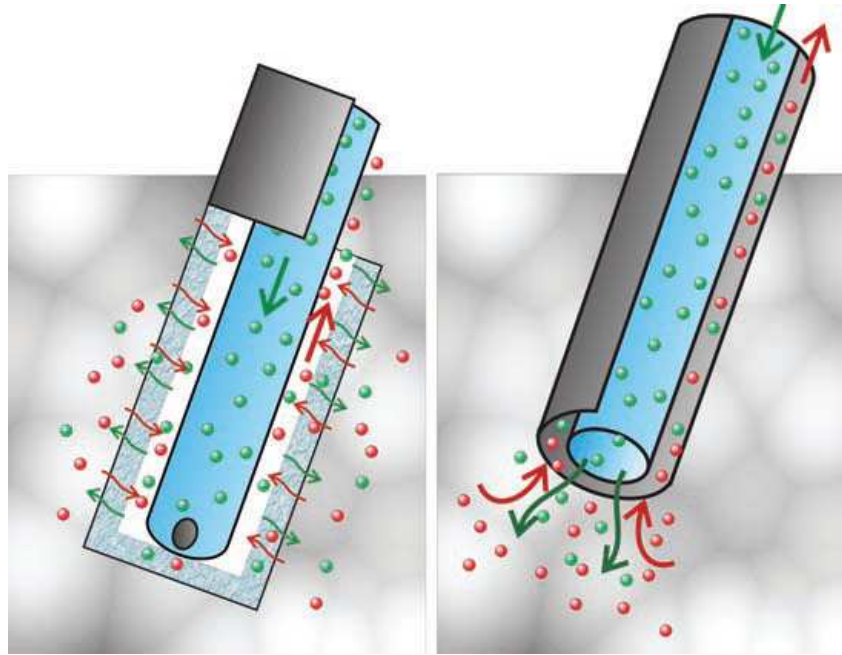


Fig. 8: Working principle of MD (left) and OFM (right): MD uses a membrane as tissue-interface, while OFM provides a direct contact to the cerebral tissue.

The slick surface avoids adhesion of immunoreactive cells and proteins to any probe surface that accesses the brain during implantation-related bleeding and through the penetrated meninges (Fitch et al. 1999, Stenken et al. 2010). These immunoreactive factors tend to amplify tissue reactions finally leading to the formation of a glial scar. During sampling a structure with large multiple lumina with smooth and inert surfaces would be desirable to provide a large exchange area at the tip of the probe and low probability of jammed lumina due to blood coagulation. The application of inert surfaces minimizes unspecific adsorption of lipophilic substances to the inner surface of the probe lumen (Fig. 9).

The following cOFM probe design was implemented taking into account all of these published findings and practical considerations as well as some limitations in material technology especially in the area of tube manufacturing using different materials and material coatings.

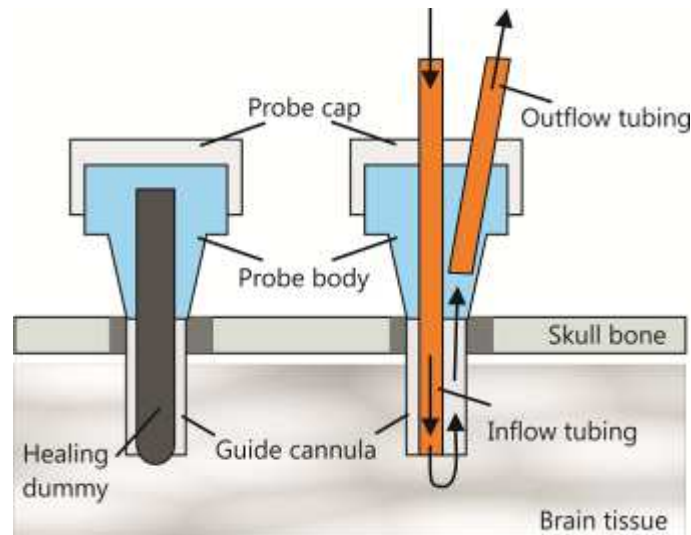


Fig 9: The probe consists of the probe body with a 20 Ga guide cannula that extends into brain tissue and a probe cap that fixes the two cartridge elements: (1) The healing dummy (stainless steel) provides mechanical stability during probe insertion, allows tissue regeneration, and prevents tissue ingrowth into guide tubing. (2) The inflow/outflow tubing replaces the healing dummy after the healing period in order to allow sampling.

3.2 cOFM probe

In contrast to the standard linear design of the OFM probe, the cOFM probe features a concentric design that allows implantation with minimal trauma and an exact navigation to address different brain regions. Exact navigation requires a stiff probe and this mechanical stability is provided by the healing dummy during probe implantation. The healing dummy is inserted into the inner lumen of the probe's guide cannula (Fig. 9). The healing dummy's design and material allows tissue regeneration and prevents tissue migration into the guide tubing. It remains in place until the implantation trauma has healed and the BBB is re-established. Immediately before sampling, the healing dummy is replaced by inflow/outflow tubing and perfusion fluid is pushed into brain tissue (via inflow tubing) and withdrawn at the same speed (Fig. 13).

Early versions of the cOFM probe used the linear design like the standard OFM probe. A linear probe for brain application needs an entrance opening in the skull that is different from the exit opening. The skull in rodents is bordered by chewing muscles that need to be unharmed, as tissue damage would be very painful and lead to a decreased food uptake. Both starving and pain lead to stress situation that could open the BBB. Therefore, using a linear approach in rat brain requires the probe to be inserted in a circular pathway in order to avoid the big muscle groups (Fig. 10). This approach was not pursued any further due to high tissue damage across the implantation path and linear probe instability that led to tissue constriction.

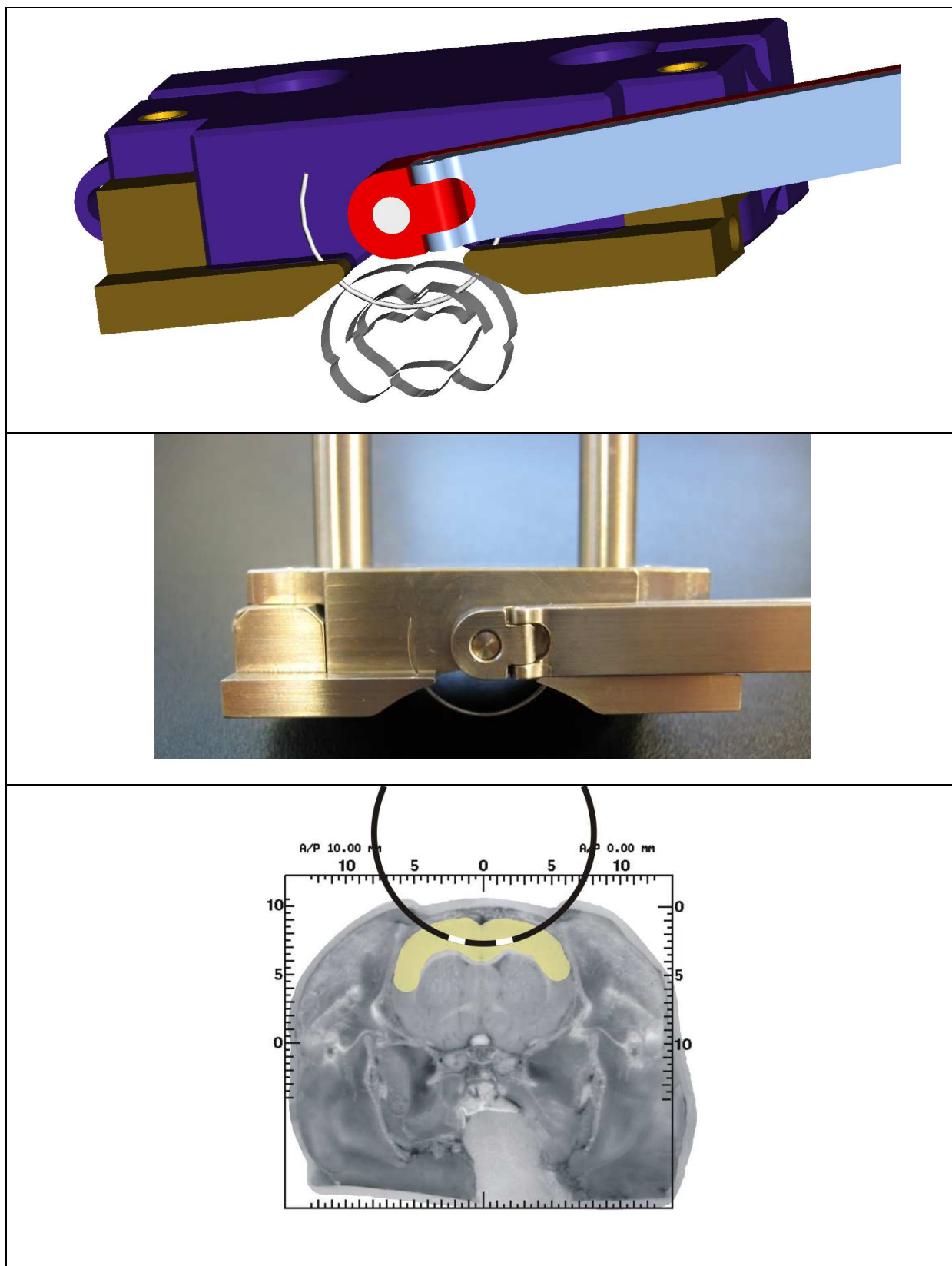


Fig 10: Top picture shows the design of the linear-circular probe implantation device, below a picture of the actual device designed to be mounted on a stereotactical implantation frame. The figure at the bottom shows the planned implantation pathway, the two white sections mark the exchange area in the hippocampus with the implantation pathway avoiding the big muscle groups.



Fig. 11: Magnified photo of the probe tip: The outer white transparent tubing is the guide cannula; the inner orange tubing is the inflow tubing.

The guide cannula is the part of the probe that is inserted through a hole in the skull, into the brain and is therefore the main contact surface between brain tissue and cOFM probe. The guide cannula is made of fluorinated ethylene propylene (FEP) a material with a slick, non-reactive surface with low friction, easily formable and therefore highly flexible. The healing dummy, made of stainless steel, fits into the guide cannula and provides the mechanical stability needed for implantation. The tip of the healing dummy is the second surface of the cOFM probe that is in direct contact with brain tissue. The tip of the healing dummy is rounded and polished in order to create a similar slick and non-reactive surface like the guide cannula. This design fulfils the requirements during implantation and healing and remains in-situ until the BBB is re-established after the implantation trauma.

Immediately before sampling the healing dummy is replaced by a sampling inlet with inflow and outflow tubing that allows the establishment of a fluidic pathway through the probe and brings the perfusate in direct contact with the brain tissue. The inflow tubing is exactly in-line with the guide cannula in order to avoid any new traumatisation during inlet exchange. At the same time it maximizes the contact between perfusate and tissue. A short inflow tubing would lead to a fluidic pathway that is too short to involve brain tissue. The spacer allows precise positioning of the inflow tubing as it maintains a constant distance between the probe cap and the probe body independent of manufacturing variability and the moment of torque at the probe cap.

The guide cannula is made of FEP, the inflow tubing's outer surface is coated with Polytetrafluorethylen (PTFE) and the outflow tubing is entirely made of PTFE. All surfaces on the entire outflow pathway are made of non-reactive surfaces in order to minimize unspecific adsorption of lipophilic substances sampled in the brain. Adsorption would exclude the substance from analysis and would therefore lead to underestimation of the concentration in the brain.

3.3 cOFM sampling system

The inflow/outflow tubing is connected to syringe pumps that allow operation under very closely controlled conditions regarding flow-rate precision and the balance between delivered and withdrawn fluid. The peristaltic pump as used in standard OFM does not allow the necessary exactness in the fluidic pathway – an imbalance of in- and out flow can lead to increased cranial pressure due to a liquid excess in the brain with fatal consequences (respiratory depression, stem brain damage and ultimately death). In order to maintain a constant and closely controlled flow through the cOFM probe in this setup we used syringe pumps (Aladdin, World Precision Instruments, Germany) (Fig. 12, Table 2).



Fig. 12: The syringe pump used in the cOFM setup is an Aladdin, World Precision Instruments capable of push and pull mode. It is driven by a microcontroller system connected to a step motor, allowing a large range of flow rates configured to the inside diameter of the used syringe. The syringe is connected to the motor via a drive-screw and drive-nut mechanism.

Table 2: Syringe pump features (World Precision Instruments, Aladdin –programmable syringe pump instruction manual)

SYRINGE SIZES	Up to 60 ml
NUMBER OF SYRINGES	1
MOTOR TYPE	Step Motor
STEPS PER REVOLUTION	400
SPEED (max.min.)	3.06 cm/min / 0.03 cm/hr
MOTOR TO DRIVE SCREW RATIO	15/28
PUMPING RATE	1019 ml/hr with 60 ml syringe / 5.8 µl/hr with 1 ml syringe
MAXIMUM FORCE	110 N at min. speed, 45 N at max. speed
NUMBER OF PROGRAM PHASES	41
SYRINGE INSIDE DIAMETER	0.1 to 50 mm
POWER	Wall adapter 9V DC @ 1000 mA
DIMENSIONS	22.9 x 14.6 x 11.4 cm (8.75 x 5.75 x 4.5 in.)

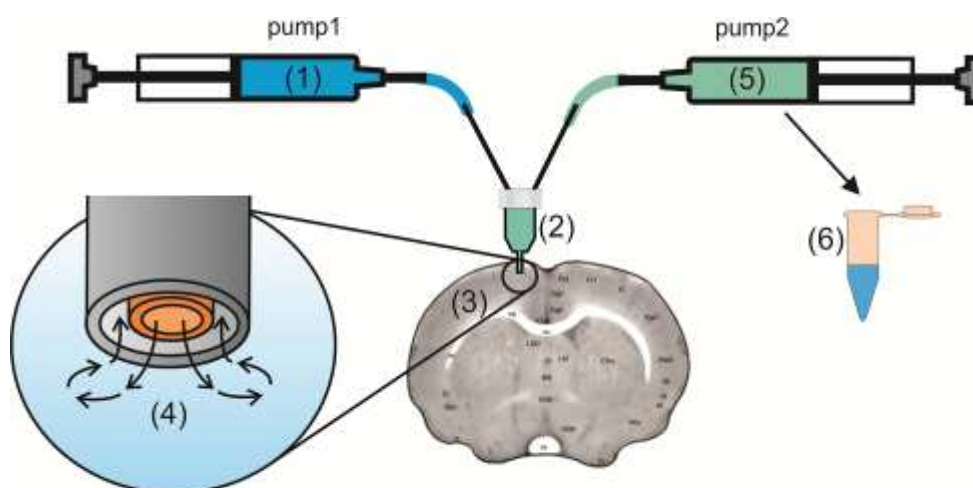


Fig 13: Pump1 pushes perfusate (1) through the cOFM probe (2), which is inserted in the frontal lobe of the left hemisphere of the rat brain (3). At the tip of the probe (4) there is exchange between interstitial fluid and perfusate. The resulting mixture of fluids is withdrawn by pump2 (5) and collected at regular intervals in vials (6). The open structure of the cOFM device puts perfusate in direct contact with brain tissue and brain interstitial fluid, which allows sampling of lipophilic and large molecules.

CHAPTER IV

Testing of BBB intactness after cOFM probe implantation

The blood-brain barrier (BBB) limits substance transport to the brain and is therefore the major hurdle to overcome when developing neuroactive drugs. Cerebral open flow microperfusion (cOFM) is a novel probe-based technique that allows continuous in vivo sampling of the interstitial fluid of the brain with subsequent measurement of drug transport across the intact BBB. Similar to other invasive probe techniques, cOFM probe insertion causes trauma and damage to the BBB. However, the design of the cOFM probe and its constituent materials allows tissue healing and re-establishment of BBB function without influencing cOFM sampling efficacy.

To characterize the healing process, BBB permeability was assessed at different time points following cOFM probe insertion for up to 15 days using Evans Blue (EB). EB is an established marker for BBB leakage as it does not cross the intact BBB. EB levels in the brain tissue 11 days after probe insertion were found identical to a non-altered BBB.

To further characterize BBB behavior after complete healing, the sensitive low-molecular-weight marker, sodium fluorescein (Naf), was administered intravenously. Naf crosses the intact BBB to a small extent, with increasing BBB permeability the extravasation rate increases rapidly; this behavior is used to monitor even small changes in BBB permeability. Significantly increased Naf levels were found in the interstitial fluid when hyperosmolar mannitol (known to open the BBB) was introduced via cOFM, which indicated a partial opening of the BBB surrounding the cOFM probe.

cOFM allows continuous sampling of any substance in the cerebral interstitial fluid. The use of Naf allows testing of BBB intactness in each sample.

1. Introduction

In recent years transport across the BBB has largely been investigated by using microdialysis (MD). MD is a probe-based method that facilitates exchange between tissue and perfusate across a thin membrane. While the membrane protects the fluidic pathway, it excludes high-molecular-weight and lipophilic substances, which are thus not accessible for sampling and subsequent analysis. Another possible technique for in vivo sampling is push-pull perfusion. While push-pull perfusion was among the first methods developed for sampling in brain tissue (Myers, 1986), it has largely been abandoned due to the greater extent of tissue damage near a push-pull sampled region due to probe size, flow rate and used materials (Kottegoda et al., 2002; Myers, 1986).

cOFM represents the latest development combining push-pull perfusion and open flow microperfusion (OFM). OFM is a relatively new technique that has been used to assess organ-specific pharmacokinetics (PK) and pharmacodynamics (PD) in the dermis (dOFM) and adipose tissue (aOFM). The main advantage of OFM over other continuous sampling techniques is that it can be used for sampling the entire range of substances including small ions, hydrophilic substances like glucose, highly lipophilic substances, antibodies, and even entire cells (Manfred Bodenlenz et al., 2005, 2012; Ellmerer et al., 1998; Holmgaard et al., 2012; Schaupp et al., 1999; Trajanoski et al., 1997). As we show here, such sampling can now be achieved for cerebral interstitial fluid, with an intact BBB, by using cOFM.

In contrast to MD, cOFM requires no membrane, it rather puts the perfusate in direct contact with brain tissue. This provides significant benefits, such as (i) no filtration is performed, which means that lipophilic and high-molecular substances can also be sampled; (ii) the sampling performance does not deteriorate over weeks, since there is no membrane occlusion due to protein clotting or biofouling (A J Rosenbloom et al., 2006; Alan J Rosenbloom, Sipe, & Weedn, 2005); (iii) BBB intactness can be monitored in each animal in each cOFM sample to ensure BBB intactness.

Like all invasive probe techniques, cOFM probe insertion causes trauma, damage to capillaries, and therefore BBB disruption. This is, however, temporary. The purpose of the present study was (i) to determine the time between cOFM probe insertion and BBB re-establishment; and (ii) to demonstrate the ability of cOFM to sample in the interstitial cerebral fluid with intact BBB.

2. Material and Methods

2.1 Chemicals, injected or infused solutions

All reagents were purchased from Sigma Aldrich, Austria (purity \geq 99%) unless stated otherwise.

2.1.1 standard cOFM perfusate

cOFM standard perfusate was composed to match brain interstitial fluid in order to avoid chemical stress for the BBB (modified from McNay and Sherwin, 2004). Perfusate composition: 123 mM NaCl, 0.4 mM MgCl₂ (purity \geq 98%), 0.7 mM CaCl₂ (purity \geq 93%), 4.3 mM KCl, 1.3 NaH₂PO₄, 21 mM Na₂HPO₄, 4 mM glucose. All reagents were dissolved in sterile water (Aqua bidest, Fresenius Kabi, Austria). In order to remove possible bacterial contamination the perfusate was filtered through a 0.22 μ m sterile filter (Thermo Fisher Scientific, Germany). All steps were carried out under sterile conditions.

2.1.2 cOFM perfusate with hyperosmolar mannitol

cOFM perfusate with hyperosmolar mannitol was prepared as for standard cOFM perfusate except that glucose was exchanged with 1000 mM mannitol (purity \geq 98%).

2.1.3 albumin-bound Evans Blue (EB)

EB marker was prepared by mixing albumin solution (7 ml Alburnorm (200 g/l), Octapharma, Austria) with Evans Blue (10 mg) and saline (1 ml; 0.9 M, Fresenius Kabi, Austria). The solution was prepared 24 h before use and was stored at +4 °C.

2.1.4 sodium fluorescein (Naf)

Naf marker was prepared by dissolving Naf (7.5 mg) in saline (1 ml; 0.9 M, Fresenius Kabi, Austria).

2.1.5 antibiotics

Antibiotics were prepared dissolving Cefotaxim (25 mg; Sandoz, Austria) in saline (1 ml; 0.9 M, Fresenius Kabi, Austria).

2.1.6 pain treatment

Pain treatment was prepared by mixing Rimadyl (0.1 ml; 5 mg Carprofen, Pfizer, Austria) with saline (5 ml; 0.9 M, Fresenius Kabi, Austria).

2.1.7 injectable narcosis

Injectable narcosis was prepared by mixing Fentanyl (1 ml; 0.05 mg/ml, Janssen-Cilag Pharma, Austria), Midazolam (1 ml; 5 mg/ml, Janssen-Cilag Pharma, Austria) and Domitor (0.5 ml; 0.1 mg/ml, Pfizer, Austria)

2.1.8 phosphate buffered saline (PBS)

151.29 mg $\text{Na}_2\text{HPO}_4 \times 2\text{H}_2\text{O}$, 20.41 mg KH_2PO_4 , 850 mg NaCl dissolved in 100 ml deionized water. PBS was sterilized at 120 °C, 30 min; pH 7.2 – 7.3.

2.2 Animals

All animal protocols used in this study were approved by the Austrian Ministry for Science and Research Ref.II/10b, Vienna. After cOFM probe insertion, male Sprague-Dawley rats with a weight of 250 – 400 g (Harlan Laboratories, Udine, Italy) were housed individually in acrylic glass cages with a 12:12 h light:dark cycle, and food and water were available ad libitum. After transport, animals were allowed to acclimatize to the environment for at least one week before surgical procedures were carried out. Appropriate animal care was provided by the staff at the animal care facility (Institute for Biomedical Research, Medical University of Graz, Austria).

2.3 Surgery

Rats were anesthetized with injectable narcosis (1.5 ml/kg). The head was fixed in a stereotactic frame (KOPF Instruments, USA) and rats were prepared for surgery by shaving the head and disinfecting the skin with 70% ethanol. A 15 mm incision was made to expose the skull. The cOFM probe was slowly inserted 1 mm deep into the left frontal lobe tissue via a 1 mm hole drilled into the skull 2 mm lateral to the bregma. The probe was fixed to the skull bone using two anchor screws and biocompatible dental cement (iCEM Self Adhesive;

Heraeus, Germany). For three days following surgery a daily dose of 0.7 ml antibiotic and 1 ml pain treatment was administered subcutaneously.

2.4 Experimental design

Two different aspects of BBB intactness are under investigation:

- (i) BBB re-establishment after cOFM probe insertion (study 1)
- (ii) BBB permeability during cOFM monitoring (study 2)

(i) Evans Blue (EB) is a large standard marker to assess BBB intactness (Manaenko et al., 2011). We assessed EB concentration in brain tissue by using brain biopsies after cOFM probe insertion. For the experiment the healing dummy remained in the probe and cOFM probes were not perfused.

(ii) To assess BBB permeability during sampling we used sodium fluorescein (Naf), a small and highly sensitive marker for BBB permeability. Naf can be analyzed in cOFM samples and therefore allows monitoring of BBB permeability during sampling. In order to compare BBB re-establishment measured with two different markers, Naf concentration was also measured in brain biopsies.

2.4.1 BBB re-establishment after cOFM insertion (study 1)

cOFM probe insertion was performed as described in section 2.4. A dose of 3 mg EB/kg bodyweight was injected into the tail vein on different days after cOFM insertion (Fig. 14). After two hours of EB circulation a transcardial flushing procedure was performed with phosphate buffered saline (PBS; 50 mmHg for 15 min) to remove the intravascular EB fraction (modified from Lohman et al., 2005). Only EB that had crossed the BBB remained in the brain tissue. To determine the extent of EB staining, whole brains were extracted. Tissue was fixed in 4% paraformaldehyde and analyzed by fluorescence measurement, as described below in section 2.6. A total of 34 rats divided into 3 groups were used in this study:

Test group: 22 rats received an EB injection and were euthanized 5-15 days after cOFM probe insertion (Fig. 14 left). Positive control group: 6 rats received an EB injection immediately after cOFM insertion and were euthanized after 2 hours of EB circulation (Fig. 14 top right). Negative control group: 6 rats were euthanized 11 days after cOFM insertion without EB injection (Fig. 14 bottom right) to take into account the effect of probe insertion which always results in background fluorescence due to residual blood around the probe.

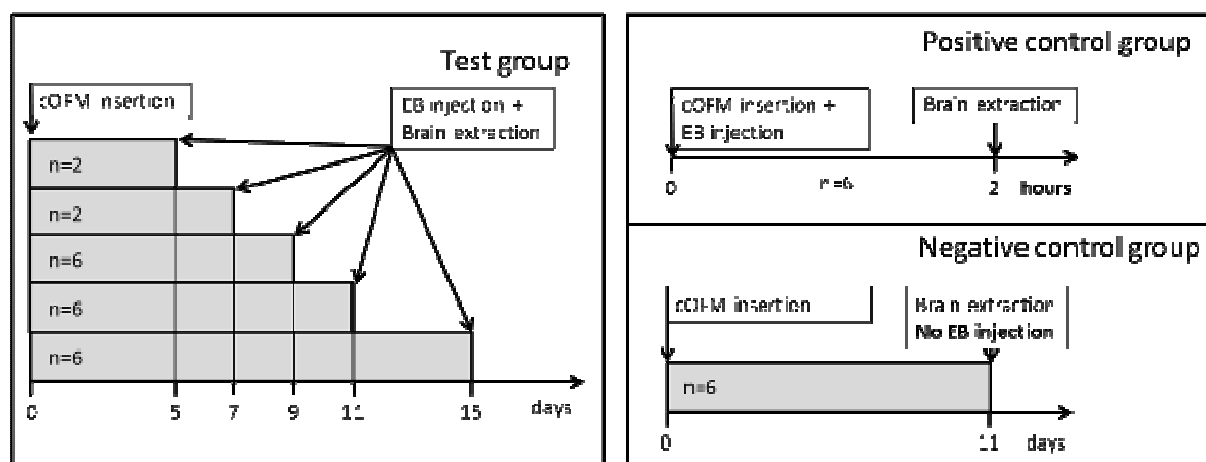


Fig. 14: Setup of study 1. The five test groups were sampled 5 - 15 days after cOFM insertion (left-hand side), while the positive and negative control groups were sampled 2 hours and 11 days, respectively, after insertion (right-hand side).

2.4.2 BBB permeability during cOFM monitoring (study 2)

A total of 24 rats divided into four groups were used in this study (Table 3):

Group 1 is a native control group with no cOFM probe inserted; therefore, BBB is intact in both hemispheres. Brain tissue and plasma samples were taken 1 hour after Naf injection.

Group 2: cOFM probe was inserted without probe perfusion; 15 days later brain tissue and plasma samples were taken 1 hour after Naf injection.

Group 3: cOFM sampling with healed BBB (15 days after implantation) using standard cOFM perfusate (Fig. 16)

Group 4: cOFM sampling with healed but open BBB (15 days after implantation) using cOFM perfusate with hyperosmolar mannitol (Fig. 16)

cOFM probe insertion into the frontal lobe of the left hemisphere of the rat's brain was performed as described in section 2.4. In groups 3 and 4 the healing dummy was exchanged by inflow/outflow tubing, 15 days after cOFM insertion, allowing cOFM sampling. Perfusion was started one hour after healing dummy exchange; sampling was started two hours after healing dummy exchange, and was performed hourly for five hours (Fig. 16). During cOFM sampling, rats were anesthetized with inhaled isoflurane (1% in 0.5 l/min oxygen, Abbott, Canada). These anesthetic conditions do not lead to an opening of the BBB in the frontal lobe (Tétrault et al., 2008). A bolus injection of Naf (11 mg/kg in physiological saline) was administered into the femoral vein to all rats in every group. For groups 3 and 4 the bolus was followed by a constant infusion of Naf (11 mg/kg/h in physiological saline) to maintain a steady Naf concentration in the blood.

In all groups, brain tissue biopsies 2 mm lateral to the bregma on the left and right hemisphere (Fig. 15) were taken after the transcardial flushing procedure (PBS; 50 mmHg for 2 min).

Table 3: Summary of all groups in study 2 in the Naf trial including types of Naf injection and samples collected.

	Naf injection	cOFM samples	plasma samples	brain samples	comment
Group 1 (n=6)	Bolus: 11 mg/kg	no	1x	1x	no probe inserted
Group 2 (n=6)	Bolus: 11 mg/kg	no	1x	1x	cOFM probe insertion without sampling
Group 3 (n=6)	Bolus: 11 mg/kg Infusion: 11 mg/kg/h	5x	5x	1x	Standard cOFM perfusate
Group 4 (n=6)	Bolus: 11 mg/kg Infusion: 11 mg/kg/h	5x	5x	1x	cOFM perfusate with hyperosmolar mannitol

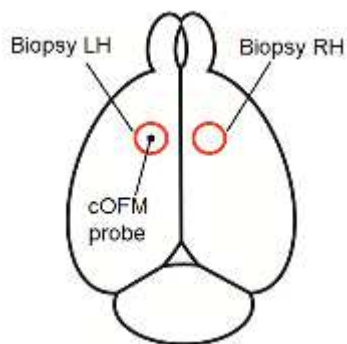


Fig. 15: Sketch of localization of biopsies in rat brain in left hemisphere (LH) and right hemisphere (RH).

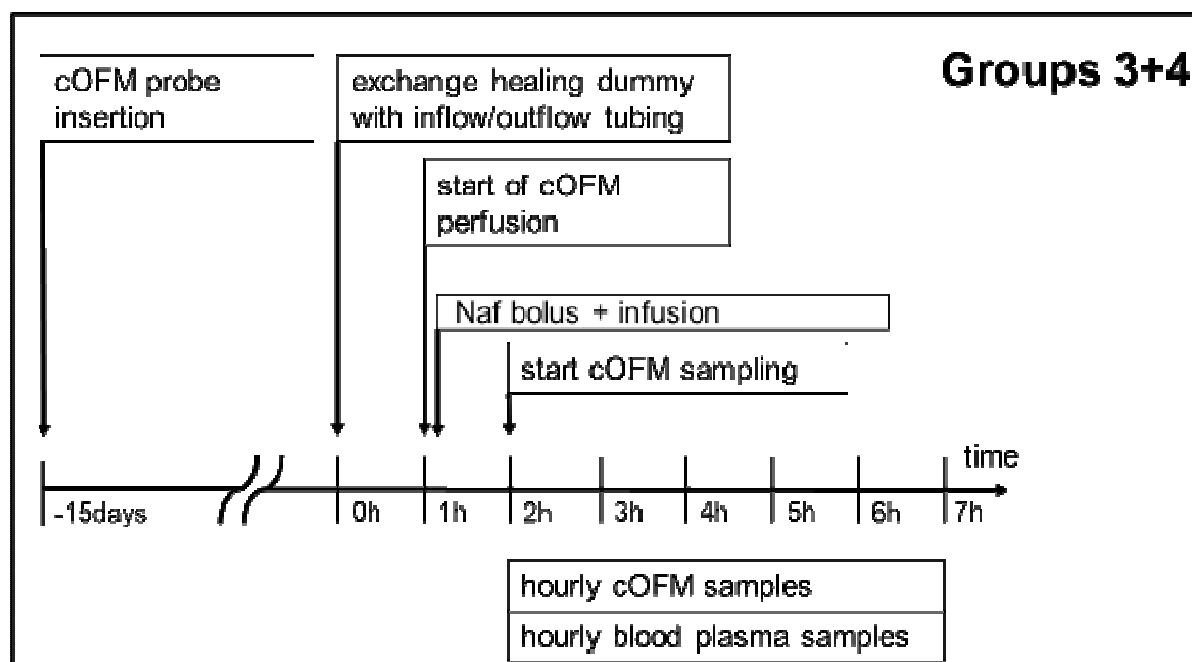


Fig. 16: Timing chart of experimental procedures in groups 3+4.

2.5 Analytical methods

All analytical methods except for the Maestro in vivo imaging systems (conducted by Birngruber) were conducted in the bioanalytical facility of Joanneum Research by trained and experienced personnel.

Three different types of samples (cOFM, plasma and brain tissue) were analyzed for EB and Naf. Sample pretreatment is required for all matrices.

Sample pretreatment: Protein precipitation was performed for cOFM and plasma samples, whereby 25 μ l of sample was mixed with 25 μ l of acetonitrile at room temperature. For brain tissue, samples were homogenized in Tris buffer (20 mM containing 1 % Triton X-100, pH 7.4; 2 μ l Tris buffer/mg brain tissue) by using a mortar and pestle. After centrifugation (all samples; 5 min at 2,000 g, RT) the supernatant was transferred into a 384-well plate.

EB analysis: To determine the extent of EB staining, whole brains were extracted and tissue was fixed in 4% paraformaldehyde. EB fluorescence was measured with the Maestro in vivo imaging system (CRi, USA). The filter set used was emission: longpass with a wavelength of 515 nm, and excitation: bandpass with a wavelength of 445 – 490 nm. Images were analyzed with ImageJ (vers. 1.44p) using a circular region of interest (ROI) with 2.5 mm diameter around the probe position.

Naf analysis: Naf concentration was determined by using a fluorescence microplate reader (Fluostar Optima, BMG labtech, Germany). Detailed information about system settings and linearity ranges are shown in Table 4.

Table 4: Sodium fluorescein system settings and linearity ranges.

	System characteristics
detection mode	fluorescence intensity
measurement mode	endpoint, bottom reading
excitation filter	485 nm
emission filter	520 nm
linearity for cOFM samples (LLOQ – ULOQ)	2.1 – 1,000 ng/ml
linearity for plasma samples (LLOQ – ULOQ)	205 – 100,000 ng/ml
linearity for brain tissue (LLOQ – ULOQ)	4.1 – 1,000 ng/ml

2.6 Statistical methods

A two-sample Wilcoxon rank test was used to examine the differences in mean EB fluorescence values between the test group and the negative control group in study 1. In study 2 the Grubbs outlier test for two outliers (Grubbs, 1950) was performed, which revealed two outliers with extremely high Naf concentration in cOFM samples in group 3. Both identified subjects were excluded from further analysis. The Kruskal-Wallis rank sum test was performed to compare Naf ratios of left hemisphere (LH) to right hemisphere (RH) in the brain biopsy analysis. A two-sample Wilcoxon rank test was used to compare group 3 (standard perfusate) and group 4 (mannitol) at each time point. All statistical analyses were performed with R version 2.13.1 (R Development Research Group, 2008), and with the statistical significance set at $p < 0.05$.

3. Results

The cOFM probe was stereotactically inserted into the left frontal lobe and probe position in the frontal lobe was confirmed by histological analysis. cOFM sampling was performed under well standardized conditions with anesthesia and surgery protocols that were well tolerated by rats, all rats survived and recovered completely within two hours after surgery.

3.1 Local BBB re-establishment after cOFM insertion (study 1)

EB was used as a marker to measure BBB permeability to high-molecular-weight substances after cOFM insertion in whole, extracted and fixed brains. Macroscopic inspection showed that all brains were free of blood, which indicates that the transcatheter flushing procedure had been effective. The removal of intravascular blood and EB by transcatheter flushing allows precise measurement of extravascular EB fluorescence, which indicates a leaky BBB.

In the positive control group EB fluorescence measurements immediately after probe insertion showed high fluorescence in the region of interest (2.5 mm circle around the probe). Brain biopsies taken 2 hours after cOFM probe insertion showed visible penetration of EB into the brain tissue surrounding the cOFM probe.

Fluorescence of EB in the brain tissue decreased with increasing healing time. Setting EB brain tissue staining in the positive control group to 100%, staining decreased to 30% in the samples taken after 5 and 7 days, and to 14.1 ± 6.8 (SD)% in the group sampled after 9 days but was still significantly higher than the negative control group (5.2 ± 0.1 (SD)% $p \leq 0.02$, Fig. 17). After 11 days (5.1 ± 1.4 (SD) %) and 15 days (5.5 ± 9.95 (SD) %), the extracted brains showed fluorescence levels similar to those of the negative control group (5.2 ± 0.1 (SD) % (Fig. 17).

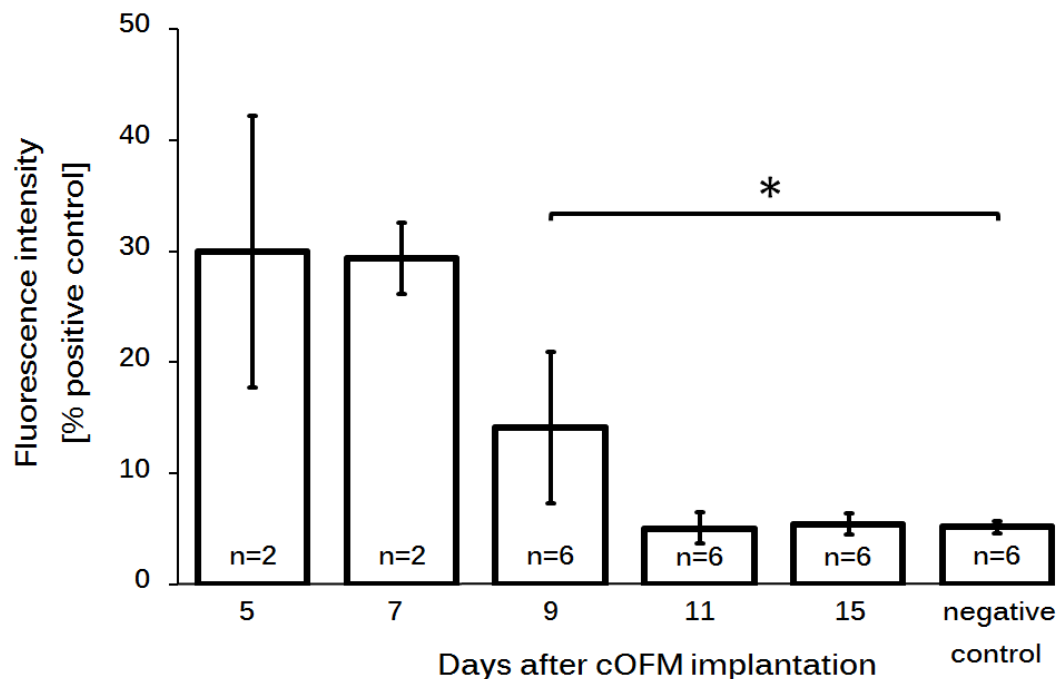


Fig. 17: Fluorescence intensity as a measure for BBB permeability for Evans Blue after various healing times (study 1).

3.2 BBB permeability characterization by brain biopsy

Naf concentrations in brain biopsies from the left hemisphere (LH) containing the probe insertion site were compared to biopsies from the right hemisphere (RH) with intact brain tissue. The Naf (LH)/Naf (RH) ratio offers information on BBB permeability surrounding the probe and allows a comparison of groups with different Naf injection modes (bolus vs. continuous infusion). Ratios were similar in groups 1 and 2. Group 3, which received standard cOFM perfusate, had a lower Naf ratio than group 1. Group 4, which received cOFM perfusate with hyperosmolar mannitol, had higher ratios (2.1 ± 1.2) than group 1; however, none of these differences were statistically significant (Fig.18).

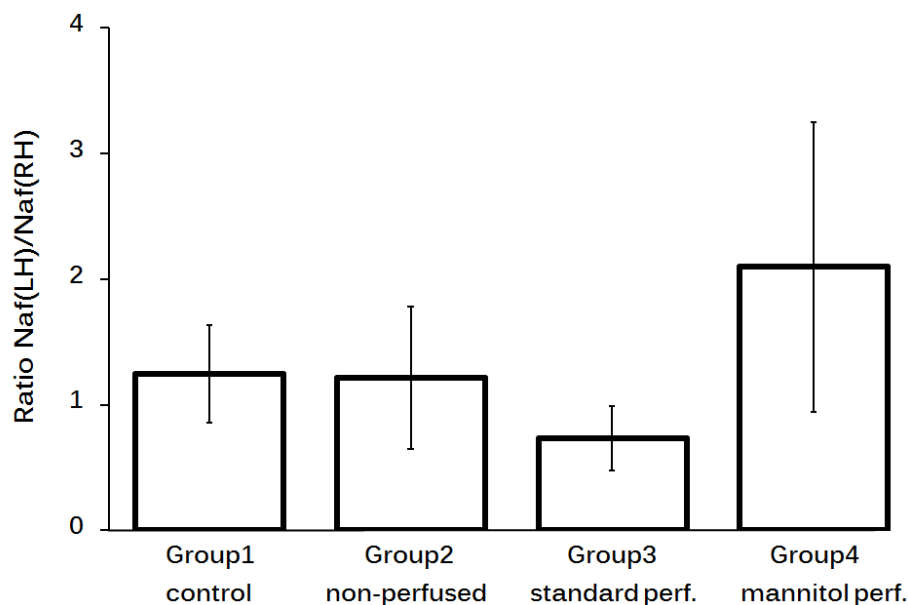


Fig. 18: The ratios of Naf levels in brain biopsies surrounding the probe (left hemisphere, LH) to the corresponding area on the contralateral hemisphere (right hemisphere, RH) for the four groups. Group 1 + 2 received one bolus injection. Group 3 + 4 received one bolus injection and a constant infusion.

3.3 BBB permeability during cOFM monitoring (study 2)

Two significant outliers were identified in group 3 using the Grubbs test ($p \leq 0.001$); these two were excluded from further analysis and replaced with new animals. Naf plasma concentration was stable (at 44 to 112 $\mu\text{g/ml}$) for all subjects over the entire experiment (Fig. 19). Naf concentrations in cOFM samples with standard perfusate (group 3) were about 15 times lower than in cOFM samples with mannitol (group 4). Groups 3 and 4 show significant differences at each investigated time point ($p \leq 0.002$, Fig. 19). The same trends can be seen when plotting the ratio of cOFM to plasma Naf concentration. Group 4 had a significantly higher ratio than group 3 at each investigated time point ($p \leq 0.002$, Fig. 19).

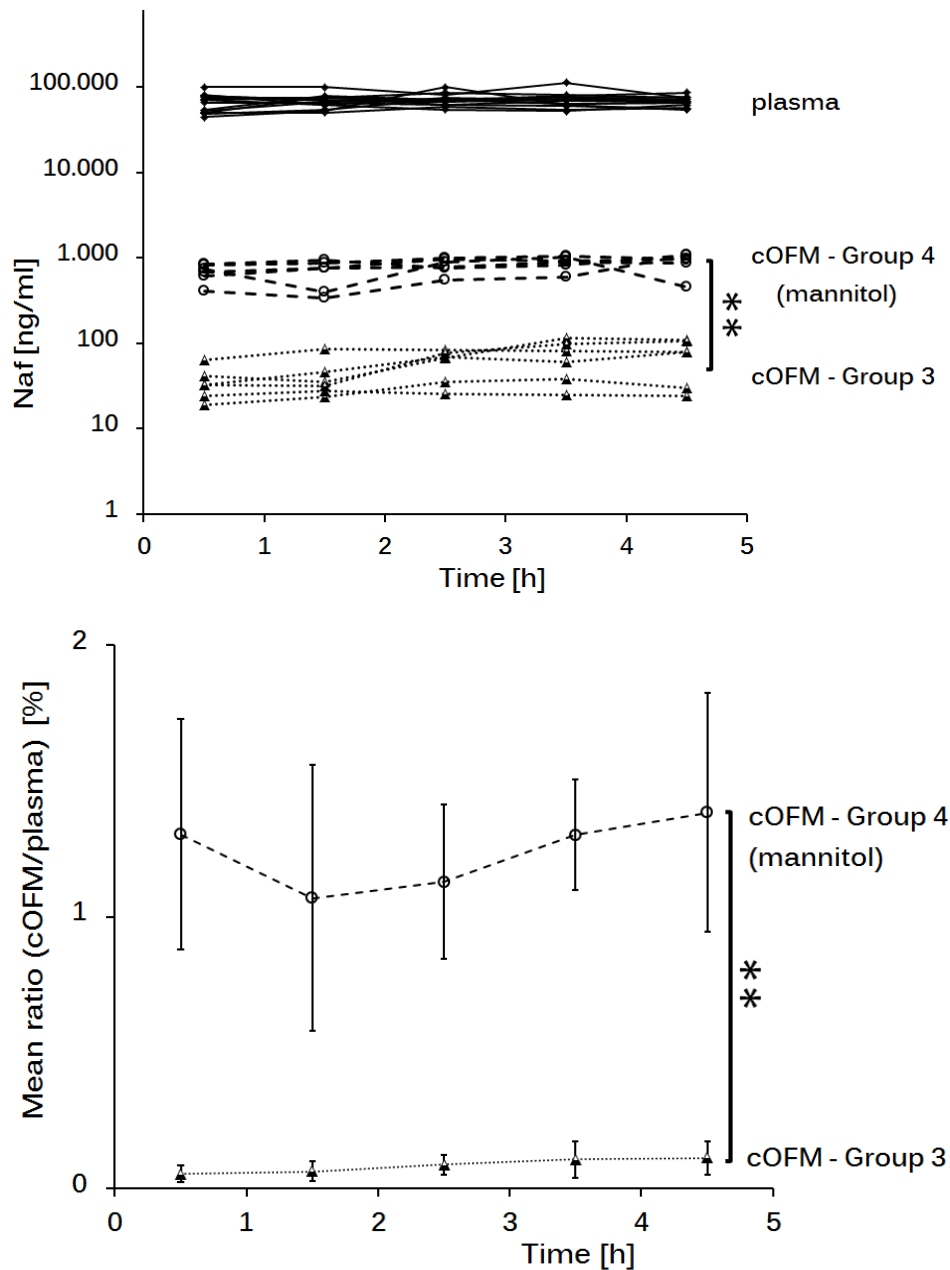


Fig. 19: Concentration of Naf in plasma and cOFM perfusate samples in groups 3 and 4.

4. Discussion

Like all invasive probe techniques, cOFM causes trauma during probe insertion, which leads to local disruption of the BBB surrounding the cOFM probe. In the case of MD, the time needed for local re-establishment of the BBB is still under debate. Earlier MD studies reported intact BBB as early as three hours after probe insertion (Aasmundstad, Mørland, & Paulsen, 1995; Benveniste, Drejer, Schousboe, & Diemer, 1984) but there are also reports of altered BBB permeability up to 24 h following MD probe insertion (Morgan, Singhal, &

Anderson, 1996; Westergren, Nyström, Hamberger, & Johansson, 1995). A later study even reported increased BBB permeability up to 28 days after MD insertion and also described a biphasic elevation of BBB permeability immediately after insertion and two days later, followed by a slow decline in permeability (Groothuis et al., 1998). Marburger et al., 2000 suggested that inflammatory damage related to the MD membrane could play a role in delayed BBB re-establishment. The seemingly contradictory nature of these findings shows that the determination of BBB permeability after probe insertion is complex and depends on diverse factors such as (i) probe size and materials, (ii) the insertion procedure, (iii) inflammatory processes and (iv) possible vasoconstriction due to traumatization. Vasoconstriction suggests an intact BBB within a few hours of insertion supported by the observation of decreased local blood flow and decreased glucose metabolism after insertion (Benveniste, Drejer, Schousboe, & Diemer, 1987). Taking into account the complex characteristics of BBB permeability after cOFM probe insertion, we applied only one constant flow rate of 1 μ l/min and selected the frontal lobe for probe insertion thus minimizing insertion trauma.

We took a stepwise approach to measuring BBB intactness, with two established markers: albumin-bound Evans Blue (EB), which has a total MW of ~66 kDa and does not cross the intact BBB but will stain brain tissue when the BBB is damaged (Manaenko, Chen, Kammer, Zhang, & Tang, 2011), and sodium fluorescein (Naf), a low-molecular-weight marker (376 Da) that crosses the intact BBB to a limited extent. Naf is a sensitive marker even for subtle changes in BBB permeability (Kaya & Ahishali, 2011; Kozler & Pokorný, 2003; Lenzser et al., 2007). We measured Naf in cOFM perfusate, blood and brain tissue samples.

Visible penetration of EB into the brain tissue surrounding the cOFM probe indicates local disruption of the BBB. cOFM insertion trauma was pronounced in the positive control group where EB was injected at the same time as probe insertion. Visible EB staining was restricted to a maximum diameter of 2 mm around the cOFM probe, therefore the region of interest for the image analysis was set to a diameter of 2.5 mm surrounding the probe. In the test group EB staining in brain tissue surrounding the probe decreased with increasing healing time (Fig. 17). Subjects with a healing time of up to 9 days still showed significant differences from the negative control group, suggesting that the BBB was not fully healed. Whereas after healing times of 11 and 15 days, extracted brains showed fluorescence levels similar to brains where no EB had been injected, indicating local re-establishment of the BBB. High standard deviations until day 9 after insertion reflect individual BBB permeability during the healing process. Consistently small standard deviations after day 11 support BBB intactness for EB. To ensure complete local BBB re-establishment around cOFM probes the time span between cOFM probe insertion and the sampling start is set to 15 days for future experiments (Fig. 17).

In order to compare native brain tissue with brain tissue surrounding the cOFM probe, brain tissue biopsies from the left frontal lobe (LH - probe insertion site) and the contralateral right hemisphere (RH - native) of the same rat were compared. The deviation from the expected ratio of 1 which indicates similarity of the two hemispheres may be due to residual intravascular Naf. A residual intravascular fraction is caused by the short transcatheterial perfusion time (2 min) that is required to avoid marker wash-out from brain tissue. Ratios and standard deviations were similar without probe insertion and 15 days after probe insertion, indicating that the BBB surrounding the cOFM probe was intact. The Naf ratio decreased when cOFM sampling was performed, possibly due to local Naf wash-out caused by cOFM sampling. When hyperosmolar mannitol was added to the perfusate, an increase in Naf levels indicated endothelial cell shrinkage and increased permeability in the already healed BBB (Bálint et al., 2007; Brown, Egleton, & Davis, 2004; Wang, Etu, & Joshi, 2007). Results indicate an intact BBB 15 days after cOFM probe insertion but none of the differences between the four groups were statistically significant.

Analysis of Naf concentrations in cOFM samples showed 15 times higher Naf levels with hyperosmolar mannitol than with standard perfusate supporting the local opening of the BBB found in brain biopsies. In contrast to results based on brain biopsies, the differences in Naf levels in cOFM samples were highly significant. cOFM Naf levels plotted against individual Naf plasma concentrations clearly showed that differences between the two groups were not influenced by individual variations in Naf plasma levels (Fig.19).

Differences in Naf concentrations demonstrate the potential of cOFM to detect BBB permeability changes in vivo and to deliver substances (mannitol) directly to brain tissue. Changes in BBB permeability during PK/PD experiments lead to altered substance transport rates across the BBB. Continuous monitoring of BBB permeability by using cOFM in combination with Naf can detect changes in each individual subject at any sampling point. Proximate control of BBB permeability provided by continuous BBB monitoring is of fundamental importance for PK studies in the CNS. The combination of substance sampling with cOFM and parallel monitoring of BBB permeability provides powerful insight into the interaction of a drug with the BBB.

5. *Conclusion*

We have shown that cOFM can be inserted reproducibly into the frontal lobe, and that insertion trauma is healed within 15 days of probe insertion. BBB permeability was monitored by determination of Naf levels in cOFM samples with a steady-state concentration of Naf in

blood. Naf can be used to monitor the state of the BBB for each animal and each sample obtained. The use of Naf can significantly enhance the quality of the results obtained, especially if PK/PD of drug candidates are investigated.

CHAPTER V

Evaluation of tissue reaction as a result of cOFM probe implantation

This study investigated the histological tissue reaction to long-term implanted cerebral open flow microperfusion (cOFM) probes in the frontal lobe of rat brain. Most probe-based cerebral fluid sampling techniques are limited in application time due to the formation of a glial scar that hinders substance exchange between brain tissue and the probe. Glial scar not only functions as a diffusion barrier but also alters metabolism and signaling in extracellular brain fluid. cOFM is a recently developed probe-based technique to continuously sample extracellular brain fluid with an intact blood-brain barrier. After probe implantation, a 2 weeks healing period is needed for blood-brain barrier reestablishment. Therefore, cOFM probes need to stay in place and functional for at least 15 days after implantation to ensure functionality even after a long implantation period. The design of the probe and used materials are optimized to evoke minimal tissue reaction. Qualitative and quantitative histological tissue analysis revealed no continuous glial scar surrounding the cOFM probe during 30 days after implantation and a similar tissue reaction to perfused and non-perfused probes.

1. Introduction

Implantable microelectrodes, biosensors and sampling probes are used to investigate the metabolism and the chemical composition of interstitial fluid in brain tissue. All of these devices critically depend on substance exchange with the surrounding tissue (Wisniewski et al. 2001). Histological studies have reported a glial scar, a tissue reaction that surrounds long-term implanted probes. The compact nature of the scar tissue hampers substance transport and therefore the function of an implanted probe (Polikov et al. 2005). Formation of glial scar and biofouling on probe surfaces and interface membranes are major factors decreasing probe performance over time. Compared to biofouling, the glial scar has a 3-5 times higher impact on a decreased transport of small substances (Winslow & Tresco 2010). The precise mechanisms that influence the extent of tissue response to artificial implants are not completely understood (Turner et al. 1999; Kim et al. 2004; Polikov et al. 2005; Kawano et al. 2012; Wanner et al. 2008). Though all invasive techniques cause implantation stress, perfusion probes like microdialysis and push pull cannulas have additional stress factors caused by the chemical properties of the perfusate or shear forces due to perfusate flow passing brain tissue (Myers 1986; Chefer et al. 2009).

Cerebral open flow microperfusion (cOFM) is a relatively new sampling technique based on OFM to sample large and lipophilic substances in brain interstitial fluid (L Schaupp et al. 1999; Manfred Bodenlenz et al. 2005; Manfred Bodenlenz et al. 2012; Holmgaard et al. 2012). All materials used in the design of cOFM probes are chosen in order to minimize tissue reaction and glial scar formation. Compared to standard microdialysis sampling, cOFM sampling is not based on a membrane and allows direct, unfiltered mixing of perfusate and interstitial brain fluid. Avoiding a membrane also minimizes adhesion of cells and substances to the probe's surface, avoids cell invasion into the membrane, and continuous irritation of surrounding tissue due to a jagged membrane surface (Dahlin et al. 2012; Scopelliti et al. 2010). The functional principle of cOFM is very similar to that of push-pull perfusion which was one of the first techniques developed to sample in brain tissue. Histological studies identified heavy tissue damage caused by the push-pull probe which represents a major drawback for the technology (Myers et al. 1998; Kottegoda et al. 2002).

In the present study we aimed to evaluate the effect of the materials and design used in a long-term implanted cOFM probe in regard to brain tissue reaction. We compared the histology of brain tissue surrounding the cOFM probe with native frontal lobe tissue of the contralateral hemisphere and studied the effects of probe perfusion.

2. Material and Methods

2.1 Animals

All animal protocols used in this study were approved by the Austrian Ministry of Science and Research Ref.II/10b, Vienna. A total of 36 adult male Sprague Dawley rats (Harlan Laboratories, Udine, Italy) with a weight of 300 – 450 g were used in this study. Animals were allowed to acclimatize to the environment for at least one week after transportation before any surgical procedures were carried out. After probe implantation animals were housed individually in acrylic glass cages with a 12:12 h light:dark cycle, and food and water were available ad libitum. Appropriate animal care was provided by the staff at the animal care facility (Institute for Biomedical Research, Medical University of Graz, Austria).

2.2 Implantation of cOFM probe

For cOFM probe implantation, the rats were anesthetized with a combination (2:2:1) of Fentanyl® (0.05 mg/ml; Janssen-Cilag Pharma, Austria), Midazolam® (5 mg/ml; Janssen-Cilag Pharma, Austria) and Domitor® (0.1 mg/ml, Pfizer Corporation, Austria). A dose of 0.015 ml/kg body weight was injected subcutaneously. The head was fixed in a stereotactic frame (KOPF Instruments, USA) and rats were prepared for surgery by shaving the head and disinfecting the skin with 70% ethanol.

A 1 mm hole was drilled into the skull with a spherical dental drill. The dura was not harmed during drilling but punctured afterwards with a fine forceps in order to create a defined opening of the meninges.

The cOFM probes were slowly inserted into the frontal lobe using the stereotactic frame to a final position of 2 mm left from midline, 0 mm anterior to bregma and 1.5 mm below the dura. The probe was fixed to the skull bone using two anchor screws and biocompatible dental cement (iCEM Self Adhesive; Heraeus, Germany). All surgical procedures were completed within 30 min and anesthesia was terminated by subcutaneous injection of the narcosis antagonists Anexate® (0.1 mg/ml; Roche Austria GmbH) and Antisedan® (0.5 mg/ml; Pfizer Corporation, Austria). For two days after surgery a daily dose of antibiotics Claforan® (50 mg/kg, Sanofi-Aventis GmbH, Wien) and a pain treatment (Rimadyl®; 0.1 mg Carprofen; Pfizer, Austria) were administered subcutaneously.

2.3 Sampling

For cOFM sampling the rats were anaesthetized with a minimal dose of Isoflurane® (1%) for 3 hours. Initially the healing dummy was replaced with inflow/outflow tubing and connected to two glass syringes (Hamilton, USA) placed in syringe pumps (Aladdin, World Precision Instruments, Germany). cOFM perfusate was pumped into the probe with a flow rate of 1 µl/min and samples were withdrawn at the same flow rate. Sampling was conducted for 2 hours. For two days following sampling (where applicable) a daily dose of the antibiotic Claforan® (50 mg/kg, Sanofi-Aventis GmbH, Wien) was administered subcutaneously.

The cOFM perfusate was composed to match brain interstitial fluid in order to avoid chemical stress for the brain tissue, modified from (McNay & Sherwin 2004). Perfusate composition: 123 mM NaCl, 0.4 mM MgCl₂ (purity ≥ 98%), 0.7 mM CaCl₂ (purity ≥ 93%), 4.3 mM KCl, 1.3 NaH₂PO₄, 21 mM Na₂HPO₄, 4 mM glucose. All reagents were dissolved in sterile water (Aqua bidest, Fresenius Kabi, Austria). In order to remove possible bacterial contamination the perfusate was filtered through a 0.22 µm sterile filter (Thermo Fisher Scientific, Germany). All steps were carried out under sterile conditions. All reagents were purchased from Sigma Aldrich, Austria (purity ≥ 99%) unless stated otherwise.

2.4 Experimental setup

A total of 36 rats were divided into 3 groups that differed in the duration of cOFM probe implantation: 3 days (n=6), 15 days (n=24) and 30 days (n=6) between cOFM probe implantation and brain extraction. Each of the 3 groups was subdivided evenly in a perfused and a non-perfused group. The perfusion was carried out for two hours at day 1, 11 and 15 following cOFM probe implantation and sacrificed on day 3, day 15 and day 30, respectively in order to characterize and compare the morphological changes between non-perfused and perfused animals. For euthanasia at the histological endpoint every rat was deeply anaesthetized with the double dose as used for surgery. The animals were flushed transcardially with PBS at room temperature for 30 min to remove intravascular blood and avoid bleeding during cOFM probe extraction. Extracted probes were visually checked for adherent tissue. The skull was opened carefully and the brains were fixed in 4% paraformaldehyde. After complete fixation the tissue was embedded in paraffin and sectioned in coronal slices of 4 µm thickness. Slices were made serially throughout the cOFM probe implantation site.

2.5 Immunohistochemistry and staining

Haematoxylin and eosin (H&E) staining was performed in at least 5 sections with a 100 μm distance from each other following a standard protocol. Two adjacent slides were selected for Iba-1 and GFAP staining. Slides for Iba-1 were deparaffinised at 60° C for 30 min and the sections were stained following a standard protocol on a Leica Bond™ Max autostainer (Leica Biosystems, Australia). Antigen retrieval was performed with ER1 for 10 min (solution provided by the manufacturer for epitope retrieval). Iba-1 antibody (Cat. No.: ab 15690, Abcam, Austria) was diluted to 1:2,000 in Bond Primary Antibody (Cat. No.: AR9352, Leica, UK) and detected with Bond™ Polymer Refine Detection (Cat. No.: DS9800, Leica, UK). For GFAP staining, slides were incubated at 70° C for 1 h and sections were stained following a standard technique on a Ventana Benchmark ULTRA autostainer (Ventana Medical Systems, USA). Antigen retrieval was performed with CC1 for 30 min (solution provided by the manufacturer for epitope retrieval). GFAP antibody (Cat. No.: 258R-24, Cell Marque, USA) was diluted to 1:500 and visualized with ultraView Universal DAB Detection Kit (Cat. No.: 760-500, Ventana Medical Systems, USA).

2.6 Histological analysis

Brain sections stained with H&E were examined under the optical microscope in order to localize the probe implantation site. Quantitative analysis of Iba-1 and GFAP positive cells was performed in the 15 days group. Tissue surrounding the probe was divided into areas with different distances to the probe tip (0 – 140 μm , 140 – 350 μm , 350 – 700 μm) using a light microscope (Axiocam, Nikon) at magnification 200x using an optical grid (Fig. 20). A comparable area on the contralateral hemisphere in the same section was analysed in the same way as the internal control. Two independent observers selected representative grid squares in the three areas and counted Iba-1 and GFAP positive cells and calculated the mean value in cells/mm². Quantitative analysis was performed blinded by two independent, qualified persons. Qualitative assessment was carried out in all groups.

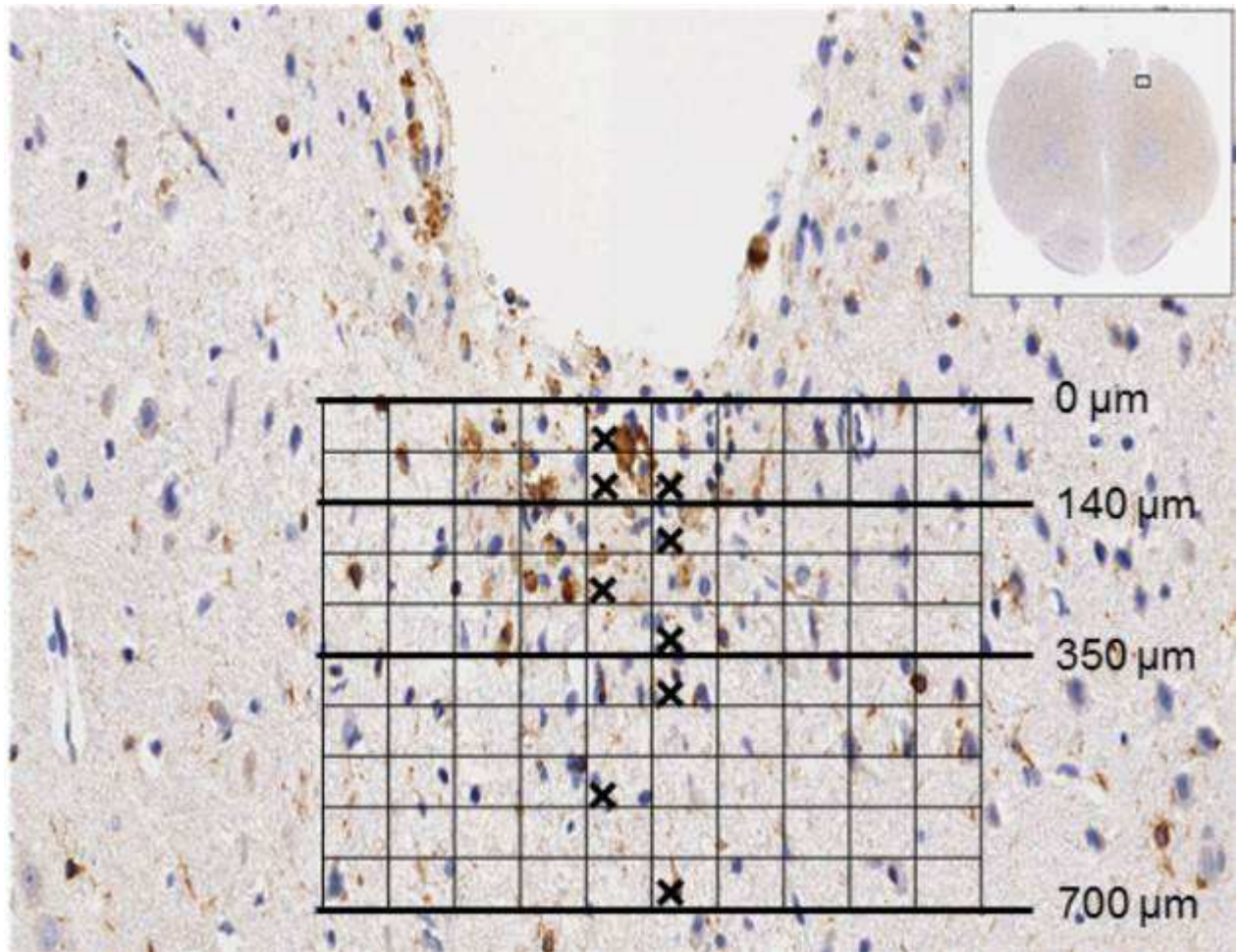


Fig. 20: Schematic representation of quantification pattern. Each square has a size of $4,900 \mu\text{m}^2$; 200x magnification. Marked squares indicate the areas selected for cell count.

2.7 Statistical analysis

Statistical analyses of the quantitative results of Iba-1 and GFAP staining were treated in the same way and performed with R 2.13.1

The Friedman-Test for repeated measurement was performed for testing the differences between the numbers of counted cells in four related groups (three different regions around the probe tip and the control region), this was done separately for perfused and non-perfused rats; The significance level was set to 5%.

Post hoc testing was done using the two samples paired Wilcoxon Rank Sum Test to determine statistical differences between the numbers of counted cells in two paired groups (regions in the same animal). The initial level of significance (5%) was adjusted by the Bonferroni correction for the multiple comparisons between different brain regions.

3. Results

For histological examination the cOFM probes were removed and visual examination showed no adhering tissue on the probe surface. Tissue removed together with the probe would lead to underestimation of glial scar in the remaining tissue section.

3.1 H&E

Microscopic analysis of H&E stained samples **3 days** after implantation showed residual erythrocytes at the tip of the probe indicating bleeding after probe implantation in both groups but less pronounced in the perfused group. Edema formation with minor tissue debris below the probe tip in implantation direction was detected in close vicinity (Fig. 21). At **day 15** after probe implantation residual blood and tissue debris dissolved completely, minimal edema was detected. In the close vicinity of the probe changes in neuron morphology (decreased volume of soma), especially in neurons with direct contact were observed, neurons in a distance of more than 140 μm showed no signs of changes in morphology (Fig. 22). At **day 30** after probe implantation edema, residual blood and tissue debris was completely regressed, hemosiderophages were detected occasionally.

None on the sections showed pronounced glial scar or tissue reaction in response to the probe that could form a diffusion barrier (Fig. 27). No considerable differences between perfused and non-perfused group was found.

3.2 GFAP

GFAP stains astroglia, the cell type mainly responsible for glial scar formation and probe encapsulation. At **day 3** after cOFM probe implantation GFAP immunoreactivity was slightly elevated in both groups being more pronounced in the perfused group (Fig. 25 B, D). At **day 15** after probe implantation quantitative analysis in different areas surrounding the probe and native tissue from a comparable region on the contralateral side as control was performed (Fig. 22 C, F, I, L). The quantitative analysis revealed no significant difference between the regions surrounding the probe and the control region. Perfused and non-perfused groups showed no significant difference (Fig. 23, Table 5). At **day 30** after probe implantation only a minor astrocytic reaction was observed in both groups surrounding the cOFM probe (Fig. 26 B, D). In none of the animals a continuous astroglial scar was formed surrounding the cOFM probe that could create a diffusion barrier.

3.3 Iba-1

Iba-1 stains microglia that is activated after CNS injury, microglia the second most important cell type involved in glial scar formation. At **day 3** after cOFM probe implantation microglia activation was detected in direct vicinity of the probe surface, slightly more pronounced in perfused animals (Fig. 25 B, D). At **day 15** after probe implantation the quantitative analysis shows only in close proximity (0 – 140 μm) of the probe tip a significantly higher number of Iba-1 positive cells: 374 ± 60 ($p \leq 0.05$) in non-perfused and 419 ± 66 ($p \leq 0.01$) in perfused brains, p-values are calculated comparing to the control region on the contralateral hemisphere; non-perfused control (164 ± 54) and perfused control (158 ± 61) (Fig. 22 B, E, H, K). Regions further away (140 – 350 μm) and (350 – 700 μm) from the probe tip showed no significant difference. Perfused and non-perfused group showed no difference (Fig. 24, Table 6). At **day 30** after probe implantation only a minor Iba-1 immunoreactivity was observed at the implantation site (Fig. 26 A, C).

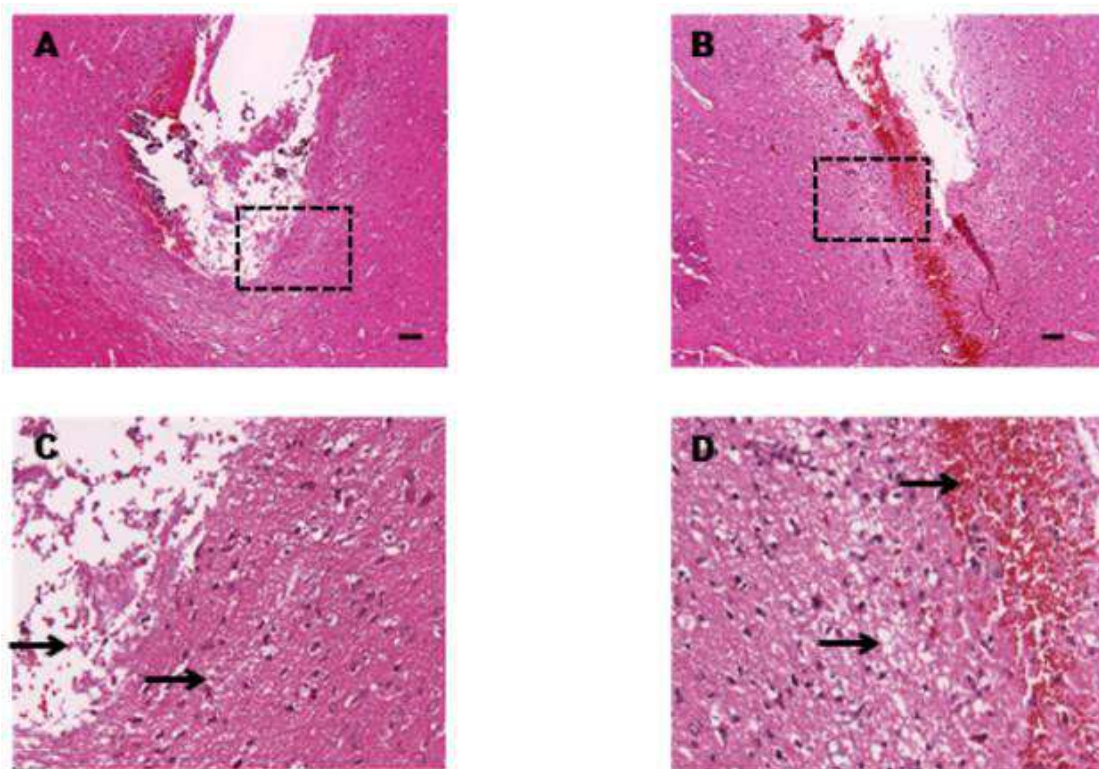


Fig. 21: Representative H&E images of non-perfused (A, C) and perfused (B, D) rat brain 3 days after cOFM probe implantation. Rectangles with broken line in A and B (50x) are shown at higher magnification (200x) in C and D. Arrows in C and D show edema and erythrocytes respectively. Scale bar = 100 μm .

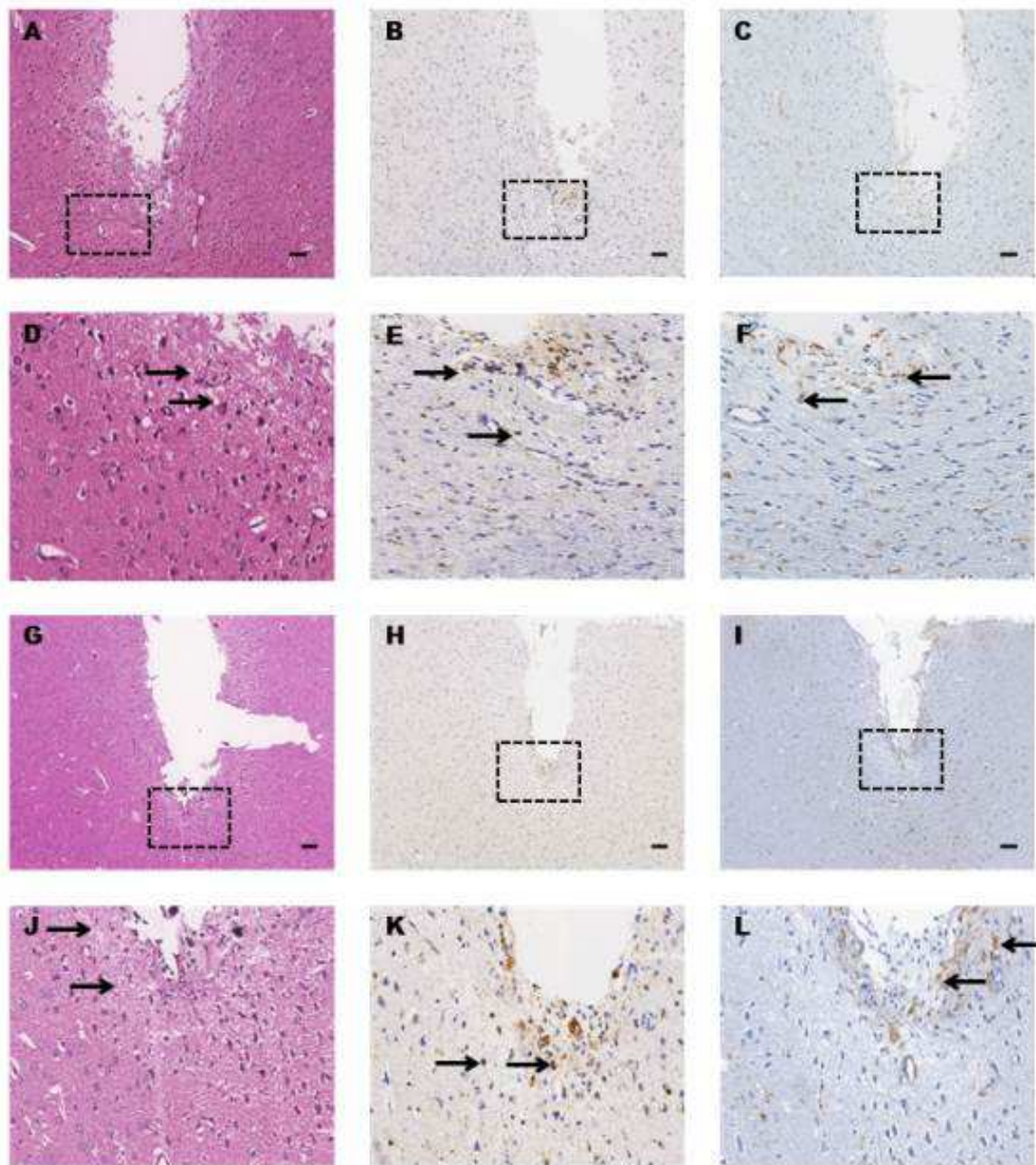


Fig. 22: Microscopy of the cOFM probe implantation site in prefrontal cortex after 15 days. Representative images of non-perfused (A-F) and perfused (G-L) rat brains. Adjacent brain slides were stained with H&E (A, D, G, J), Iba-1 for microglia (B, E, H, K) and GFAP for astrocytes (C, F, I, L). Rectangles with broken line in A-C and G-I (50x) are shown at higher magnification (200x) in D-F and J-L respectively. At this stage only a minimal residual edema is detectable at H&E staining in both non-perfused and perfused animals. Only a minor microglia (E, K) and astrocyte (F, L) reaction directly adjacent to the cOFM probe implantation site is visible. Scale bar = 100 μ m.

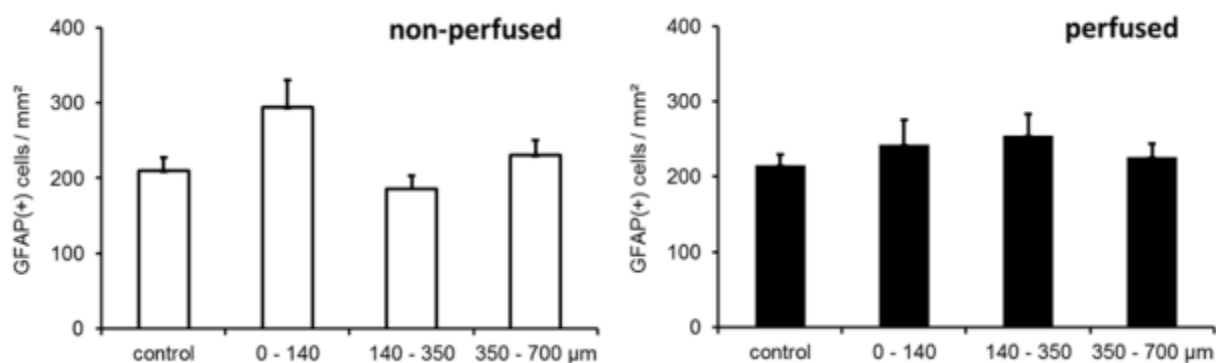


Fig. 23:Quantification of GFAP the positive cells 15 days after cOFM probe implantation at different distances from probe tip and in the corresponding region on the contralateral hemisphere (control).

Table 5: Quantification of GFAP positive cells 15 days following cOFM probe implantation. (p values were calculated comparing GFAP positive cell count at each distance from cOFM probe tip with contralateral control area).

Area	Non-perfused cells / mm ²		Perfused cells / mm ²	
	mean ± SEM	p value	mean ± SEM	p value
control	209 ± 18	-	215 ± 14	-
0 - 140 μm	294 ± 36	0.067	243 ± 33	0.687
140 - 350 μm	186 ± 17	0.140	254 ± 29	0.236
350 - 700 μm	230 ± 20	0.553	226 ± 17	0.774

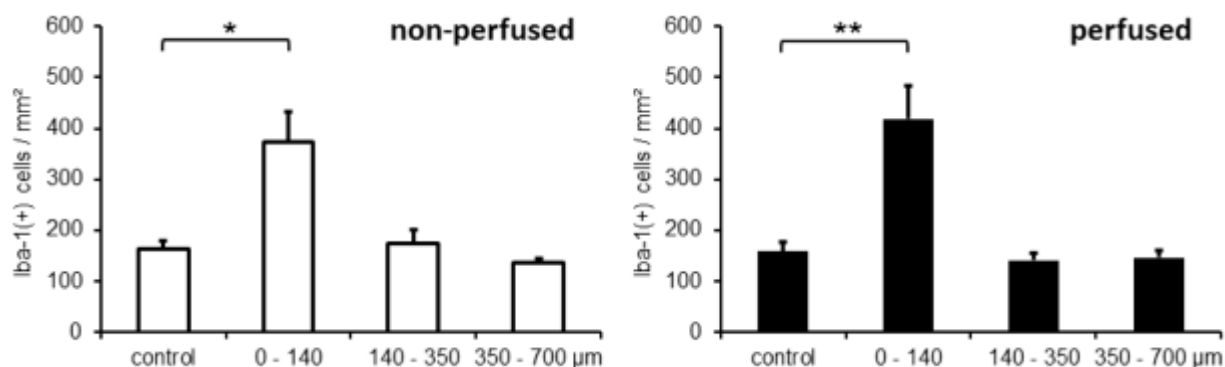


Fig. 24: Quantification of Iba-1 positive cells 15 days after cOFM probe implantation at different distances from probe tip and in the corresponding region on the contralateral hemisphere (control).

Table 6: Quantification of Iba-1 positive cells after 15 days following cOFM probe implantation (p values were calculated comparing Iba-1 positive cell count at each distance from cOFM probe tip with contralateral control area)

Area	Non-perfused cells / mm ²		Perfused cells / mm ²	
	mean ± SEM	p value	mean ± SEM	p value
control	164 ± 16	-	158 ± 18	-
0 - 140 µm	374 ± 60	0.019	419 ± 66	0.006
140 - 350 µm	175 ± 27	0.837	141 ± 13	0.390
350 - 700 µm	135 ± 8	0.121	147 ± 14	0.457

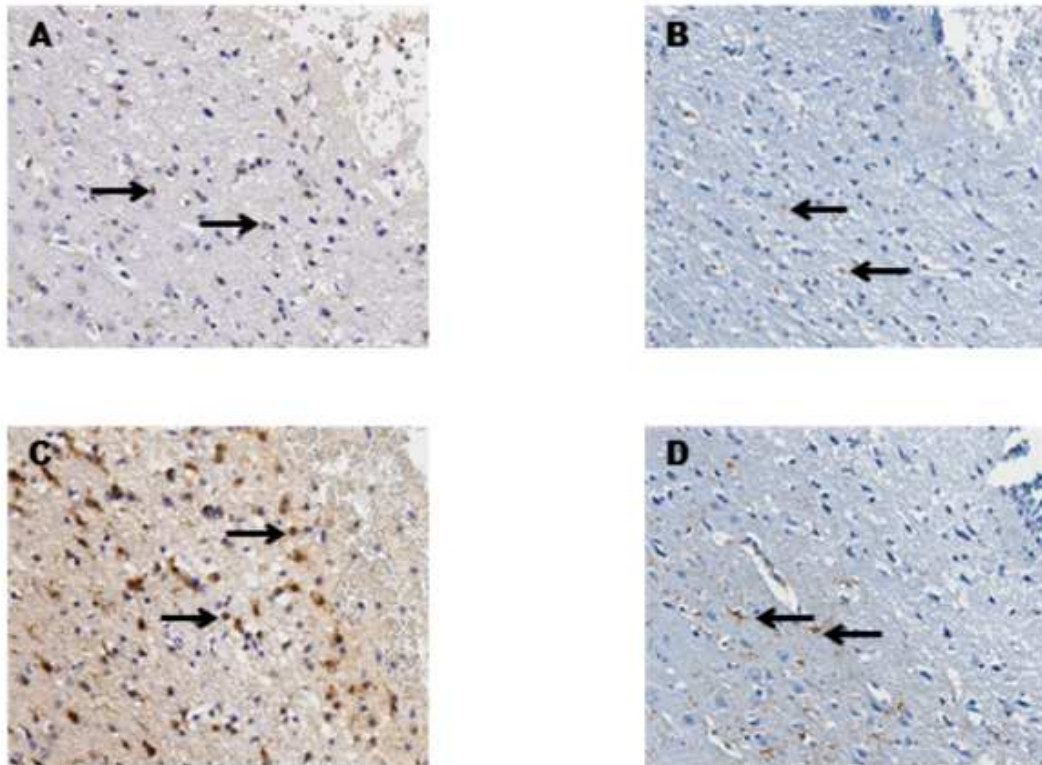


Fig. 25:Microscopy of Iba-1 (A, C) and GFAP immunoreactivity (B, D) 3 days after cOFM probe implantation (200x). Representative images of non-perfused (A, B) and perfused (C, D) rat brains. Arrows in A and C show Iba-1 positive microglia. GFAP positive astrocytes are marked with arrows in B and D.

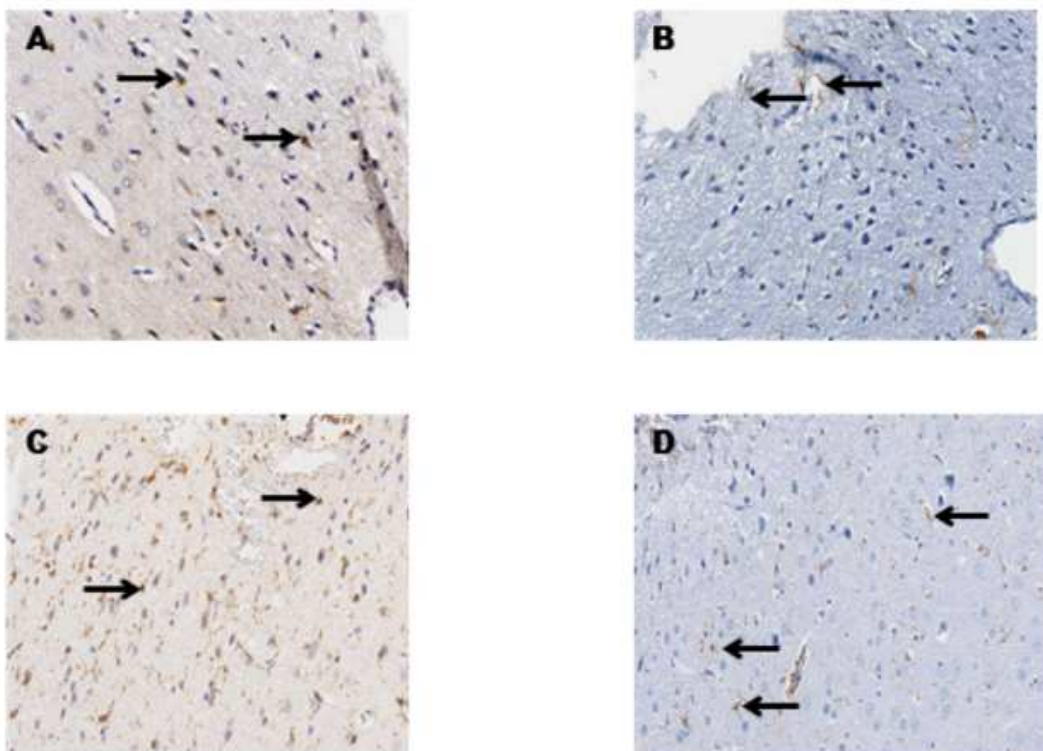


Fig. 26:Microscopy of Iba-1 (A, C) and GFAP immunoreactivity (B, D) 30 days after cOFM probe implantation (200x). Representative images of non-perfused (A, B) and perfused (C, D) rat brains. Arrows in A and B show Iba-1 positive microglia. GFAP positive astrocytes are marked with arrows in C and D.

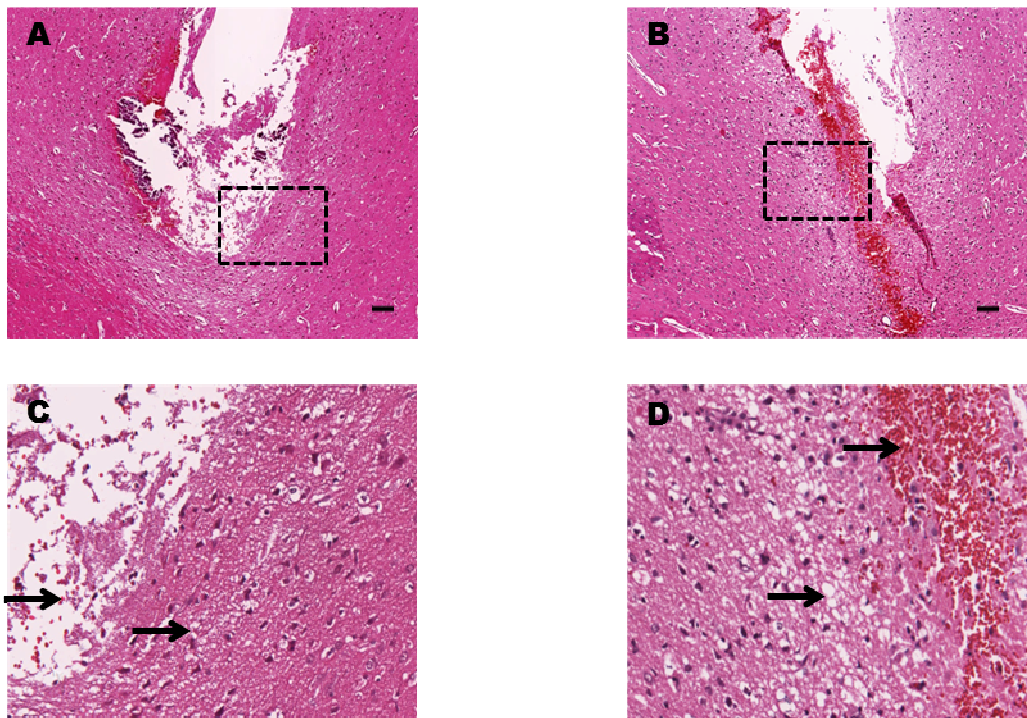


Fig. 27: Microscopy of cOFM probe implantation site 30 days after cOFM probe implantation. Representative images of non-perfused (A) and perfused (B) brains. Scale bar = 100 μ m.

4. Discussion

In this study we assessed the histopathological effects of long-term implanted cOFM probes in the frontal lobe with a special focus on the formation of a glial scar forming a diffusion barrier surrounding the cOFM probe. As a secondary aim we determined tissue reaction following probe perfusion with a physiological fluid, the cOFM perfusate. Results on tissue reaction due to probe perfusion provide information whether repeated perfusion is possible and therefore an extended experimental setup without significant alteration is feasible. Glial scar formation encapsulating the probe after cOFM probe implantation affects substance exchange between brain tissue and the implanted probe and would therefore strongly limit cOFM sampling. In a previous study we have found that BBB function is reestablished 15 days after cOFM probe implantation. The current study was thus specifically designed to assess quantitative tissue changes on day 15 after probe implantation focused on the exchange area at the tip of the cOFM probe. The main components of the glial scar are astrocytes and microglia and therefore the focus of our investigation (Azemi, Lagenaur, & Cui, 2011). The quantitative analysis of Iba-1 (microglia) staining on day 15 after cOFM probe implantation revealed only a moderate increase in microglial reaction in the immediate vicinity of the probe tip ($< 140 \mu$ m). In regions farther away from the probe no changes in microglial activation were observed. Also, GFAP (astrocytes) staining showed no significant

astrocytic reaction along the implantation track at 3, 15 and 30 days. Comparable microdialysis studies have observed a high degree of cell loss, nerve fiber damage, and elevated numbers of astrocytes and microglia up to 300 μm from the probe implantation tracks after 3-14 days (Borland, Shi, Yang, & Michael, 2005; Clapp-Lilly et al., 1999; Hascup et al., 2009). After a longer implantation time of 30 - 60 days microdialysis probes induced the formation of a 2 mm wide glial scar (Benveniste & Diemer, 1987; E. C. de Lange, Danhof, Zurcher, de Boer, & Breimer, 1995). Compared to the microdialysis probes, cOFM probes caused only minor tissue reactions and no continuous glial scarring or encapsulation at any time (Fig. 28). The formation of a continuous glial scar impairs the function of the probe because it acts as a diffusion barrier between brain tissue and the probe and therefore hampers substance exchange. Methodological investigations showed that the encapsulation of an implanted probe led to decreased sensitivity and an underestimation of the extracellular substance concentrations particularly for larger molecules (Bungay, Newton-Vinson, Isele, Garris, & Justice, 2003). The absence of a glial scar after cOFM probe implantation allows unhindered diffusion and emphasizes the potential of cOFM for long-term sampling of a wide range of molecular weights under physiological conditions in brain tissue.

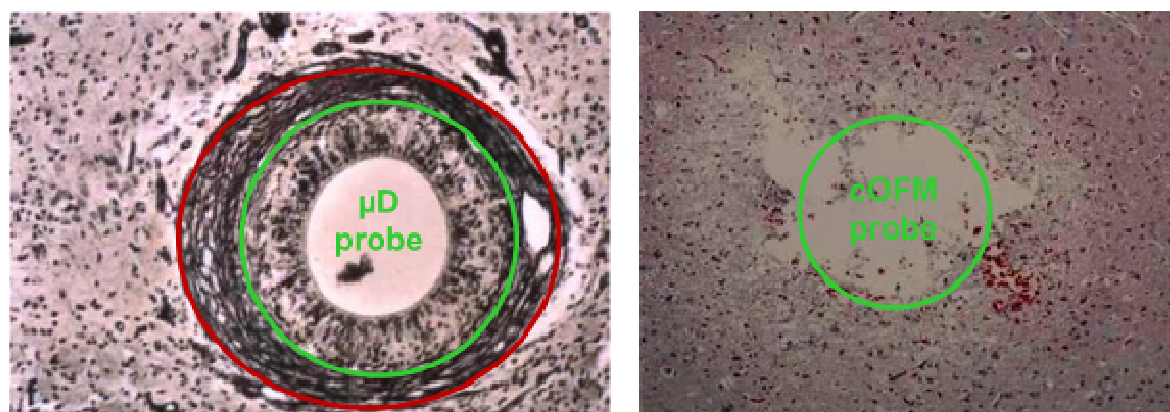


Fig. 28: Formation of a glial scar surrounding a microdialysis probe (left) and surrounding the cOFM probe (right). The green circle indicates the outer surface of the probes and the red line indicates the extent of glial scar formation. (left picture adapted from (Benveniste & Diemer, 1987))

Such minor tissue reactions are probably the consequence of cOFM design and materials used for the probe. All materials which are in direct contact with brain tissue were chosen with the intention to minimize tissue reaction.

The **cOFM guide cannula** is made of FEP (fluorinated ethylene propylene), which is very flexible and has a slick and biologically inert surface. The flexibility of the cOFM guide cannula reduces mechanical stress caused by micro-motions of the brain floating in cerebrospinal fluid while the probe is fixed to the skull (Seymour & Kipke, 2007). Brain tissue reactions are considerably increased when rigid implants are anchored to the skull compared to the same probe implanted intraparenchymally without fixation to the skull (Kim, Hitchcock, Bridge, & Tresco, 2004). Increasing flexibility of an implanted probe decreases thickness of

the glial scar and improves neuronal viability in the close vicinity of the implant (Harris et al., 2011). The slick surface of the cOFM guide cannula avoids adhesion of immunoreactive cells and proteins that access the brain when blood vessels are ruptured and meninges are penetrated during implantation (Abnet, Fawcett, & Dunnett, 1991; Maxwell, Follows, Ashhurst, & Berry, 1990). Cell adhesion to rough surfaces or even cell migration into porous structures such as microdialysis membranes (Fitch, Doller, Combs, Landreth, & Silver, 1999; von Grote, Venkatakrishnan, Duo, & Stenken, 2011) were therefore avoided in the cOFM design. The **cOFM healing dummy**, a thin steel rod, provides mechanical stability during the implantation process. The open space between guide cannula and healing dummy is needed to facilitate easy removal of the healing dummy which allows the guide cannula to follow the brains' micro-motions. The tip of the healing dummy is rounded and polished in order to provide a biologically inert surface similar to the guide cannula. The **cOFM perfusate** is adapted to the actual cerebral interstitial fluid in terms of ion content and pH value in order to avoid chemical stress for the brain. The perfusate flow rate was set to 1 $\mu\text{l}/\text{min}$ in order to minimize mechanical shear stress to the tissue. The placement of inflow and outflow tubing warms up the perfusate before it reaches the brain tissue and thus avoids temperature stress (E. C. M. Lange, Danhof, Boer, & Breimer, 1997). The perfusion of the cOFM probe had no significant effect on the astrocytic or microglial reaction, with only a slightly higher cell count in the area up to 140 μm around the probe in the non-perfused group.

Glial scar formation surrounding the probe is the main limiting factor for long-term implanted sampling systems (Grabb, Sciotti, Gidday, Cohen, & van Wylen, 1998; Thelin et al., 2011). We found that the implantation a cOFM probe did not cause any major tissue reaction like the formation of a continuous glial scar encapsulation during the observed period of 30 days. Glial scar formation was not affected by perfusion of the cOFM probe with optimized perfusate.

5. *Conclusion*

Previous studies (see chapter IV) revealed that it takes 15 days for full BBB reestablishment after cOFM implantation. In this study we show that up to 30 days after cOFM implantation no formation of a glial scar is detected that could cause encapsulation of the probe and hamper diffusion between healthy brain tissue and the cOFM probe. Perfusion of the probes had no effect on the tissue surrounding the implantation track so that repeated sampling is feasible.

CHAPTER VI

Application of cOFM in a pharmaceutical study: Enhanced delivery of doxorubicin to the brain by formulation in targeted nanocarriers

The neuroprotective blood-brain barrier (BBB) keeps many drug candidates below therapeutic levels in the CNS. A targeted nanocarrier formulation, glutathione pegylated liposomal doxorubicin (2B3-101) has been developed by to-BBB to safely enhance the delivery of doxorubicin to brain tumors. However, the drug concentration in the extracellular brain fluid cannot be measured reliably using conventional techniques. OFM is able to sample a wide range of substances including high molecular weight and lipophilic drugs.

In this trial, 12 rats received an intravenous administration of either 2B3-101 or the non-targeted pegylated liposomal doxorubicin (generic Caelyx), both at a dose of 7 mg/kg. Doxorubicin concentrations in rat brains were measured for 5 hours using cOFM. A steady-state infusion of sodium fluorescein (Naf) was used as BBB integrity marker. Two animals were excluded from analysis because of an impaired BBB intactness, one in each treatment group.

Average Naf concentrations in the brain were equal after administration of either 2B3-101 or generic Caelyx. The brain doxorubicin concentration in the brain was 4.8-fold higher after administration of 2B3-101 compared to generic Caelyx ($p=0.0016$).

In conclusion, cOFM can be used to determine concentrations of lipophilic doxorubicin in the brain. The administration of 2B3-101, a novel brain-targeted chemotherapeutic, resulted in increased brain doxorubicin concentrations. This adds to the proof-of-concept of 2B3-101 for improved treatment of brain cancer.

1. Introduction

Various strategies are being developed to enhance drug delivery to the brain, including targeting of endogenous transporters at the BBB, such as the transferrin receptor, the insulin receptor, the low-density lipoprotein receptor-related protein (LRP), and more recently the glutathione transporter (Lindqvist, Rip, Gaillard, Björkman, & Hammarlund-Udenaes, 2013). Glutathione-pegylated liposomes (G-Technology®) have been developed by the company to-BBB and used as a brain drug-delivery platform for the development of several treatments; the most advanced is 2B3-101, glutathione pegylated (GSH-PEG) liposomal doxorubicin, for the treatment of patients with brain cancer. Proof-of-concept studies with 2B3-101 showed its efficacy against experimental brain tumors. Furthermore, 2B3-101 is currently being investigated in a phase I/IIa clinical study in patients with solid tumors and brain metastases or recurrent malignant glioma (clinicaltrials.gov NCT01386580).

Due to the lipophilic and sticky properties of doxorubicin, it has not been possible to estimate brain extracellular doxorubicin concentrations using the classical semi-permeable membrane-based method of microdialysis to elucidate the extent and/or mechanism of transport across the BBB. In previous experiments, brain uptake was determined using homogenates; however, despite transcardial flushing to eliminate the intravascular drug fraction, it was not possible to obtain an accurate and reliable value for the level of brain uptake of the free drug (Gaillard, Visser, Appeldoorn, & Rip, 2012).

Cerebral open flow microperfusion (cOFM) is designed to monitor the concentration of any drug in brain, including high molecular weight and lipophilic drugs, without affecting the integrity of the blood-brain barrier (BBB). Therefore, cOFM can be used to determine whether lipophilic drugs cross the BBB and their retention time; i.e., their effective concentration. Open flow microperfusion (OFM) was initially developed to determine substance concentrations in the interstitial fluids of adipose (aOFM) and dermal (dOFM) tissue, and is now being used in clinical settings (M Bodenlenz et al., 2013; Manfred Bodenlenz et al., 2005, 2012; Holmgaard et al., 2012). More recently, a new form of OFM has been devised for the purpose of measuring brain uptake. The cOFM technology uses implantable probes similar to those used with microdialysis, yet with the crucial difference that the cOFM probe is membrane free, thereby avoiding problems such as adsorption of lipophilic substances or sampling being limited to substances below a particular molecular weight. In addition, glial scar formation around the probe is a problem associated with the use of many intra-cerebral probes. The scar tissue's dense nature hampers substance transport and therefore the function of the implanted probe. The cOFM probe design and the probe materials used allow long-term implantation (>30 days) without formation of glial scar encapsulation (chapter 5).

This study aims to compare the concentration of doxorubicin in brain after the i.v. application of 2B3-101 or Caelyx®, the generic version of the product Doxil®. Caelyx is a similar, non-targeted pegylated liposomal formulation. cOFM was used to measure doxorubicin in brain interstitial fluid and Naf was used as a marker for BBB intactness during sampling.

2. Material and Methods

2.1 Animals

All animal protocols used in this study were approved by the Austrian Ministry for Science and Research Ref.II/10b, Vienna. Male Sprague-Dawley rats with a body weight of 300 – 400 g were obtained from Harlan Laboratories (Udine, Italy). Animals were housed in acrylic glass cages with a 12:12 hour light:dark cycle, and food and water available ad libitum. Animals were allowed to acclimatize to the environment for at least one week before surgical procedures were carried out. Appropriate animal care was provided by the staff at the animal care facility (Institute for Biomedical Research, Medical University of Graz, Austria).

2.2 Experimental set-up

Rats were anesthetized with injectable narcosis (1.5 ml/kg; consisting of a mix of Fentanyl (1 ml; 0.05 mg/ml, Janssen-Cilag Pharma, Austria), Midazolam (1 ml; 5 mg/ml, Janssen-Cilag Pharma, Austria) and Domitor (0.5 ml; 0.1 mg/ml, Pfizer, Austria)). The head was fixed in a stereotactic frame (KOPF Instruments, USA) and rats were prepared for surgery by shaving the head and disinfecting the skin with 70% ethanol. A 15 mm incision was made to expose the skull. The cOFM probe containing a stainless steel healing dummy was slowly inserted 1.5 mm deep into the left frontal lobe via a 1 mm hole drilled into the skull 2 mm lateral to the bregma. The probe was fixed to the skull bone using two anchor screws and biocompatible dental cement (iCEM Self Adhesive; Heraeus, Germany). For three days following surgery a daily dose of 0.7 ml antibiotics (Cefotaxim® 25 mg; Sandoz, Austria, dissolved in saline) and 1 ml pain treatment (Rimadyl®; 0.1 mg Carprofen; Pfizer, Austria, diluted in saline 1:50) was administered subcutaneously. After cOFM probe implantation, animals were housed individually with a 12:12 h light:dark cycle, and food and water available ad libitum.

Based on data obtained by previous extensive model characterization with respect to BBB recovery after surgical implantation of the cOFM probe, the drug-transport experiment was carried out 15 days after implantation of the cOFM probe (chapter IV). Two hours before administration of treatments the healing dummy was exchanged for inflow/outflow tubing.

The outflow tubing is connected to a Hamilton syringe, and the inflow tubing to a 1 ml standard syringe (BBraun, Austria). Both are operated with a syringe pump (Aladdin, World Precision Instruments, Germany) at a flow rate of 1 μ l/min. One hour before administration of treatments, the cOFM perfusion was started. cOFM perfusate contained NaCl (123 mM), MgCl₂ (0.4 mM), CaCl₂ (0.7 mM), KCl (4.3 mM), NaH₂PO₄ (1.3 mM) Na₂HPO₄ (21 mM), and glucose (4 mM).

Before exchanging the healing dummy, a Tygon (Saint-Gobain, France) catheter was inserted into the femoral vein to administer sodium fluorescein (Naf) and the blinded doxorubicin formulation, another catheter was introduced into the contralateral artery for blood sampling. Blood samples had a volume of 300 μ l. Samples were immediately replaced by saline injection (0.9 M, Fresenius Kabi, Austria), which also prevented blood coagulation in the catheters.

All animals received Naf (Sigma Aldrich, Vienna, Austria) as a marker for BBB integrity. After starting cOFM perfusion (1 h before treatment start), Naf was administered intravenously as a bolus injection (11 mg/kg), followed by a continuous infusion of 11 mg/kg/hour during the experiment. Anesthesia during sampling was carried out according to description in chapter IV and V.

2.3 Treatment

Glutathione pegylated liposomal doxorubicin (2B3-101) was manufactured by TTY Biopharm (Taipei, Taiwan, R.O.C) according to good manufacturing practices (GMP), based on protocols developed by to-BBB technologies BV. The production of 2B3-101 was performed according to the manufacturing process of Caelyx (TTY Biopharm) in order to allow good comparability in terms of size of the liposomes and amount of doxorubicin payload. As a non-targeted comparator, the generic Caelyx product was obtained from TTY Biopharm. Researchers at Joanneum Research received these products labeled as A and B, which were blinded until the analysis was completed. Both 2B3-101 (n=4 animals) and generic Caelyx (n=8 animals) were administered as intravenous bolus injections (1.5 ml/min) at a dose of 7 mg/kg. This dose was based on the maximum tolerated dose for repeated administrations in rats as determined in the regulated preclinical studies of the product before it had been allowed to enter the clinical trial. The amount of animals per group was a result of problems due to exceeded storage time of one batch of 2B3-101, animals that received this batch died immediately after injection and were excluded from analysis.

Plasma samples were taken at 30, 90, 150, 210 and 270 min. Blood samples were heparinized (Na-Heparin) and fractionated by centrifugation (1,000 g, 10 min, RT). The

plasma fraction was separated and frozen at -80°C . cOFM samples were collected hourly (approximately 60 μl per sample) and immediately stored at -20°C until further analysis.

2.4 Analysis

All analytical methods were conducted in the bioanalytical facility of Joanneum Research by trained and experienced personnel.

Sodium fluorescein (Naf) concentration in cOFM and plasma samples was determined by fluorescence detection using a microplate reader (excitation/emission: 485/520 nm). Samples and calibration standard respectively (0 – 10 $\mu\text{g/ml}$ Naf in either cOFM or plasma) were diluted 1:1 with acetonitrile (ACN), vortexed and centrifuged (5 min, 2,000 g, RT). 35 μl of the supernatant were transferred into a 384-well plate for analysis.

Doxorubicin in cOFM and plasma samples was determined by HPLC-MS. The samples were chromatographed on a Zorbax SB C18 Agilent LC column (3.5 μm , 35 x 0.5 mm). The mass spectrometer with ESI interface probe was operated in positive-ion mode. Since potentially free doxorubicin as well as intact liposomes with doxorubicin as payload were sampled in cOFM and plasma samples. In order to create comparable conditions in terms of matrix effects 2B3-101 was used to prepare the calibration curve (0-100 ng/ml doxorubicin). Samples were mixed with acidic isopropanol, internal standard (daunorubicin 40 ng/ml in 30% ACN), and water before centrifugation (15 min, 4 $^{\circ}\text{C}$, 21,000 g). The supernatant (7.5 μl) was transferred to the HPLC-MS system.

2.5 Sodium fluorescein (Naf) as BBB integrity marker

Naf was used as a marker for intactness of the BBB, as described previously (chapter IV). Briefly, during a 5-h Naf infusion a stable plasma concentration was achieved. The ratio of the area under the curve (AUC) of the Naf concentration in cOFM samples and the Naf concentration in plasma samples was determined in 6 control rats and in 6 rats in which the BBB was opened by mannitol perfusion through the cOFM probe (Fig. 19 chapter IV). This study indicates that the ratio in rats with an intact BBB was 0.09 ± 0.04 (mean % \pm SD). In contrast, rats that were subjected to mannitol-induced BBB disruption presented a ratio of 1.1 ± 0.2 (mean % \pm SD). Therefore, in the current study animals with a ratio of >0.5 % (indicative of an impaired BBB functionality) were excluded from further analysis based on results in chapter IV and additional preliminary studies (data not shown).

3. RESULTS

Healthy rats with an implanted cOFM probe received an intravenous bolus injection of 2B3-101 (n=4) or non-targeted pegylated liposomal doxorubicin generic - Caelyx (n=8). Two animals were excluded from the data analysis: 1 animal in the 2B3-101 group was shown to have an impaired BBB function (a ratio of >0.5 % of Naf in the cOFM sample versus plasma) and cOFM samples showed visible fractions of blood; while 1 animal in the generic Caelyx group was excluded due to blood loss caused by leaky arterial catheterization. The ratio of the AUC of the Naf concentration in cOFM and the Naf concentration in plasma for animals receiving the generic Caelyx was 0.10 ± 0.06 (mean % \pm SD, n=7). This ratio was 0.22 ± 0.18 (mean % \pm SD, n=3; p=0.13 vs generic Caelyx, unpaired t-test) for animals receiving 2B3-101. There was no statistically significant difference between the Naf permeability across the BBB after the generic Caelyx and 2B3-101 administrations. In both treatment groups, the plasma concentrations of Naf showed accumulation over time, while brain concentrations remained the same.

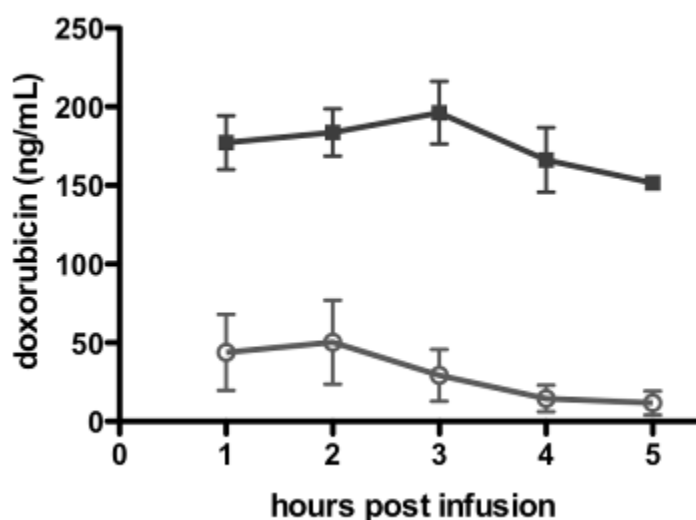


Fig. 29: Concentration-time profile of doxorubicin in cOFM after administration of 2B3-101 (closed squares) or generic Caelyx (open circles). The concentrations are plotted at the end of a 1-hour sampling period.

The mean doxorubicin concentrations in the cOFM samples showed that 2B3-101 was present in significantly higher concentrations (5.8 fold) than generic Caelyx (Fig. 29), based on AUC of the cOFM concentrations. Doxorubicin concentrations in plasma were significantly higher (1.3 fold, based on plasma AUC) after 2B3-101 administration compared to administration of generic Caelyx. Therefore, to correct for a potential influence of the 1.3-fold higher systemic exposure, brain and plasma AUCs for each individual animal were calculated and the brain:plasma ratios were determined. These results demonstrate that a statistically

significant 4.8-fold higher doxorubicin concentration was measured in brain after administration of 2B3-101 ($p=0.0016$, unpaired two-tailed t-test; Fig. 30).

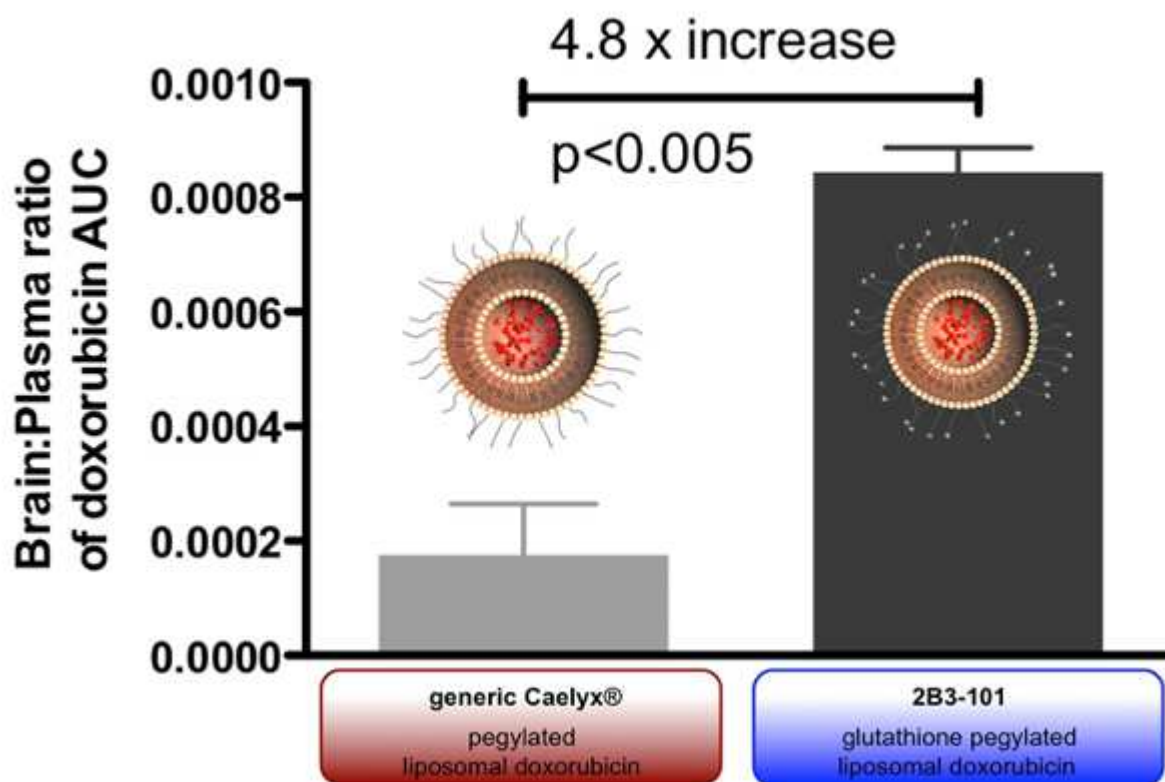


Fig. 30: Brain:plasma ratios of the AUCs after administration of 2B3-101 (dark grey bar) and generic Caelyx (light grey bar). 2B3-101 shows a significantly higher (4.8-fold) brain delivery ($p < 0.005$, unpaired two-tailed t-test)

4. Discussion

Using a new form of open flow microperfusion, i.e. cerebral OFM (cOFM), we were able to show that glutathione pegylated liposomal doxorubicin (2B3-101) enhances doxorubicin concentration in brain extracellular space by a factor of 5 relative to the non-targeted formulation (generic Caelyx). By continuous infusion of sodium fluorescein (Naf) we demonstrated that the BBB was intact 15 days after implantation of the cOFM probe in the left frontal lobe, and remained intact during drug exposure.

OFM was originally developed to analyse drug compounds in adipose tissue. The most recent development, cerebral OFM, has several advantages over other methods for determining uptake of drug compounds into the brain. Whole brain homogenates, for example, will never be fully depleted of the vascular component, despite perfusion (de Boer,

Visser, & Gaillard, 2013; Gaillard et al., 2012; Gaillard, 2011). Contamination of remaining drug in such vascular components is especially problematic when using drug delivery technologies that result in very high plasma levels of encapsulated drug relative to the free drug levels in the brain parenchyma and Microdialysis, a technique that is often used to determine free (unbound) drug in brain extracellular fluid, can only be applied to relatively small and less lipophilic compounds. Since cOFM uses a membrane-free probe without a nominal cut-off, larger and more lipophilic compounds can be sampled. Doxorubicin is an example of a lipophilic drug that cannot be measured using microdialysis (Whitaker & Lunte, 2010).

Previously, the improved efficacy of 2B3-101 was shown in a xenograft brain tumor model, as compared to non-targeted pegylated liposomal doxorubicin (Gaillard, 2013, unpublished results), while the toxicity remained essentially the same. In the current study, brain levels of doxorubicin were also determined, but in whole brain homogenates without making a distinction between free doxorubicin and doxorubicin bound in 2B3-101. Twenty-one hours after administration of 2B3-101 and non-targeted pegylated liposomal doxorubicin, an approximately 1.5-fold higher brain level of doxorubicin was found for 2B3-101 compared to pegylated liposomal doxorubicin, despite lower plasma concentrations. Four days after administration a 1.7-fold difference was found; 2B3-101 showed a higher sustained brain level. These combined results have already led to the development of a clinical trial for 2B3-101 (clinicaltrials.gov NCT01386580).

In the current study, a significantly higher (4.8-fold) doxorubicin concentration was found in the brain after administration of 2B3-101 relative to that found after administration of Caelyx. Even though cOFM allows direct sampling of brain interstitial fluid, the brain to blood ratio was calculated to correct for the observed higher plasma concentration of 2B3-101 relative to generic Caelyx. Such correction is important for mechanistic interpretations, to avoid an overestimation of the enhanced brain uptake simply by passive, plasma-concentration driven delivery of 2B3-101 across the BBB. Obtained results indicate an enhanced uptake into brain by functionalizing the pegylated liposomes with conjugated glutathione (GSH). It should be considered that the higher GSH-mediated brain uptake compared to previous results might be influenced by the animal model (rats vs. mice), the shorter measurement time (up to 5 hours after administration), or the more reliable cOFM brain sampling method, i.e. no blood contamination was detectable in the samples. However, since similar results were observed when comparing microdialysis concentrations to brain homogenates of water-soluble compounds (Lindqvist et al., 2013) we assume that the cOFM method is the most appropriate measurement method applied so far with 2B3-101. We did not distinguish between liposomal doxorubicin and free doxorubicin in the cOFM samples in this study. Such

a distinction will be possible in the future; although the low sample volumes always result in challenging analytics.

The continuous infusion of Naf allowed BBB function to be monitored constantly throughout the experiment. Naf was co-measured with doxorubicin, rather than having to obtain separate samples, which reduced costs and experimental efforts. We have previously observed that the BBB is disrupted by cOFM probe implantation and BBB re-establishment takes 11-15 days (chapter IV).

We used a constant rate Naf infusion in the current experiment, with a similar rate and dose level based on result in steady-state plasma concentrations in a previous study (chapter IV), an increase of Naf in plasma over time was observed. However the Naf concentration in brain did not increase another indication of an intact BBB. The increase in plasma levels could have been due to an interaction of liposomes and Naf.

In conclusion, we have shown that cOFM can be used to directly measure and compare the concentrations of two liposomal doxorubicin formulations in the interstitial fluid of the brain. Glutathione pegylated liposomal doxorubicin (2B3-101) enhanced the doxorubicin delivery to the brain relative to generic Caelyx. This is an indication that this chemotherapeutic drug improves treatment of brain cancer. The experimental design of glutathione pegylated liposomes (G-Technology) and monitoring with cOFM is applicable to other drugs and formulations, indicating the versatility of cOFM for the development of neuroactive drugs and vectorized formulations for drug delivery across BBB.

As this was a commissioned study in cooperation with an industrial partner, it was not entirely designed to demonstrate scientific. Therefore a few methodological drawbacks have to be recognized:

- The group size of 4(3) and 8(7) for group A and B is too small to result in a significant statistics and therefore only indicates an improved doxorubicin delivery of 2B3-101 rather that provide solid evidence.
- To our knowledge, the exclusion criteria based on Naf measurement in cOFM samples is the first method to monitor BBB permeability using a sampling method. A reference method is not available yet and complete proof of an intact BBB is therefore missing. First steps towards a verification of the method are described in chapter IV and the inclusion of Naf as a marker definitely allows the detection of BBB permeability variations and therefore represents a significant leap towards standardized monitoring of BBB permeability.

Summary

1. Summary

The aim of this doctoral thesis was the conception and the development of a new application of the open flow microperfusion (OFM) in the brain tissue. Cerebral open flow microperfusion (cOFM) was designed as a sampling technique that provides access to interstitial brain fluid in-vivo in rats and that allows the measurement of local substance concentrations with an intact BBB. The cOFM probe is inserted into the brain tissue which causes tissue damage and capillary rupture and thus a disruption of the BBB. In order to minimize implantation trauma, the site of implantation was located in the frontal lobe, an area in the cerebral cortex. A mild trauma in this area is not life threatening, the frontal lobe is positioned on the outer surface of the brain, easy to address with a short implantation path and the damage caused is therefore small.

Measurement of substance transport across the BBB requires an unaltered BBB in the surroundings of the cOFM probe. Therefore, the time until BBB re-establishment after disruption during the probe implantation was determined. BBB re-establishment was measured with albumin bound Evans Blue, a widely used marker for BBB intactness. Subjects with a healing time of up to 9 days after cOFM implantation still showed a significantly increased BBB permeability, indicating that the BBB was not fully healed. After a healing time of 11 and 15 days after cOFM probe implantation the BBB was fully re-establishment with a permeability similar to the BBB in comparable, uninvolved areas of the brain (chapter IV: 3.1). These results were confirmed with a second marker for BBB permeability, i.e. sodium fluorescein (Naf) (chapter IV: 3.2). By using Naf as a marker for BBB permeability throughout the whole sampling procedure the BBB status can be monitored in each individual sample. This is important since the BBB is a very sensitive structure which is easily influenced by factors such as stress, hormonal status and mechanical influences like

percussion. Naf was found an important quality control marker and therefore integrated into the standardized cOFM procedure (chapter IV: 3.3).

The necessary healing time of two weeks until the BBB is re-established after cOFM probe implantation is associated with several problems:

1. probe encapsulation due to glial scar formation around the implantation site
2. inactivation of the cOFM probe due to clogging of the tubing
3. continuous irritation of brain tissue due to the probe

(Ad 1.): Encapsulation of the probe due to the formation of a glial scar surrounding the implantation site is a widespread problem affecting all kinds of microelectrodes, biosensors and sampling probes. The function of all of these devices critically depends on substance exchange with the surrounding tissue. The dense structure of the glial scar hampers substance transport and would therefore strongly limit cOFM usability. In a histological study we were able to show that up to 30 days after cOFM implantation no significant glial scar is formed which could cause probe encapsulation and hamper diffusion between healthy brain tissue and the cOFM probe. Probe perfusion had no effect on the tissue at the tissue surrounding the probe. This remarkably small tissue reaction can be attributed to the choice of materials, especially to fluorinated ethylene propylene (FEP) that is present at most of the interfaces between cOFM probe and brain tissue. The underlying hypothesis on this interaction is described and discussed in chapter V.

(Ad 2.): The inactivation of the cOFM probe due to clogging of the tubing was avoided by an inserted healing dummy during the implantation and the healing phase. The healing dummy is a thin steel rod that provides mechanical stability process and prevents tissue from entering the guide cannula during the implantation. During the healing process the healing dummy seals the guide cannula towards the brain tissue and prevents tissue ingrowth. During sampling the healing dummy is removed and replaced by inflow/outflow tubing that allows sampling.

(Ad 3.): Continuous irritation of brain tissue due to the presence of the probe hampers re-establishment of the BBB and promotes formation of a glial scar. Due to the flexibility and the slick and biologically inert surface of the cOFM probe brain tissue irritation was minimized.

cOFM allows sampling of highly lipophilic substances and substances with a high molecular weight. This was of particular important in the first industrial study that was carried out with cOFM (chapter VI). Doxorubicin, a drug used in cancer therapy, is lipophilic and small. So that it can cross the BBB easily. But it is a substrate for the P-gp efflux transporter and therefore efficiently extracted from brain. Doxorubicin was applied in a liposomal nanocarrier formulation with a size of ~100 nm. A non-vectorized pegylated liposomal formulation and a

pegylated liposomal formulation vectorized with glutathione, a substrate for an influx transporter, were used. The free doxorubicin (lipophilic) and the nanocarrier formulation (high molecular size) were sampled and analyzed in the cOFM study. Naf was used to monitor BBB permeability and as a valid argument for outlier exclusion due to a hampered BBB. This study represents a typical industrial application for cOFM and results are in line with investigations carried out with other methods. cOFM has several advantages over other methods for determining brain uptake of drug compounds (chapter II).

2. Conclusions

cOFM probes:

- can measure transport across the BBB
- can deliver substances into brain tissue, bypassing the BBB
- can measure changes in BBB permeability in addition to PK/PD as quality control in each animal
- causes minimal tissue reaction

cOFM future work will focus on:

- investigating PK and PD of neuroactive substances
- examining histological changes surrounding the probe
- using cOFM with neurodegenerative animal models
- the role of BBB permeability in neurodegenerative disease

3. Outlook and ongoing investigations:

Current research and development aim to further standardize all components and processes involved in the cOFM concept. Standard operating procedures will be defined for all standard applications available for different tissues in order to minimize variability and allow the cooperation with international brain research centers and the exchange of technologies.

To facilitate the use of OFM systems in therapeutic applications the system will be miniaturized even further, which allows including the great variety of mouse models in cOFM trials. The absolute quantification of analytes will be a great enhancement and allow new types of investigations. cOFM can achieve a more complete picture of the whole metabolism

when OFM samples are analyzed using metabolomics instead of focusing on particular analytes. We plan to use metabolomics with cOFM for searching new biomarkers.

An ongoing project is the improvement of the Experimental Autoimmune Encephalomyelitis (EAE) rat model, an animal model for autoimmune diseases with brain degenerative effects mimicking multiple sclerosis. The established EAE animal model has some important disadvantages; firstly, the experimental lesions commonly affect predominantly the spinal cords. Secondly the exact localization where a lesion is about to form is not predictable. Our new method will allow to predictably produce an EAE lesion in the neocortex of the rat around the cOFM probe. Therefore monitoring of all stages of lesion formation, changes in metabolism and the influences of the BBB in the development of the disease can be investigated.

PUBLICATIONS

During the work on this doctoral thesis following publications were made with Thomas Birngruber as first author or with contribution of Thomas Birngruber.

1. JOURNALS

Mader JK, **Birngruber T**, Korsatko S, Deller S, Köhler G, Boysen S, Augustin T, Mautner SI, Sinner F, Pieber TR, AP@home consortium. Enhanced absorption of insulin aspart as the result of a dispersed injection strategy tested in a randomized trial in type 1 diabetic patients. *Diabetes Care* 2013 Apr; 36(4):780-785. **J.K.M. and T.B. contributed equally to this study.**

Birngruber T, Ghosh A, Perez-Yarza VA, Kroath T, Ratzner M, Pieber TR, Sinner F. Cerebral open flow microperfusion - a new in vivo technique for continuous measurement of substance transport across the intact blood-brain barrier. *Clinical and Experimental Pharmacology and Physiology*, 2013 in press.

Bodenlenz M, Aigner B, Dragatin C, Liebenberger L, Zahiragic S, Höfferer C, **Birngruber T**, Priedl J, Feichtner F, Schaupp L, Korsatko S, Ratzner M, Magnes C, Pieber TR, Sinner F. Clinical applicability of dOFM devices for dermal sampling. *Skin Res Technol*. 2013 Apr 13.

2. BOOK CHAPTERS

Birngruber T, Fröhlich E, Sinner F, Pieber T. *The Textbook of Nanoneuroscience and Nanoneurosurgery*; chapter 35: "In Vitro and In Vivo Techniques to Assess Neurotoxicity of Nanoparticles" August 12, 2013 reviewed and edited by Society for Brain Mapping & Therapeutics (SBMT) and SBMT-PLoS One NeuroMapping & Therapeutics

Pieber TR, **Birngruber T**, Bodenlenz M, Höfferer C, Mautner S, Tiffner K, Sinner F. *Microdialysis in Drug Development*; chapter 15: „Open Flow Microperfusion: An Alternative Method to Microdialysis?“ November, 2013 by AAPS Advances in the Pharmaceutical Sciences Series.

3. PROCEEDINGS

Birngruber T, Ghosh A, Perez-Yarza VA, Kroath T, Ratzer M, Pieber TR, Sinner F. cOFM: a novel in-vivo technique to continuously measure substance transport across the intact blood-brain barrier. Gordon Research Conference, Barriers of the CNS, June 16-17, 2012 Colby-Sawyer College, New London, NH, USA (poster).

Birngruber T, Mader JK, Mautner SI, Köhler G, Sinner F, Pieber TR. Microfocus computed tomography - A novel method to assess insulin distribution in subcutaneous adipose tissue. Diabetes Technology Meeting, Nov 8-10 2012, Bethesda, MD, USA (poster)

Birngruber T, Ghosh A, Perez-Yarza VA, Kroath T, Ratzer M, Pieber TR, Sinner F. cerebral Open-Flow Microperfusion (cOFM) an innovation in drug testing in-vivo. Conference on Cerebral Vascular Biology, 21 – 25 June, 2011, Leiden, the Netherlands

Birngruber T, Ghosh A., Hochmeister S, Kroath T, Pieber TR, Sinner F. cOFM for cerebral monitoring causes no significant brain tissue reaction. 7th Microdialysis Symposium 2013 - Inserm - Université de Poitiers (poster)

Birngruber T, Ghosh A, Perez-Yarza VA, Kroath T, Ratzer M, Pieber TR, Sinner F. cerebral Open-Flow Microperfusion (cOFM) eine innovative Methode zur Messung des Substanztransports über die BBB. Herrenalber Transport Tage, 30.5. – 1.6.2011 Bad Herrenalb, Germany

Birngruber T, Raml R, Gladdines W. Kroath T. Gaillard PJ, Pieber TR, Sinner F. Cerebral Open Flow Microperfusion (cOFM) enables quantification of enhanced transport of brain-targeted nanocarriers across the intact blood-brain barrier. The European CLINAM & ETPN Summit, June 23-26, 2013 (invited talk)

Mader JK, **Birngruber T**, Korsatko S, Deller S, Köhler G, Boysen S, Augustin T, Mautner SI, Sinner F, Pieber TR. Verbesserte pharmakodynamische Eigenschaften von Insulin aspart durch eine veränderte Applikationsmethode bei Patienten mit Typ-1-Diabetes. 40. Jahrestagung der OEDG, Nov 15-17 2012, Salzburg, Austria. Wien. Klin. Wochenschr. 2012, 124, Supplement 1: p. 17-18. (poster)

Mader JK, **Birngruber T**, Korsatko S, Deller S, Köhler G, Boysen S, Augustin T, Mautner SI, Sinner F, Pieber TR. Enhanced pharmacodynamic properties of insulin aspart due to a modified injection strategy in subjects with type 1 diabetes. 72nd Scientific Sessions of the ADA (American Diabetes Association), June 8-12 2012, Philadelphia, PA, USA; Poster Presentation. (poster)

Hochmeister S, **Birngruber T**, Zeitelhofer-Adzemovic M, Haindl M, Sinner F. A new model of focal inflammatory demyelination in the neocortex of the rat. XXI World Congress of Neurology. September 2013 (poster)

Ghosh A, **Birngruber T**, Sinner F, Pieber TR. Cerebral Open Flow Microperfusion (cOFM): a histological study. Abstract Book of 100th Indian Science Congress. 2013; -100th Indian Science Congress; JAN 3-7, 2013; Kolkata, India. (oral presentation)

Ghosh A, **Birngruber T**, Sinner F, Pieber TR. Cerebral Open Flow Microperfusion (cOFM): a histological study. A novel technique to explore extracellular milieu in brain. Abstract Book of 99th Indian Science Congress. 2012; -99th Indian Science Congress; 3 to 7 January, 2012; Bhuwaneswar, India. (oral presentation)

Publications

Bodenlenz M, Hoefferer C, Feichtner F, Magnes C, Schaller R, Priedl J, **Birngruber T**, Sinner F, Schaupp L, Korsatko S, Pieber TR. Novel catheters for in vivo research and pharmaceutical trials providing direct access to extracellular space of target tissues. 2010; The 12th Mediterranean Conference on Medical and Biological Engineering and Computing – MEDICON 2010; May 27-30, 2010; Porto Carras, Chalkidiki, Greece. (oral presentation)

Kraitsy K, **Birngruber T**, Fischerauer S, Patz S, Pichler K, Suppan M, Widni EE, Pistracher K, Grünbacher G, Kresse A, Kuess A, Eder HG, Fasching U, Sinner F, Weinberg A, Schäfer U. Open Flow Microperfusion; A novel method to continuously evaluate and quantify modulations in the hippocampal microenvironment. 8th World Congress on Brain Injury; MAR 9-15, 2010; Washington DC, USA. 2010. (oral presentation)

References

- Aasmundstad, T. A., Mørland, J., & Paulsen, R. E. (1995). Distribution of morphine 6-glucuronide and morphine across the blood-brain barrier in awake, freely moving rats investigated by in vivo microdialysis sampling. *Journal of Pharmacology and Experimental Therapeutics*, 275(1), 435–441.
- Abbott, N J. (1987) Neurobiology. Glia and the blood-brain barrier. *Nature*, 325(6101), 195.
- Abbott, N Joan. (2013). Blood-brain barrier structure and function and the challenges for CNS drug delivery. *Journal of inherited metabolic disease*.
- Abbott, N. Joan. (2004). Prediction of blood–brain barrier permeation in drug discovery from in vivo, in vitro and in silico models. *Drug Discovery Today: Technologies*, 1(4), 407–416.
- Abnet, K., Fawcett, J. W., & Dunnett, S. B. (1991). Interactions between meningeal cells and astrocytes in vivo and in vitro. *Brain Research. Developmental Brain Research*, 59(2), 187–196.
- Agus, D. B., Gambhir, S. S., Pardridge, W. M., Spielholz, C., Baselga, J., Vera, J. C., & Golde, D. W. (1997). Vitamin C crosses the blood-brain barrier in the oxidized form through the glucose transporters. *The Journal of clinical investigation*, 100(11), 2842–2848.
- Alavijeh, M. S., Chishty, M., Qaiser, M. Z., & Palmer, A. M. (2005). Drug metabolism and pharmacokinetics, the blood-brain barrier, and central nervous system drug discovery. *NeuroRx: the journal of the American Society for Experimental NeuroTherapeutics*, 2(4), 554–571.
- Amara, S. G., Grillner, S., Insel, T., Nutt, D., & Tsumoto, T. (2011). Neuroscience in recession? *Nature reviews. Neuroscience*, 12(5), 297–302.
- Andlin-Sobocki, P., & Rössler, W. (2005). Cost of psychotic disorders in Europe. *European Journal of Neurology*, 12 Suppl 1(10), 74–77.
- Azemi, E., Lagenaur, C. F., & Cui, X. T. (2011). The surface immobilization of the neural adhesion molecule L1 on neural probes and its effect on neuronal density and gliosis at the probe/tissue interface. *Biomaterials*, 32(3), 681–692.
- Badaut, J., Brunet, J.-F., & Regli, L. (2007). Aquaporins in the brain: from aqueduct to “multi-duct”. *Metabolic brain disease*, 22(3-4), 251–263.

References

- Bálint, Z., Krizbai, I. a, Wilhelm, I., Farkas, A. E., Párducz, A., Szegletes, Z., & Váró, G. (2007). Changes induced by hyperosmotic mannitol in cerebral endothelial cells: an atomic force microscopic study. *European Biophysics Journal*, 36(2), 113–120.
- Benveniste, H., & Diemer, N. H. (1987). Cellular reactions to implantation of a microdialysis tube in the rat hippocampus. *Acta Neuropathologica*, 74(3), 234–238.
- Benveniste, H., Drejer, J., Schousboe, a, & Diemer, N. H. (1987). Regional cerebral glucose phosphorylation and blood flow after insertion of a microdialysis fiber through the dorsal hippocampus in the rat. *Journal of neurochemistry*, 49(3), 729–734.
- Benveniste, H., Drejer, J., Schousboe, A., & Diemer, N. H. (1984). Elevation of the extracellular concentrations of glutamate and aspartate in rat hippocampus during transient cerebral ischemia monitored by intracerebral microdialysis. *Journal of Neurochemistry*, 43(5), 1369–1374.
- Bloch, O., & Manley, G. T. (2007). The role of aquaporin-4 in cerebral water transport and edema. *Neurosurgical focus*, 22(5), E3.
- Boado, R. J. (2008). A new generation of neurobiological drugs engineered to overcome the challenges of brain drug delivery. *Drug news & perspectives*, 21(9), 489–503.
- Bodenlenz, M, Aigner, B., Dragatin, C., Liebenberger, L., Zahiragic, S., Höfferer, C., Sinner, F. (2013). Clinical applicability of dOFM devices for dermal sampling. *Skin research and technology : official journal of International Society for Bioengineering and the Skin (ISBS) [and] International Society for Digital Imaging of Skin (ISDIS) [and] International Society for Skin Imaging (ISSI)*.
- Bodenlenz, Manfred, Höfferer, C., Magnes, C., Schaller-Ammann, R., Schaupp, L., Feichtner, F., Pieber, T. R. (2012). Dermal PK/PD of a lipophilic topical drug in psoriatic patients by continuous intradermal membrane-free sampling. *European Journal of Pharmaceutics and Biopharmaceutics*, 81(3), 635–641.
- Bodenlenz, Manfred, Schaupp, L. a, Druml, T., Sommer, R., Wutte, A., Schaller, H. C., Pieber, T. R. (2005). Measurement of interstitial insulin in human adipose and muscle tissue under moderate hyperinsulinemia by means of direct interstitial access. *American Journal of Physiology - Endocrinology and Metabolism*, 289(2), E296–E300.
- Bodor, N., & Buchwald, P. (1999). Recent advances in the brain targeting of neuropharmaceuticals by chemical delivery systems. *Advanced drug delivery reviews*, 36(2-3), 229–254.
- Bonate, P. L. (1995). Animal models for studying transport across the blood-brain barrier. *Journal of neuroscience methods*, 56(1), 1–15.
- Borland, L. M., Shi, G., Yang, H., & Michael, A. C. (2005). Voltammetric study of extracellular dopamine near microdialysis probes acutely implanted in the striatum of the anesthetized rat. *Journal of Neuroscience Methods*, 146(2), 149–158.
- Bourasset, F., Bernard, K., Muñoz, C., Genissel, P., & Scherrmann, J.-M. (2005). Neuropharmacokinetics of a new alpha-amino-3-hydroxy-5-methyl-4-isoxazole propionic acid (AMPA) modulator, S18986 [(S)-2,3-dihydro-[3,4]cyclopentano-1,2,4-benzothiadiazine-1,1-dioxide], in the rat. *Drug metabolism and disposition: the biological fate of chemicals*, 33(8), 1137–1143.

References

- Bricker, B., Jackson, T., Boateng, B., Zhu, X. Y., & Ablordeppey, S. Y. (2012). Evaluation of the behavioral and pharmacokinetic profile of SYA013, a homopiperazine analog of haloperidol in rats. *Pharmacology, biochemistry, and behavior*, *102*(2), 294–301.
- Brooks, D. J., Beaney, R. P., Lammertsma, A. A., Leenders, K. L., Horlock, P. L., Kensett, M. J., Jones, T. (1984). Quantitative measurement of blood-brain barrier permeability using rubidium-82 and positron emission tomography. *Journal of cerebral blood flow and metabolism: official journal of the International Society of Cerebral Blood Flow and Metabolism*, *4*(4), 535–545.
- Brown, R. C., Egleton, R. D., & Davis, T. P. (2004). Mannitol opening of the blood-brain barrier: regional variation in the permeability of sucrose, but not 86Rb+ or albumin. *Brain Research*, *1014*(1-2), 221–227.
- Bundgaard, M., & Abbott, N. J. (2008). All vertebrates started out with a glial blood-brain barrier 4-500 million years ago. *Glia*, *56*(7), 699–708.
- Bungay, P. M., Newton-Vinson, P., Isele, W., Garris, P. A., & Justice, J. B. (2003). Microdialysis of dopamine interpreted with quantitative model incorporating probe implantation trauma. *Journal of Neurochemistry*, *86*(4), 932–946.
- Butt, A. M., Jones, H. C., & Abbott, N. J. (1990). Electrical resistance across the blood-brain barrier in anaesthetized rats: a developmental study. *The Journal of physiology*, *429*, 47–62.
- Caruso, A., Sanchez, R. A., Hillebrecht, A., Poirier, A., Schuler, F., Lave, T., ... Belli, S. (2013). PK/PD assessment in CNS drug discovery: Prediction of CSF concentration in rodents for P-glycoprotein substrates and application to in vivo potency estimation. *Biochemical pharmacology*.
- Cecchelli, R., Berezowski, V., Lundquist, S., Culot, M., Renftel, M., Dehouck, M.-P., & Fenart, L. (2007). Modelling of the blood-brain barrier in drug discovery and development. *Nature reviews. Drug discovery*, *6*(8), 650–661.
- Chen, Y., & Liu, L. (2012). Modern methods for delivery of drugs across the blood-brain barrier. *Advanced drug delivery reviews*, *64*(7), 640–665.
- Clapp-Lilly, K. L., Roberts, R. C., Duffy, L. K., Irons, K. P., Hu, Y., & Drew, K. L. (1999). An ultrastructural analysis of tissue surrounding a microdialysis probe. *Journal of Neuroscience Methods*, *90*(2), 129–142.
- Claude, P., & Goodenough, D. A. (1973). Fracture faces of zonulae occludentes from “tight” and “leaky” epithelia. *The Journal of cell biology*, *58*(2), 390–400.
- Cornford, E., & Hyman, S. (1999). Blood-brain barrier permeability to small and large molecules. *Advanced drug delivery reviews*, *36*(2-3), 145–163.
- Dahlin, A., Royall, J., Hohmann, J. G., & Wang, J. (2009). Expression profiling of the solute carrier gene family in the mouse brain. *The Journal of pharmacology and experimental therapeutics*, *329*(2), 558–570.
- De Boer, M., Visser, C. C., & Gaillard, P. J. (2013). Upcycling drugs for brain-related diseases: a sustainable future for targeted drug delivery. *Therapeutic delivery*, *4*(4), 435–438.

References

- De Lange, E. C., Danhof, M., de Boer, A. G., & Breimer, D. D. (1997). Methodological considerations of intracerebral microdialysis in pharmacokinetic studies on drug transport across the blood-brain barrier. *Brain research. Brain research reviews*, 25(1), 27–49.
- De Lange, E. C., Danhof, M., Zurcher, C., de Boer, A. G., & Breimer, D. D. (1995). Repeated microdialysis perfusions: periprobe tissue reactions and BBB permeability. *Brain Research*, 702(1-2), 261–265.
- De Lange, E. C., de Boer, A. G., & Breimer, D. D. (2000). Methodological issues in microdialysis sampling for pharmacokinetic studies. *Advanced drug delivery reviews*, 45(2-3), 125–148.
- Dehouck, B., Dehouck, M. P., Fruchart, J. C., & Cecchelli, R. (1994). Upregulation of the low density lipoprotein receptor at the blood-brain barrier: intercommunications between brain capillary endothelial cells and astrocytes. *The Journal of cell biology*, 126(2), 465–473.
- Dingemanse, J., Sollie, F. A., Breimer, D. D., & Danhof, M. (1988). Pharmacokinetic modeling of the anticonvulsant response of oxazepam in rats using the pentylenetetrazol threshold concentration as pharmacodynamic measure. *Journal of pharmacokinetics and biopharmaceutics*, 16(2), 203–228.
- Dolman, D., Drndarski, S., Abbott, N. J., & Rattray, M. (2005). Induction of aquaporin 1 but not aquaporin 4 messenger RNA in rat primary brain microvessel endothelial cells in culture. *Journal of neurochemistry*, 93(4), 825–833.
- Doran, A., Obach, R. S., Smith, B. J., Hosea, N. A., Becker, S., Callegari, E., ... Zhang, C. (2005). The impact of P-glycoprotein on the disposition of drugs targeted for indications of the central nervous system: evaluation using the MDR1A/1B knockout mouse model. *Drug metabolism and disposition: the biological fate of chemicals*, 33(1), 165–174.
- Egleton, R. D., & Davis, T. P. (2005). Development of neuropeptide drugs that cross the blood-brain barrier. *NeuroRx: the journal of the American Society for Experimental NeuroTherapeutics*, 2(1), 44–53.
- Ellmerer, M., Schaupp, L., Sendlhofer, G., Wutte, A., Brunner, G. A., Trajanoski, Z., Pieber, T. R. (1998). Lactate metabolism of subcutaneous adipose tissue studied by open flow microperfusion. *The Journal of Clinical Endocrinology and Metabolism*, 83(12), 4394–4401.
- Elmqvist, W. F., & Sawchuk, R. J. (1997). Application of microdialysis in pharmacokinetic studies. *Pharmaceutical research*, 14(3), 267–288.
- Eskow Jaunarajs, K. L., Dupre, K. B., Ostock, C. Y., Button, T., Deak, T., & Bishop, C. (2010). Behavioral and neurochemical effects of chronic L-DOPA treatment on nonmotor sequelae in the hemiparkinsonian rat. *Behavioural pharmacology*, 21(7), 627–637.
- Ewing, J. R., Knight, R. A., Nagaraja, T. N., Yee, J. S., Nagesh, V., Whitton, P. A., Fenstermacher, J. D. (2003). Patlak plots of Gd-DTPA MRI data yield blood-brain transfer constants concordant with those of ¹⁴C-sucrose in areas of blood-brain opening. *Magnetic resonance in medicine: official journal of the Society of Magnetic Resonance in Medicine / Society of Magnetic Resonance in Medicine*, 50(2), 283–292.

References

- Fitch, M. T., Doller, C., Combs, C. K., Landreth, G. E., & Silver, J. (1999). Cellular and molecular mechanisms of glial scarring and progressive cavitation: in vivo and in vitro analysis of inflammation-induced secondary injury after CNS trauma. *J Neurosci.*, *19*(19), 8182–8198.
- Fukuuchi, Y., Tomita, M., & Koto, A. (Eds.). (2001). *Ischemic Blood Flow in the Brain*. Tokyo: Springer Japan.
- Gaillard, P. J. (2011). Case study: to-BBB's G-Technology, getting the best from drug-delivery research with industry-academia partnerships. *Therapeutic delivery*, *2*(11), 1391–1394.
- Gaillard, P. J., Visser, C. C., Appeldoorn, C. C. M., & Rip, J. (2012). Targeted blood-to-brain drug delivery -10 key development criteria. *Current pharmaceutical biotechnology*, *13*(12), 2328–2339.
- Grabb, M. C., Sciotti, V. M., Gidday, J. M., Cohen, S. A., & van Wylen, D. G. (1998). Neurochemical and morphological responses to acutely and chronically implanted brain microdialysis probes. *Journal of Neuroscience Methods*, *82*(1), 25–34.
- Groothuis, D. R., Ward, S., Schlageter, K. E., Itskovich, a C., Schwerin, S. C., Allen, C. V, Levy, R. M. (1998). Changes in blood-brain barrier permeability associated with insertion of brain cannulas and microdialysis probes. *Brain research*, *803*(1-2), 218–230.
- Gustavsson, A., Svensson, M., Jacobi, F., Allgulander, C., Alonso, J., Beghi, E., ... Olesen, J. (2011). Cost of disorders of the brain in Europe 2010. *European neuropsychopharmacology : the journal of the European College of Neuropsychopharmacology*, *21*(10), 718–779.
- Harris, J. P., Capadona, J. R., Miller, R. H., Healy, B. C., Shanmuganathan, K., Rowan, S. J., Tyler, D. J. (2011). Mechanically adaptive intracortical implants improve the proximity of neuronal cell bodies. *Journal of Neural Engineering*, *8*(6), 066011.
- Hascup, E. R., af Bjerken, S., Hascup, K. N., Pomerleau, F., Huettl, P., Strömberg, I., & Gerhardt, G. a. (2009). Histological studies of the effects of chronic implantation of ceramic-based microelectrode arrays and microdialysis probes in rat prefrontal cortex. *Brain Research*, *1291*, 12–20.
- Hawkins, B. T., & Davis, T. P. (2005). The Blood-Brain Barrier / Neurovascular Unit in Health and Disease, *57*(2), 173–185.
- Hilbert, J. M., & Battista, D. (1991). Quazepam and flurazepam: differential pharmacokinetic and pharmacodynamic characteristics. *The Journal of clinical psychiatry*, *52 Suppl*, 21–26.
- Holmgaard, R., Benfeldt, E., Nielsen, J. B., Gatschelhofer, C., Sorensen, J. a, Höfferer, C., ... Sinner, F. (2012). Comparison of Open-Flow Microperfusion and Microdialysis Methodologies When Sampling Topically Applied Fentanyl and Benzoic Acid in Human Dermis Ex Vivo. *Pharmaceutical Research*, 1808–1820.
- IMS. (2004). IMS Retail Drug Monitor. *Health (San Francisco)*.
- Innovative Medicines Initiative (IMI). (2008). The Innovative Medicines Initiative Research Agenda, (February).

References

- Johanson, C. E. (1980). Permeability and vascularity of the developing brain: cerebellum vs cerebral cortex. *Brain research*, 190(1), 3–16.
- Josserand, V., Pélerin, H., de Bruin, B., Jegou, B., Kuhnast, B., Hinnen, F., ... Tavitian, B. (2006). Evaluation of drug penetration into the brain: a double study by in vivo imaging with positron emission tomography and using an in vitro model of the human blood-brain barrier. *The Journal of pharmacology and experimental therapeutics*, 316(1), 79–86.
- Kaliszan, R. (1996). Brain/blood distribution described by a combination of partition coefficient and molecular mass. *International Journal of Pharmaceutics*, 145(1-2), 9–16.
- Kaya, M., & Ahishali, B. (2011). Assessment of permeability in barrier type of endothelium in brain using tracers: Evans blue, sodium fluorescein, and horseradish peroxidase. *Methods in Molecular Biology*, 763, 369–382.
- Kim, Y.-T., Hitchcock, R. W., Bridge, M. J., & Tresco, P. A. (2004). Chronic response of adult rat brain tissue to implants anchored to the skull. *Biomaterials*, 25(12), 2229–2237.
- Kola, I., & Landis, J. (2004). Can the pharmaceutical industry reduce attrition rates? *Nature Reviews. Drug Discovery*, 3(8), 711–715.
- Kozler, P., & Pokorný, J. (2003). Altered blood-brain barrier permeability and its effect on the distribution of Evans blue and sodium fluorescein in the rat brain applied by intracarotid injection. *Physiological Research*, 52(5), 607–614.
- Lai, C.-H., & Kuo, K.-H. (2005). The critical component to establish in vitro BBB model: Pericyte. *Brain research. Brain research reviews*, 50(2), 258–265.
- Lai, F., Fadda, A. M., & Sinico, C. (2013). Liposomes for brain delivery. *Expert opinion on drug delivery*.
- Lange, E. C. M., Danhof, M., Boer, A. G., & Breimer, D. D. (1997). Methodological considerations of intracerebral microdialysis in pharmacokinetic studies on drug transport across the blood–brain barrier. *Brain*, 25, 27–49.
- Lenzsér, G., Kis, B., Snipes, J. A., Gáspár, T., Sándor, P., Komjáti, K., Busija, D. W. (2007). Contribution of poly(ADP-ribose) polymerase to postischemic blood-brain barrier damage in rats. *Journal of Cerebral Blood Flow and Metabolism*, 27(7), 1318–1326.
- Lindqvist, A., Rip, J., Gaillard, P. J., Björkman, S., & Hammarlund-Udenaes, M. (2013). Enhanced Brain Delivery of the Opioid Peptide DAMGO in Glutathione PEGylated Liposomes: A Microdialysis Study. *Molecular pharmaceutics*, 10(5), 1533–1541.
- Madara, J. L. (1988). Tight junction dynamics: is paracellular transport regulated? *Cell*, 53(4), 497–498.
- Manaenko, A., Chen, H., Kammer, J., Zhang, J. H., & Tang, J. (2011). Comparison Evans Blue injection routes: Intravenous versus intraperitoneal, for measurement of blood-brain barrier in a mice hemorrhage model. *Journal of Neuroscience Methods*, 195(2), 206–210.
- Marburger, A., Sohr, R., Reum, T., & Morgenstern, R. (2000). Comparison by microdialysis of striatal L-DOPA after its systemic administration in rats with probes implanted acutely or through a guide cannula. *Journal of Neuroscience Methods*, 102(2), 127–132.

References

- Maxwell, W. ., Follows, R., Ashhurst, D. E., & Berry, M. (1990). The response of the cerebral hemisphere of the rat to injury - 1. The mature rat. *Philosophical Transactions of the Royal Society of London. Series B, Biological Sciences*, 328(1250), 479–500.
- Mensch, J., Oyarzabal, J., Mackie, C., & Augustijns, P. (2009). In vivo, in vitro and in silico methods for small molecule transfer across the BBB. *Journal of pharmaceutical sciences*, 98(12), 4429–4468.
- Miller, G. (2002). Drug targeting. Breaking down barriers. *Science*, 297(5584), 1116–1118.
- Morgan, M. E., Singhal, D., & Anderson, B. D. (1996). Quantitative assessment of blood-brain barrier damage during microdialysis. *Journal of Pharmacology and Experimental Therapeutics*, 277(2), 1167–1176.
- Myers, R. D. (1986). Development of push-pull systems for perfusion of anatomically distinct regions of the brain of the awake animal. *Annals of the New York Academy of Sciences*, 473, 21–41.
- Neuhaus, J., Risau, W., & Wolburg, H. (1991). Induction of blood-brain barrier characteristics in bovine brain endothelial cells by rat astroglial cells in transfilter coculture. *Annals of the New York Academy of Sciences*, 633, 578–580.
- Newton, H. B. (2006). Advances in strategies to improve drug delivery to brain tumors. *Expert review of neurotherapeutics*, 6(10), 1495–1509.
- Nutt, D. J. (2011). The full cost and burden of disorders of the brain in Europe exposed for the first time. *European neuropsychopharmacology : the journal of the European College of Neuropsychopharmacology*, 21(10), 715–717.
- Ohtsuki, S. (2004). New aspects of the blood-brain barrier transporters; its physiological roles in the central nervous system. *Biological & pharmaceutical bulletin*, 27(10), 1489–496.
- Oldendorf, W. H. (1970). Measurement of brain uptake of radiolabeled substances using a tritiated water internal standard. *Brain research*, 24(2), 372–376.
- Oldendorf, W. H. (1974). Lipid solubility and drug penetration of the blood brain barrier. *Proceedings of the Society for Experimental Biology and Medicine. Society for Experimental Biology and Medicine (New York, N.Y.)*, 147(3), 813–815.
- Olesen, J., & Leonardi, M. (2003). The burden of brain diseases in Europe. *European Journal of Neurology*, 10(5), 471–477.
- Pardridge, W. M. (1995). Transport of small molecules through the blood-brain barrier: biology and methodology. *Advanced Drug Delivery Reviews*, 15(1-3), 5–36.
- Pardridge, W. M. (2005). The blood-brain barrier and neurotherapeutics. *NeuroRx*, 2(1), 1–2.
- Pardridge, W. M. (2012). Drug transport across the blood-brain barrier. *Journal of cerebral blood flow and metabolism : official journal of the International Society of Cerebral Blood Flow and Metabolism*, 32(11), 1959–1972.

References

- Patlak, C. S., Blasberg, R. G., & Fenstermacher, J. D. (1983). Graphical evaluation of blood-to-brain transfer constants from multiple-time uptake data. *Journal of cerebral blood flow and metabolism : official journal of the International Society of Cerebral Blood Flow and Metabolism*, 3(1), 1–7.
- Polt, R. (1994). Glycopeptide Enkephalin Analogues Produce Analgesia in Mice: Evidence for Penetration of the Blood-Brain Barrier. *Proceedings of the National Academy of Sciences*, 91(15), 7114–7118.
- Reichel, A. (2006). The role of blood-brain barrier studies in the pharmaceutical industry. *Current drug metabolism*, 7(2), 183–203.
- Rosenbloom, A J, Ferris, R., Sipe, D. M., Riddler, S. A., Connolly, N. C., Abe, K., & Whiteside, T. L. (2006). In vitro and in vivo protein sampling by combined microdialysis and ultrafiltration. *Journal of Immunological Methods*, 309(1-2), 55–68.
- Rosenbloom, Alan J, Sipe, D. M., & Weedn, V. W. (2005). Microdialysis of proteins: performance of the CMA/20 probe. *Journal of neuroscience methods*, 148(2), 147–153.
- Rucker, H. K., Wynder, H. J., & Thomas, W. E. (2000). Cellular mechanisms of CNS pericytes. *Brain research bulletin*, 51(5), 363–369.
- Saunders, N. R., Daneman, R., Dziegielewska, K. M., & Liddelov, S. A. (2013). Transporters of the blood-brain and blood-CSF interfaces in development and in the adult. *Molecular aspects of medicine*, 34(2-3), 742–752.
- Schaupp, L., Ellmerer, M., Brunner, G. A., Wutte, A., Sendlhofer, G., Trajanoski, Z., Wach, P. (1999). Direct access to interstitial fluid in adipose tissue in humans by use of open-flow microperfusion. *American Journal of Physiology*, 276(2 Pt 1), E401–E408.
- Seymour, J. P., & Kipke, D. R. (2007). Neural probe design for reduced tissue encapsulation in CNS. *Biomaterials*, 28(25), 3594–3607.
- Shepro, D., & Morel, N. M. (1993). Pericyte physiology. *FASEB journal : official publication of the Federation of American Societies for Experimental Biology*, 7(11), 1031–1038.
- The Innovative Medicines Initiative (IMI) Research Agenda. (2008), 2008(February).
- Thelin, J., Jörntell, H., Psouni, E., Garwicz, M., Schouenborg, J., Danielsen, N., & Linsmeier, C. E. (2011). Implant size and fixation mode strongly influence tissue reactions in the CNS. *PloS one*, 6(1), e16267.
- Trajanoski, Z., Brunner, G. A., Schaupp, L., Ellmerer, M., Wach, P., Pieber, T. R., ... Skrabal, F. (1997). Open-flow microperfusion of subcutaneous adipose tissue for on-line continuous ex vivo measurement of glucose concentration. *Diabetes Care*, 20(7), 1114–1121.
- Upton, R. N. (2007). Cerebral uptake of drugs in humans. *Clinical and Experimental Pharmacology & Physiology*, 34(8), 695–701.
- Verkman, A. S. (2005). More than just water channels: unexpected cellular roles of aquaporins. *Journal of cell science*, 118(Pt 15), 3225–3232.

References

- Von Grote, E. C., Venkatakrishnan, V., Duo, J., & Stenken, J. A. (2011). Long-term subcutaneous microdialysis sampling and qRT-PCR of MCP-1, IL-6 and IL-10 in freely-moving rats. *Molecular bioSystems*, 7(1), 150–161.
- Wang, M., Etu, J., & Joshi, S. (2007). Enhanced disruption of the blood brain barrier by intracarotid mannitol injection during transient cerebral hypoperfusion in rabbits. *Journal of Neurosurgical Anesthesiology*, 19(4), 249–256.
- Weiss, N., Miller, F., Cazaubon, S., & Couraud, P.-O. (2009). The blood-brain barrier in brain homeostasis and neurological diseases. *Biochimica et biophysica acta*, 1788(4), 842–857.
- Westergren, I., Nyström, B., Hamberger, a, & Johansson, B. B. (1995). Intracerebral dialysis and the blood-brain barrier. *Journal of neurochemistry*, 64(1), 229–234.
- Whitaker, G., & Lunte, C. E. (2010). Investigation of microdialysis sampling calibration approaches for lipophilic analytes: doxorubicin. *Journal of pharmaceutical and biomedical analysis*, 53(3), 490–496.
- Wittchen, H. U., Jacobi, F., Rehm, J., Gustavsson, A., Svensson, M., Jönsson, B., ... Steinhausen, H.-C. (2011). The size and burden of mental disorders and other disorders of the brain in Europe 2010. *European neuropsychopharmacology : the journal of the European College of Neuropsychopharmacology*, 21(9), 655–679.
- Wolburg, H., Neuhaus, J., Kiesel, U., Krauss, B., Schmid, E. M., Ocalan, M., Risau, W. (1994). Modulation of tight junction structure in blood-brain barrier endothelial cells. Effects of tissue culture, second messengers and cocultured astrocytes. *Journal of cell science*, 107 (Pt 5, 1347–1357).
- Wolf, S., Seehaus, B., Minol, K., & Günter Gassen, H. (1996). Die Blut-Hirn-Schranke: Eine Besonderheit des cerebralen mikrozirkulationssystems. *Naturwissenschaften*, 83(7), 302–311.

CURRICULUM VITAE



Personal Data

Date of birth: 01. 10. 1978
Nationality: Austrian
Address: Steyrergasse 35
8010 Graz
Austria
Email: thomas.birngruber@joanneum.at

Education

1993 – 1998 Höhere technische Lehranstalt Steyr – Elektronik und Informatik

1999 – 2006 Study of Biomedical Engineering at the Graz University of Technology
Master thesis: “Faseroptische, quenching basierte Sauerstoffmessung im Fettgewebe unter Verwendung von Mikrodialyse. “

2006 – 2013 Doctoral study at the Graz University of Technology, Graz, Austria in cooperation with
Joanneum Research HEALTH – Institute of Biomedicine and Health Sciences, Graz, Austria

Affiliations

2006 - 2007 Medical University of Graz, Department of Radiology
Magnetic resonance imaging research - MRI

2007 - 2010 Medical University of Graz, Department of Endocrinology
Brain research – establishment and testing of surgical and behavioral research facilities including sampling and imaging techniques

2010 – 2013 Joanneum Research – HEALTH Institute of Biomedicine and Health Sciences - Brain research – cerebral open flow microperfusion (cOFM)

Current position

Scientist at Joanneum Research – HEALTH Institute of Biomedicine and Health Sciences
Team leader - cerebral PK/PD – cerebral open flow microperfusion (cOFM)

Mader JK, **Birngruber T**, Korsatko S, Deller S, Köhler G, Boysen S, Augustin T, Mautner SI, Sinner F, Pieber TR, AP@home Consortium.

Enhanced absorption of insulin aspart as the result of a dispersed injection strategy tested in a randomized trial in type 1 diabetic patients. Diabetes Care 2013 Apr; 36(4):780-5.

J.K.M. and T.B. contributed equally to this study.

Enhanced Absorption of Insulin Aspart as the Result of a Dispersed Injection Strategy Tested in a Randomized Trial in Type 1 Diabetic Patients

JULIA K. MADER, MD¹
THOMAS BIRNGRUBER, MS²
STEFAN KORSATKO, MD¹
SIGRID DELLER, MD¹
GERD KOHLER, MD¹
SUSANNE BOYSEN, MS³

THOMAS AUGUSTIN, PhD²
SELMA L. MAUTNER, PhD^{1,2}
FRANK SINNER, PhD^{1,2}
THOMAS R. PIEBER, MD^{1,2}
ON BEHALF OF THE AP@HOME CONSORTIUM

OBJECTIVE—We investigated the impact of two different injection strategies on the pharmacokinetics and pharmacodynamics of insulin aspart in vivo in an open-label, two-period crossover study and verified changes in the surface-to-volume ratio *ex vivo*.

RESEARCH DESIGN AND METHODS—Before the clinical trial, insulin aspart was injected *ex vivo* into explanted human abdominal skin flaps. The surface-to-volume ratio of the subcutaneous insulin depot was assessed by microfocus computed tomography that compared 1 bolus of 18 IU with 9 dispersed boluses of 2 IU. These two injection strategies were then tested in vivo, in 12 C-peptide-negative type 1 diabetic patients in a euglycemic glucose clamp (glucose target 5.5 ± 1.1 mmol/L) for 8 h after the first insulin administration.

RESULTS—The *ex vivo* experiment showed a 1.8-fold higher mean surface-to-volume ratio for the dispersed injection strategy. The maximum glucose infusion rates (GIR) were similar for the two strategies (10 ± 4 vs. 9 ± 4 ; $P = 0.5$); however, times to reach maximum GIR and 50% and 10% of the maximum GIR were significantly reduced by using the 9×2 IU strategy (68 ± 33 vs. 127 ± 93 min; $P = 0.01$; 38 ± 9 vs. 49 ± 16 min; $P < 0.01$; 23 ± 6 vs. 30 ± 10 min; $P < 0.05$). For 9×2 IU, the area under the GIR curve was greater during the first 60 min (219 ± 89 vs. 137 ± 75 ; $P < 0.01$) and halved until maximum GIR (242 ± 183 vs. 501 ± 396 ; $P < 0.01$); however, it was similar across the whole study period ($1,361 \pm 469$ vs. $1,565 \pm 527$; $P = 0.08$).

CONCLUSIONS—A dispersed insulin injection strategy enhanced the effect of a fast-acting insulin analog. The increased surface-to-volume ratio of the subcutaneous insulin depot can facilitate insulin absorption into the vascular system.

Diabetes Care 36:780–785, 2013

Fast-acting insulin analogs have been developed to avoid postprandial glucose peaks (1,2). Some studies suggest that postprandial hyperglycemia can contribute to elevated levels of hemoglobin A_{1c} (3,4) and lead to the development of short- and long-term diabetes complications (5,6). Although currently available fast-acting insulin analogs have

been designed for a better match with meal-induced glucose excursions, insulin absorption and insulin action still lag behind (7,8). Even bolus administration of fast-acting insulin analogs immediately before meals does not completely avoid postprandial glucose peaks. Modern fast-acting insulin analogs still only insufficiently mimic physiological insulin

profiles; however, their effect could be further improved by accelerating insulin absorption from the injection site into the vascular system.

Accelerated insulin absorption in response to an increased blood flow has been described for heated injection sites (9) or coadministered adjuvants such as hyaluronidase (10–12) but also for a larger distribution of the subcutaneous insulin depot achieved with a modified injection strategy. Human insulin absorption has been tested with a “sprinkler needle” that has 14 holes in its walls and a sealed tip, thus dispersing the insulin bolus at the injection site. With the sprinkler needle, insulin was absorbed more rapidly and glucose levels were less raised relative to a regular injection needle (13). A dispersed insulin bolus should have an increased surface-to-volume ratio and could further contribute to even faster insulin absorption of modern already fast-acting insulin analogs.

The aim of our study was to test whether the absorption rate of a fast-acting insulin analog (insulin aspart) could be further accelerated through the dispersion of a single predefined insulin bolus into nine separate insulin injections. We compared the two different injection strategies *ex vivo* by using microfocus computed tomography (micro-CT) to assess the increase in the surface-to-volume ratio and in vivo by assessing the pharmacokinetic and pharmacodynamic response in a clinical trial.

RESEARCH DESIGN AND METHODS

Insulin administration

The fast-acting insulin analog aspart (NovoRapid; Novo Nordisk A/S, Baegsvard, Denmark) was administered with a FlexPen with an 8-mm pen needle (NovoFine 30G; Novo Nordisk) *ex vivo* and in vivo by a trained study nurse. Insulin was administered either as a single bolus of 18 IU or as nine boluses of 2 IU each in a predefined 10-mm grid pattern (Fig. 1A). To assess the dosing accuracy of each

From the ¹Division of Endocrinology and Metabolism, Department of Internal Medicine, Medical University of Graz, Graz, Austria; the ²Joanneum Research GmbH, HEALTH-Institute for Biomedicine and Health Sciences, Graz, Austria; and ³Novo Nordisk A/S, Maaloev, Denmark.

Corresponding author: Thomas R. Pieber, endo@meduni-graz.at.

Received 5 July 2012 and accepted 4 September 2012.

DOI: 10.2337/dci12-1319. Clinical trial reg. no. NCT01399346, clinicaltrials.gov.

J.K.M. and T.B. contributed equally to this study.

© 2013 by the American Diabetes Association. Readers may use this article as long as the work is properly cited, the use is educational and not for profit, and the work is not altered. See <http://creativecommons.org/licenses/by-nc-nd/3.0/> for details.

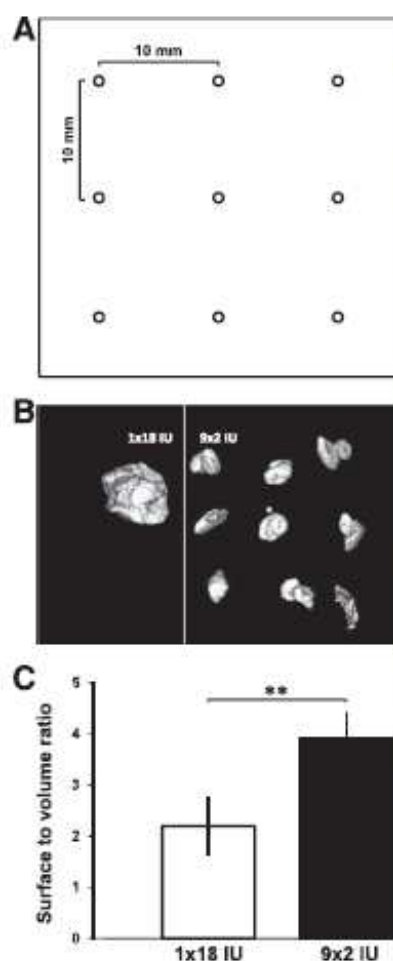


Figure 1—A: Individual injection sites for the dispersed injection strategy (9×2 IU) were separated by 10 mm. B: A 3D reconstruction of the micro-CT measurements. C: Mean surface-to-volume ratios comparing two injection strategies (1×18 IU vs. 9×2 IU). ** $p < 0.01$.

insulin pen used in the study, two insulin doses were injected into vials with both application strategies (1×18 IU and 9×2 IU), and then each dose was weighed with a microbalance (Sartorius, Göttingen, Germany). In total, 36 insulin pens were used (3 per subject to allow insulin injection within 1 min for the dispersed injection strategy). Injected insulin weights were the same for the two injection strategies ($18.3 \pm 0.4 \mu\text{g}$ for 1×18 IU vs. $18.3 \pm 0.3 \mu\text{g}$ for 9×2 IU).

Micro-CT

The ex vivo micro-CT experiment was performed to compare the surface-to-volume

ratio of the two injection strategies before their use in the in vivo clamp study. The two injection strategies were applied to explanted abdominal skin flaps; surface and volume of each resulting subcutaneous liquid depot were measured with micro-CT. To enhance the contrast between the liquid depots and the surrounding adipose tissue, 10% (by weight) of the insulin aspart solution in the FlexPen was replaced with a contrast agent (Iopamiro, iodine 200 mg/mL; Bracco s.p.a., Milan, Italy). The contrast agent was selected for its high iodine content and low viscosity, providing good contrast enhancement at minimal viscosity changes of the insulin solution. Twelve abdominal skin flaps with a minimal size of 50×50 mm and at least 20 mm of subcutaneous adipose tissue were collected from BioBank (Medical University of Graz, Austria). All skin samples had been explanted during pendulous abdomen resections after massive weight loss. The time span between explantation and injection of the insulin/contrast agent solution never exceeded 5 h. During this time, skin flaps were kept at room temperature.

Immediately after injection of the insulin and contrast agent solution, skin flaps were scanned with a micro-CT scanner (Inveon Multimodality System, Siemens, Germany) with Siemens Inveon Acquisition Workplace software (version 1.2.2.2). To optimize contrast, acquisition time, and resolution, the scanning sequence was set to a voltage of 50 kV, a current of 300 μA , and an exposure time of 500 ms. A rotation of 210° in 180 rotation steps led to a resolution with an effective pixel size of 53 μm . For three-dimensional (3D) image reconstruction, a downsample factor of 1 was used. The system supports a 3D reconstruction of an acquired data set of two-dimensional projections by using back projection of a filtered projection algorithm. Analysis of the 3D model was performed with Siemens Inveon Research Workplace. The volume of interest was selected by a region-growing algorithm, with a spot of high intensity selected manually as a starting point. Regions with decreasing levels of intensity were added to the volume of interest until the predefined injection volume ($180 \pm 1.8 \mu\text{L}$) was reached. The surface of the selected volume of interest was calculated for both injection strategies (1×18 IU and 9×2 IU) (Fig. 1B).

Clinical euglycemic clamp study

A monocentric, randomized, controlled, two-period crossover euglycemic clamp

study was performed in 12 type 1 diabetic patients at the Clinical Research Centre at the Medical University of Graz between April and June 2011. The study was approved by the local ethics committee and performed in accordance with the Declaration of Helsinki and the principles of Good Clinical Practice. Participants gave written, informed consent after the purpose, nature, and potential risks of the study had been explained and before any study-related activities were started. Participants had to fulfill all inclusion criteria (fasting C-peptide <0.3 nmol/L; BMI 20.0 – 28.0 kg/m 2 ; hemoglobin A $_{1c}$ $<10\%$) and none of the exclusion criteria (i.e., insulin aspart use, lipodystrophy, smoking). The study consisted of four visits: one screening visit, two clamp visits separated by a washout phase of 5–21 days, and one follow-up visit. To avoid any residual action of their regular insulin regimens, participants were instructed to follow a specific regimen: participants on multiple daily injections administered their last dose of short-acting insulin at least 5 h before the clamp visit. Participants on long-acting insulin analogs were transferred to NPH insulin 2 days before the clamp visit and received the last injection of NPH insulin 20 h before the clamp visit. Participants on continuous subcutaneous insulin infusion stopped their insulin infusion at least 5 h before the clamp visit. Participants abstained from strenuous exercise 24 h before the clamp visits. Participants attended the research facility under fasting conditions and remained fasting throughout each clamp visit. One 18-gauge venous catheter was inserted in each arm: one was used for insulin and glucose infusion; the other was used for blood sampling. The arm used for blood sampling was put under a heating blanket at 55°C to obtain arterialized venous blood. The euglycemic clamp procedure was started by using a variable intravenous human insulin infusion (Actrapid; Novo Nordisk) or glucose infusion to obtain a stable plasma glucose (target 5.5 ± 1.1 mmol/L) during the run-in period (3–7 h). During the last hour of the run-in period, the insulin infusion was tapered and finally switched off. At time 0 (between 11 A.M. and 2 P.M.), a dose of 18 IU insulin aspart was injected into the subcutaneous adipose tissue of the abdominal wall. The insulin dose was administered either as 1×18 IU or as 9×2 IU. On arrival, the participant number was entered into the computer program

Insulin absorption with dispersed injection

Randomizer, which assigned the participant randomly to one of the injection strategies. The other injection strategy was then administered on the second clamp visit. The dosing sequence was also randomly assigned by using Randomizer according to parameters provided by the Institute for Medical Informatics, Statistics and Documentation (Medical University of Graz). For the 9×2 IU injection strategy, where administration took <1 min, a transparent grid was used that separated the individual injection sites from each other by exactly 10 mm (Fig. 1A). The euglycemic glucose clamp was continued at a level of 5.5 ± 1.1 mmol/L for 8 h after the insulin bolus administration or until plasma glucose rose above 200 mg/dL. Euglycemia was maintained by variable glucose infusion (glucose 10%; Fresenius Kabi, Bad Homburg, Germany), which was administered with a perfusion pump (B. Braun, Melsungen, Germany). Arterialized venous blood samples were drawn in 5- to 10-min intervals throughout the euglycemic clamp. Plasma glucose was measured in duplicate on site with a Super GL 2 Glucose Analyzer (Müller Gerätebau, Freital, Germany). Plasma samples for insulin determination were taken at baseline (0 min), every 5 min up to 120 min, every 15 min from 120 to 180 min, every 30 min from 180 to 240 min, and then at 60-min intervals until study end (480 min). Plasma samples for insulin determination were deep frozen on site, and insulin measurements were subsequently performed at the laboratories of Novo Nordisk A/S (Maaloev, Denmark) by means of a homogenous immunoassay with analog-specific antibody for aspart determination.

Data analysis

Primary pharmacokinetic and secondary pharmacodynamic study end points were derived from insulin concentration profile and exogenous glucose infusion rate (GIR). Pharmacokinetic data included time to maximum insulin concentration, times to 10% and 50% of maximum insulin concentration, and maximum insulin concentration. Pharmacodynamic data included time to maximum GIR, times to 10% and 50% of maximum GIR, and maximum GIR. Area under the curve (AUC) was calculated for insulin concentration and GIR up to 480 min after insulin administration and for the time to reach maximum insulin concentration and maximum GIR.

All data were tested for normal distribution with a Shapiro-Wilk test. The paired measurements were analyzed with paired *t* tests or Wilcoxon signed rank tests, depending on whether the paired differences were normally distributed. The unpaired measurements from the micro-CT experiment were analyzed with Mann-Whitney *U* tests. AUCs were estimated with the trapezoidal rule for defined time points. $P < 0.05$ was considered to indicate a significant difference. Bonferroni corrections were used to correct for multiple testing of the pharmacokinetic and pharmacodynamic results. Unless otherwise specified, data are reported as mean \pm SD. All statistical analyses were performed with the software package R (v.2.10.1).

RESULTS

Ex vivo

To directly compare the calculated surface-to-volume ratios of the subcutaneous insulin depots with each other, the two injection strategies (1×18 IU and 9×2 IU) were applied with the same total volume. Although the measured mean volume of the dispersed injection strategy

was thus similar to that of the single injection strategy (179.6 ± 0.96 mm³ vs. 180.6 ± 0.70 mm³), the mean surface of the dispersed injection strategy was significantly larger than the single injection surface (703.6 ± 83.8 mm² vs. 396.6 ± 101.1 mm²; $P < 0.01$). The dispersed injection strategy thus enhanced the surface-to-volume ratio by a factor of 1.8 (3.9 ± 0.48 vs. 2.2 ± 0.57 ; $P < 0.01$), which is in line with the expected increase in surface calculated from geometric analysis according to the assumption of spherical liquid depots (Fig. 1C).

Clinical euglycemic clamp study

We included 12 C-peptide-negative type 1 diabetic patients (age 32 ± 9 years; 6 females; BMI 23.9 ± 2.5 kg/m²; hemoglobin A_{1c} $7.3 \pm 0.6\%$; diabetes duration 19 ± 10 years). All participants completed both clamp visits, no clinically relevant adverse events were observed, and all collected data were used for subsequent statistical analysis.

Maximum insulin concentrations were similar for both injection strategies (Table 1). Time to reach maximum insulin concentration was shorter for 9×2

Table 1—Pharmacokinetic and pharmacodynamic parameters for the two injection strategies

	1×18 IU	9×2 IU	<i>P</i> value
Pharmacokinetics			
Insulin t_{max10} (min)	14.2 ± 5.6	9.2 ± 4.2	0.03
Insulin t_{max50} (min)	35.0 ± 8.3	24.6 ± 7.5	0.001
Insulin t_{max} (min)	66.3 ± 38	56.3 ± 14	0.3
C-INS _{max} (mU/L)	526.0 ± 275	546.0 ± 243	0.7
AUC-INS ₀₋₃₀	$13,279 \pm 7,220$	$16,507 \pm 8,575$	0.2
AUC-INS ₀₋₆₀	$3,044 \pm 1,982$	$5,595 \pm 4,432$	0.04
AUC-INS ₀₋₁₂₀	$13,042 \pm 7,635$	$18,866 \pm 11,476$	0.01
AUC-INS ₀₋₁₈₀	$31,817 \pm 16,759$	$37,443 \pm 9,843$	0.1
AUC-INS ₀₋₂₄₀	$52,288 \pm 27,458$	$51,824 \pm 27,240$	0.9
AUC-INS ₀₋₃₆₀	$61,024 \pm 33,138$	$57,417 \pm 30,145$	0.4
AUC-INS ₀₋₄₈₀	$66,202 \pm 36,516$	$60,312 \pm 31,699$	0.2
Pharmacodynamics			
GIR t_{max10} (min)	29.6 ± 9.9	22.5 ± 6.2	0.05
GIR t_{max50} (min)	48.8 ± 15.7	37.5 ± 8.7	0.001
GIR t_{max} (min)	126.7 ± 92.8	68.3 ± 33.3	0.01
C-GIR _{max} (mg · kg ⁻¹ · min ⁻¹)	8.8 ± 3.5	10.0 ± 3.9	0.5
AUC-GIR ₀₋₃₀	501 ± 396	242 ± 183	0.007
AUC-GIR ₀₋₆₀	10 ± 10	21 ± 15	0.07
AUC-GIR ₀₋₁₂₀	137 ± 75	219 ± 89	0.001
AUC-GIR ₀₋₁₈₀	571 ± 249	678 ± 216	0.1
AUC-GIR ₀₋₂₄₀	$1,275 \pm 510$	$1,258 \pm 394$	0.9
AUC-GIR ₀₋₃₆₀	$1,494 \pm 524$	$1,351 \pm 448$	0.2
AUC-GIR ₀₋₄₈₀	$1,565 \pm 527$	$1,361 \pm 469$	0.08

AUC-GIR, area under the curve for GIR; AUC-INS, area under the curve for insulin; C-GIR_{max}, maximum GIR value; C-INS_{max}, maximum insulin concentration; t_{10-180} , times 130–480 min; t_{max} , time to reach maximum concentration or rate; t_{max10} , time to reach 10% of maximum concentration or rate; t_{max50} , time to reach 50% of maximum concentration or rate.

IU, although the differences were only significant for the time to reach 10% ($P < 0.03$) and 50% ($P < 0.001$) of the maximum insulin concentrations (Fig. 2A).

The time to reach maximum GIR was almost 50% shorter for 9×2 IU than for 1×18 IU (Table 1). The times taken to reach 10% and 50% of maximum GIR were still significantly lower for the dispersed injection strategy (Fig. 2B), whereas the concentrations at maximum insulin action were similar for both injection strategies. Individual GIR data for times to reach 10% of maximum GIR, 50% of maximum GIR, and maximum GIR are indicated in Fig. 3A–C. The AUC for glucose was significantly larger for 9×2 IU during the first 60 min, whereas the AUC until time of maximum GIR was smaller for 9×2 IU (Table 1). After 120 min, all AUCs for GIR were similar for both injection strategies.

CONCLUSIONS—Although fast-acting insulin analogs are designed for a more rapid absorption into the vascular system, it is still difficult to achieve a physiological insulin profile. To accelerate insulin absorption of the fast-acting insulin aspart, we tested whether a dispersed injection strategy would affect insulin absorption in comparison with a regular single-bolus insulin injection by using ex vivo micro-CT in explanted abdominal skin flaps and by assessing pharmacokinetic and pharmacodynamic parameters in vivo in a euglycemic clamp study in type 1 diabetic patients.

After injection, insulin aspart solutions form liquid depots in the tissue. Liquid depots with a higher surface-to-volume ratio can be absorbed faster, because a larger depot surface involves more capillaries and enhances absorption into the vascular system. Enhanced drug absorption with increased surface-to-volume ratio has been demonstrated in a canine model (14), and in humans an increased volume slowed the speed of pharmacokinetics in large versus small skin blisters (15). By using micro-CT, a nondestructive 3D imaging technique, we were able to compare quantitatively the surface-to-volume ratio of subcutaneous insulin depots of a dispersed injection strategy (9×2 IU) with that of a single insulin injection (1×18 IU). For the dispersed injection strategy, we found a 1.8-fold higher surface-to-volume ratio, which is in line with theoretical calculations from spherical liquid depots.

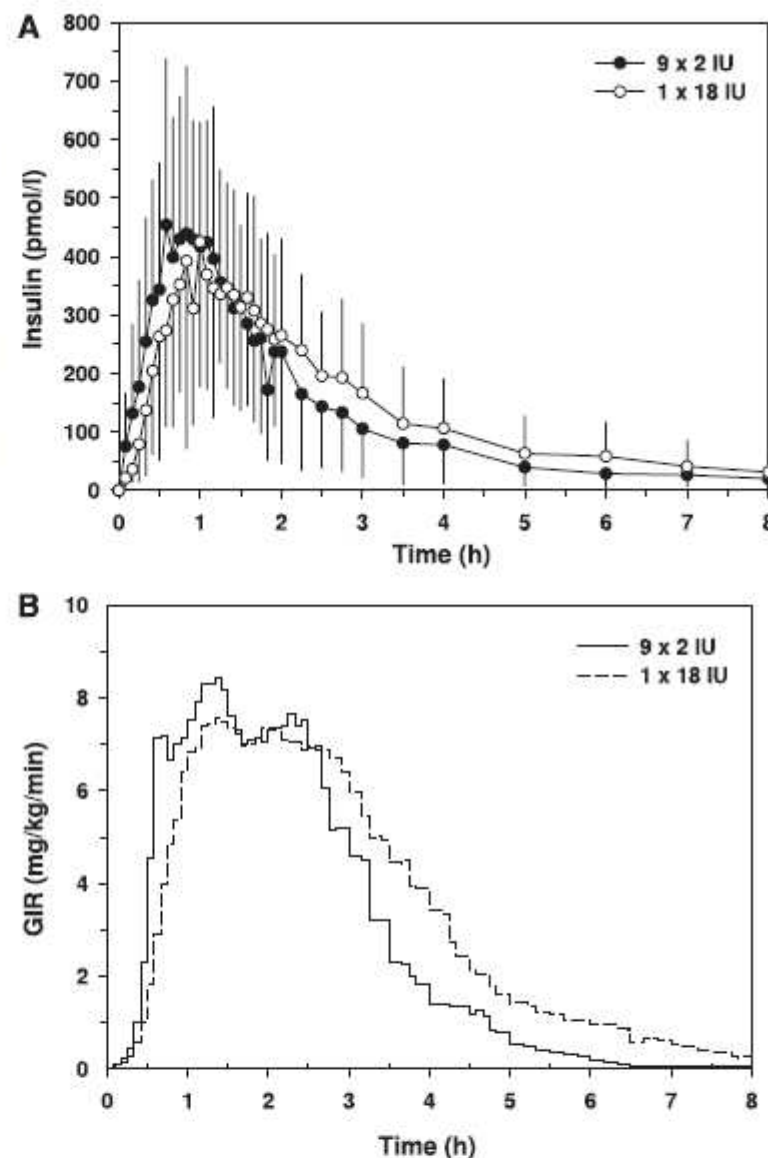


Figure 2—A: Mean insulin curve for 9×2 IU (●) and 1×18 IU (○) injections of insulin aspart. Values represent mean \pm SD (only one direction shown for clarity). B: Mean glucose infusion rate curve for 9×2 IU (solid line) and 1×18 IU (dashed line) injections of insulin aspart.

A recently developed technology for morphometric tissue analysis, micro-CT is mainly used in bone and dental structure analysis (16–18). In combination with a CT contrast agent, micro-CT provided excellent resolution, fast analysis, and exact semiautomated volume and surface calculations for each individual insulin depot. Because micro-CT measurements require no tissue fixation and only minimal tissue

manipulation, we were able to assess unaltered samples that closely matched in vivo conditions immediately after insulin injection.

Insulin pharmacokinetic and pharmacodynamic data collected during the clinical trial in type 1 diabetic patients supported the micro-CT findings. The lag time between insulin injection and insulin appearance in blood plasma was

Insulin absorption with dispersed injection

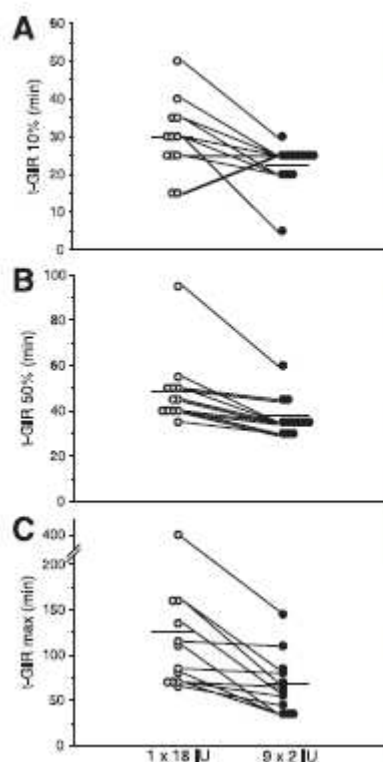


Figure 3—Individual GIR profile data showing time to 10% of maximum GIR (A), time to 50% of maximum GIR (B), time to maximum GIR (C). Horizontal bars indicate means for the 1 × 18 IU and 9 × 2 IU injection strategies.

significantly reduced when the fast-acting insulin aspart was administered with a dispersed injection strategy. Other approaches to accelerate insulin absorption, such as the use of hyaluronidase to facilitate the dissociation of insulin hexamers into more easily absorbed monomers and dimers, have also been associated with faster insulin absorption and an earlier onset of insulin action (12,19). Adding hyaluronidase to a fast-acting insulin analog reduced time to reach maximum insulin concentration by 51% (19) and resulted in an even more pronounced effect in comparison with our dispersed injection strategy (15%). The decrease in the time to reach 50% of maximum insulin concentrations with the dispersed injection strategy (29%) was comparable with the hastening of the onset of insulin action by adding hyaluronidase (34%). Application of local heating to the injection site, which locally increases the blood flow, has also been demonstrated to result in an

accelerated insulin absorption and more rapid onset of insulin action (9). Heating the injection site reduced time to maximum insulin concentration by 42% and time to 50% of maximum insulin concentration by 29%. The very similar twice as fast onset of insulin action of a dispersed insulin bolus is most likely caused by an increase in the number of capillaries involved in the absorption of insulin into the vascular system, comparable with the effect of intradermal injections with microneedles that access a more dense capillary network (20). In a study that compared insulin injection of a fast-acting insulin analog using a jet injector, time to maximum insulin concentration and insulin action were halved in comparison to an insulin pen (21). This was attributed to a cone-like dispersion pattern with a large surface area caused by the jet injector, as described earlier by Mitragotri et al. (22).

Use of the dispersed injection strategy not only reduced the lag time but also improved all other pharmacokinetic parameters during the first 60 min after insulin injection. Additionally, duration of insulin action was shorter for the dispersed injection strategy. The shorter duration of insulin action can contribute to reduced late postprandial hypoglycemia, which occurs when the carbohydrate content of a meal is already consumed but insulin action is still present. Although pharmacokinetic data are important for the development of new insulin analogs, pharmacodynamic results from glucose infusion rates provide relevant data for more efficient glycemic control. In our *in vivo* clamp study in type 1 diabetic patients, the time to reach maximum GIR was almost halved when the insulin bolus was evenly dispersed among nine injection sites compared with a single injection site, indicating a much faster onset of insulin action. In combination with fast-acting insulin analogs, the effect of a dispersed injection strategy can lead to a clinically relevant improvement of glycemic control. Although we have shown that multiple injection sites significantly accelerate the absorption of a fast-acting insulin analog, the simultaneous injection of multiple small boluses is not feasible for routine diabetes care. The use of a sprinkler needle concept is one way to translate our findings into a technology acceptable for patients. Enhanced absorption of human insulin with flatter blood glucose profiles and less pronounced blood glucose peaks has been found

with the sprinkler needle relative to a regular injection needle (13).

Although the lag time between insulin injection and insulin appearance is already reduced in fast-acting insulin analogs, an earlier onset of insulin action would enable diabetic patients to inject insulin regularly after meals without having to take into account the delayed action of currently available insulins. This would be of considerable benefit for glycemic control in pediatric diabetic patients, in whom the consumed carbohydrates and the resulting blood glucose are difficult to predict because of highly variable eating habits and activity levels (23) and in geriatric patients with varying levels of appetite depending on their health status. These patient populations always bear an increased risk of postprandial hypoglycemic events when applying premeal insulin boluses without complete consumption of the planned meal.

Maintenance of good glucose control in diabetic pregnancy is also essential to avoid adverse fetal outcomes, such as fetal growth acceleration (24,25). Glucose uptake, endogenous glucose production, and insulin requirements strongly vary throughout pregnancy. Especially in late gestation of type 1 diabetic pregnancies, postprandial glucose control is difficult to manage because of slower glucose disposal (26). Postprandial insulin dosing could contribute to a better glycemic control in this patient group.

Faster insulin absorption can also promote the development of closed-loop artificial pancreas systems that use subcutaneous insulin administration and continuous glucose measurement. The substantial lag time between insulin administration and the onset of insulin action is a major obstacle for the development of algorithms that control closed-loop systems (27). A shortened absorption time of fast-acting insulin analogs can lead to faster control algorithms, and a clinically feasible dispersed injection strategy would be a major step toward the successful implementation of fully closed-loop systems, which do not require a meal announcement followed by a priming bolus.

In summary, this study confirmed acceleration of insulin absorption of a fast-acting insulin analog by using a dispersed insulin bolus. A clinically feasible dispersed injection strategy might better mimic physiological insulin profiles and contribute to improvements in glycemic control. To evaluate the implications for clinical outcomes, such as a reduction

of late postprandial hypoglycemia, both reduction of glucose fluctuations and improvement in glycemic control need to be addressed in further clinical trials.

Acknowledgments—This study was partly funded by AP@home (FP7-ICT-2009-4 247138). T.R.P. is a member of the advisory board of Novo Nordisk A/S and has received speaker honoraria from Novo Nordisk A/S. J.K.M. and G.K. received speaker honoraria from Novo Nordisk A/S. S.B. is an employee of Novo Nordisk A/S. No other potential conflicts of interest relevant to this article were reported.

J.K.M. designed and performed the clinical study, interpreted data, and drafted the manuscript. T.B. designed and performed the *ex vivo* experiment, interpreted data, and drafted the manuscript. S.K., S.D., and G.K. helped to design the study, performed the study, interpreted the data, and critically reviewed the manuscript. S.B. performed the analytical insulin analysis, interpreted the data, and reviewed the manuscript. T.A. designed the study and performed statistical analysis. S.I.M. interpreted data and drafted the manuscript. F.S. contributed to the study design and discussions and critically revised the manuscript. T.R.P. designed the study, supervised the project, contributed to discussions, and critically revised the manuscript. All authors and the AP@home Consortium approved the final version of the manuscript. T.R.P. is the guarantor of this work and, as such, had full access to all the data in the study and takes responsibility for the integrity of the data and the accuracy of the data analysis.

Parts of this study were presented in abstract form at the 72nd Scientific Sessions of the American Diabetes Association, Philadelphia, Pennsylvania, 8–12 June 2012.

The authors thank Helmut Schöllnast (Medical University of Graz) for providing information on micro-CT contrast agents; Martina Brunner (Medical University of Graz) for the help with the sample preparation; Martina Urschitz, Michael Wolf, Janka Gerdova, and Harold Kojzar (all, Medical University of Graz) for help with the clamp studies; Bernd Tschapeller (Joanneum Research) for data management; and Novo Nordisk A/S (Maaloev, Denmark) for the insulin measurements performed free of charge.

References

- Lindholm A, McEwen J, Riss AP. Improved postprandial glycemic control with insulin aspart. A randomized double-blind cross-over trial in type 1 diabetes. *Diabetes Care* 1999;22:801–805
- Pettrì DJ, Ospina P, Howard C, Zisser H, Jovanovic L. Efficacy, safety and lack of immunogenicity of insulin aspart compared with regular human insulin for women with gestational diabetes mellitus. *Diabet Med* 2007;24:1129–1135
- American Diabetes Association. Standards of medical care in diabetes—2012. *Diabetes Care* 2012;35(Suppl. 1):S11–S63
- Monnier L, Lapinski H, Colette C. Contributions of fasting and postprandial plasma glucose increments to the overall diurnal hyperglycemia of type 2 diabetic patients: variations with increasing levels of HbA_{1c}. *Diabetes Care* 2003;26:881–885
- Qiao Q, Tuomilehto J, Borch-Johnsen K. Post-challenge hyperglycaemia is associated with premature death and macrovascular complications. *Diabetologia* 2003;46(Suppl. 1):M17–M21
- Clement S. What are the best options for controlling prandial glycaemia? *Curr Diab Rep* 2009;9:355–359
- Plank J, Witte A, Brunner G, et al. A direct comparison of insulin aspart and insulin lispro in patients with type 1 diabetes. *Diabetes Care* 2002;25:2053–2057
- Hovorka R, Shojee-Moradie F, Carroll PV, et al. Partitioning glucose distribution/transport, disposal, and endogenous production during IVGTT. *Am J Physiol Endocrinol Metab* 2002;282:E992–E1007
- Raz I, Weiss R, Yegorchikov Y, Bitton G, Nagar R, Pesach B. Effect of a local heating device on insulin and glucose pharmacokinetic profiles in an open-label, randomized, two-period, one-way crossover study in patients with type 1 diabetes using continuous subcutaneous insulin infusion. *Clin Ther* 2009;31:980–987
- Muchmore DB, Vaughn DE. Review of the mechanism of action and clinical efficacy of recombinant human hyaluronidase coadministration with current prandial insulin formulations. *J Diabetes Sci Tech* 2010;4:419–428
- Hompesch M, Muchmore DB, Morrow L, Vaughn DE. Accelerated insulin pharmacokinetics and improved postprandial glycemic control in patients with type 1 diabetes after coadministration of prandial insulins with hyaluronidase. *Diabetes Care* 2011;34:666–668
- Vaughn DE, Muchmore DB. Use of recombinant human hyaluronidase to accelerate rapid insulin analogue absorption: experience with subcutaneous injection and continuous infusion. *Endocr Pract* 2011;17:914–921
- Edsberg B, Herly D, Hildebrandt P, Kühl C. Insulin bolus given by sprinker needle: effect on absorption and glycaemic response to a meal. *Br Med J (Clin Res Ed)* 1987;294:1373–1376
- Rosin E, Ebert S, Uphoff TS, Evans MH, Schultz-Darken NJ. Penetration of antibiotics into the surgical wound in a canine model. *Antimicrob Agents Chemother* 1989;33:700–704
- Blaser J, Rieder HL, Lüthy R. Interface-area-to-volume ratio of interstitial fluid in humans determined by pharmacokinetic analysis of netilmicin in small and large skin blisters. *Antimicrob Agents Chemother* 1991;35:837–839
- Jones AC, Milthorpe B, Averdunk H, et al. Analysis of 3D bone ingrowth into polymer scaffolds via micro-computed tomography imaging. *Biomaterials* 2004;25:4947–4954
- Swain MV, Xue J. State of the art of Micro-CT applications in dental research. *Int J Oral Sci* 2009;1:177–188
- Kraus T, Fischerauer SF, Hänzl AC, Uggowitzer PJ, Löffler JF, Weinberg AM. Magnesium alloys for temporary implants in osteosynthesis: *in vivo* studies of their degradation and interaction with bone. *Acta Biomater* 2012;8:1230–1238
- Vaughn DE, Yocum RC, Muchmore DB, et al. Accelerated pharmacokinetics and glucodynamics of prandial insulins injected with recombinant human hyaluronidase. *Diabetes Technol Ther* 2009;11:345–352
- Pettrì RJ, Ginsberg B, Hirsch L, et al. Intradermal microneedle delivery of insulin lispro achieves faster insulin absorption and insulin action than subcutaneous injection. *Diabetes Technol Ther* 2011;13:435–442
- Engwerda EE, Abbink EJ, Tack CJ, de Galan BE. Improved pharmacokinetic and pharmacodynamic profile of rapid-acting insulin using needle-free jet injection technology. *Diabetes Care* 2011;34:1804–1808
- Mittagott S. Current status and future prospects of needle-free liquid jet injectors. *Nat Rev Drug Discov* 2006;5:543–548
- Steck AK, Klingensmith GJ, Fiallo-Scharer R. Recent advances in insulin treatment of children. *Pediatr Diabetes* 2007;8(Suppl. 6):49–56
- Hernanz L, Saez-de-Ibarra I, Grande C, Pallardo LF. Non-glycemic-dependent reduction of late pregnancy A1C levels in women with type 1 diabetes. *Diabetes Care* 2007;30:1579–1580
- Kersten A, de Valk HW, Visser GHA. Increased second trimester maternal glucose levels are related to extremely large-for-gestational-age infants in women with type 1 diabetes. *Diabetes Care* 2007;30:1069–1074
- Murphy HR, Eleri D, Allen JM, et al. Pathophysiology of postprandial hyperglycemia in women with type 1 diabetes during pregnancy. *Diabetologia* 2012;55:282–293
- Eleri D, Dunger DB, Hovorka R. Closed-loop insulin delivery for treatment of type 1 diabetes. *BMC Med* 2011;9:120

Birngruber T, Fröhlich E, Sinner F, Pieber T.

The Textbook of Nanoneuroscience and Nanoneurosurgery;

chapter 35:

“In Vitro and In Vivo Techniques to Assess Neurotoxicity of
Nanoparticles”

August 12, 2013 by CRC Press.

reviewed and edited by Society for Brain Mapping & Therapeutics
(SBMT) and SBMT-PLoS One NeuroMapping & Therapeutics

35 *In Vitro* and *In Vivo* Techniques to Assess Neurotoxicity of Nanoparticles

*Thomas Birngruber, Eleonore Fröhlich,
Frank Sinner, and Thomas Pieber*

CONTENTS

Introduction.....	473
<i>In Vitro</i> Techniques	475
Basal Cytotoxicity Screening.....	475
Specific Cytotoxicity Screening.....	478
<i>In Vivo</i> Techniques	480
Histopathology	480
Imaging Techniques	480
Positron Emission Tomography	480
MRI and MRS	481
Analytical Techniques.....	481
Microdialysis.....	481
Open Flow Microperfusion	482
Behavioral Tests	483
Conclusions.....	483
References.....	484

INTRODUCTION

The basic idea of nanotoxicology is that the small size of nanoparticles (NPs) is the main cause for their adverse biological effects. Many materials—which, in bulk form, are cell compatible (e.g., polystyrene used for cell culture)—may become cytotoxic in sizes ≤ 20 nm (Fröhlich et al. 2009). NPs can be used as fluorescent biological labels—such as drug and gene delivery agents, biodetectors for pathogens, probes for DNA structure, for separation and purification of biological molecules and cells—and in tissue engineering, tumor destruction via heating, and magnetic resonance imaging (MRI) contrast enhancement (Bhaskar et al. 2010). In the central nervous system (CNS), the blood–brain barrier (BBB) functions as a protective shield against harmful substances such as viruses and toxins but also against potentially harmful NPs circulating in the bloodstream. The BBB consists of tight junctions between endothelial cells around the capillary lumen (Reese and Karnovsky 1967) (Figure 35.1) protecting the brain but also preventing potential CNS therapeutic agents from entering the brain (Miller 2002; Pardridge 2005). Some NPs can cross the BBB and have been identified as possible transporter systems to carry CNS active drugs across it. BBB permeability and toxicity of drug candidates and NPs are important parameters during CNS drug development and must be considered at an early stage of pharmaceutical development. The ability

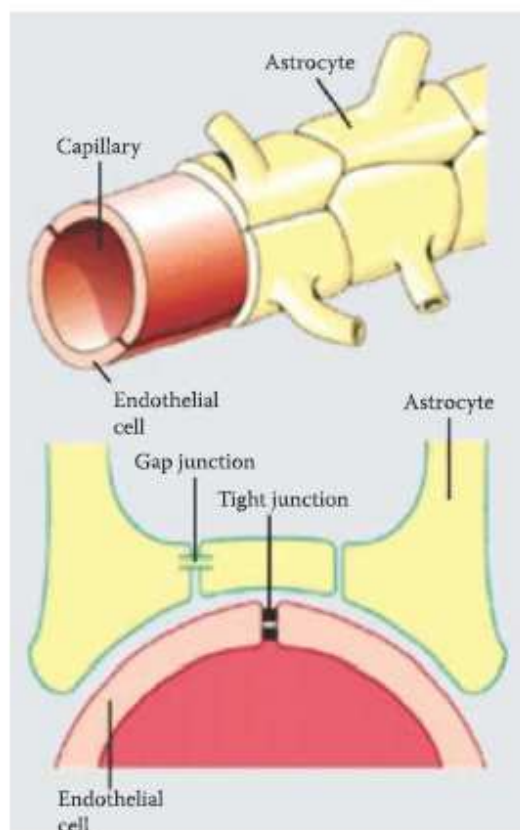


FIGURE 35.1 BBB consists of tight junctions on the vascular endothelial cells in the brain. (Reprinted with permission from Speckman, E.-J. et al., *Physiologie*, Urban & Fischer, Munich, 2008.)

of NPs to pass the BBB may also be useful for detection and therapy of brain pathologies. Whether NPs are used in terms of a pharmaceutical formulation or are taken up unintentionally from the surroundings as a result of pollution, the question of an interaction of NPs with brain cells is highly interesting.

NPs entering the brain come in contact with five brain-specific cell types: neurons, astrocytes, oligodendrocytes, ependymal cells, and microglial cells (Figure 35.2). Astrocytes and microglial cells are the most important populations to evaluate neurotoxicity *in vitro* based on their role in the brain (transmission of information, protection of neurons, and regulation of the immune system) and their quantitative representation around brain neurons. Nano-sized materials such as single-wall carbon nanotubes have been reported to cause oxidative stress in neurons leading to apoptosis and necrosis (Zhang et al. 2010) and to decrease viability not only in neurons but also in glial cells (Belyanskaya et al. 2009). Cells treated with nano-sized titanium dioxide have been reported to show intracellular accumulations of reactive oxygen species (ROS) leading to apoptosis, necrosis, and cell cycle arrest (Liu et al. 2010; Wu et al. 2010). U87 astrocytoma cells can suffer from cytotoxic effects after exposure to titanium dioxide, zinc oxide, and magnesium oxide NPs (Lai et al. 2008), whereas iron oxide NPs can interfere with adherence of astrocytes to the substratum (Au et al. 2007).

In this chapter, we provide an overview of currently available *in vitro* and *in vivo* screening techniques to assess the cytotoxicity of NPs in general and in relation to brain-specific cells in particular.

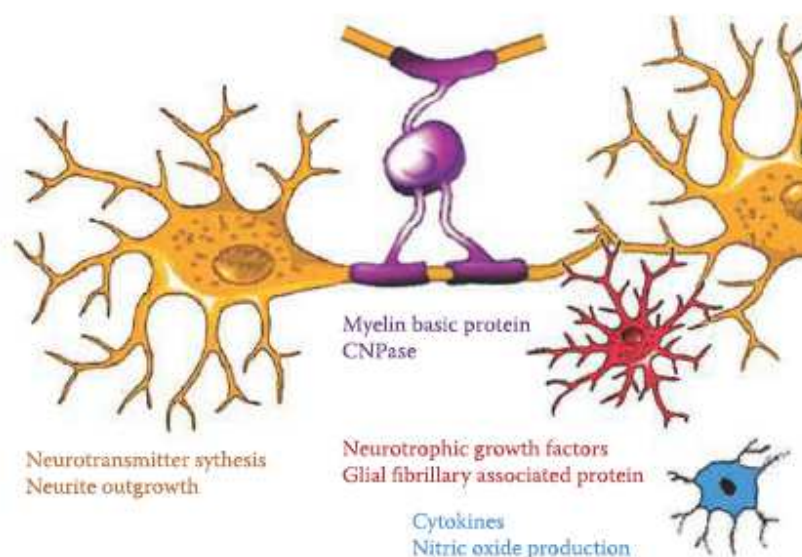


FIGURE 35.2 Important cell types in the brain and their main functions that could be used for specific neurotoxicity testing. For assessing neurons (yellow), the synthesis of neurotransmitters (e.g., tyrosine hydroxylase for DOPA synthesis) and neurite outgrowth are useful parameters. Function of oligodendrocytes (pink) can be assessed by expression of myelin basic protein and 2',3'-cyclic nucleotide 3'-phosphodiesterase (CNPase). Status of astrocytes (red) can be monitored by neurotrophic growth factor expression and glial fibrillary acidic protein expression. Changes in microglia cells (blue) can be studied in cytokine and nitric oxide production.

IN VITRO TECHNIQUES

BASAL CYTOTOXICITY SCREENING

Screening for basal cytotoxicity is the first toxicological assessment in drug development and can also be used to measure nanotoxicity (Table 35.1). Basal cytotoxicity screening assays (bCSAs) are used to identify any negative influence on cell metabolism and viability by monitoring cell functions common to all cell types such as proliferation, organelle function, and cell death. Basal cytotoxicity screening assays have been used for drug compound testing for many years to identify any potentially damaging effects. In these assays, IC_{50} values (compound concentration causing the half-maximal effect) in human cell lines show a strong correlation with LD_{50} values in blood (compound concentration death in 50% of exposed subjects) (Shrivastava et al. 1992). For bCSAs, well-characterized commercially available cell lines are used because they show higher reproducibility of growth and stimuli response than primary cells, which also have to be freshly isolated from animals or humans for each experiment. Primary cells can also vary in quality because of the isolation procedure and donor differences; additionally, they cannot be maintained in culture for a prolonged period. On the other hand, primary cells retain more cell-specific characteristics than cell lines and are therefore used when cell-specific functions are assessed. Most bCSAs are based on determining cell number (cell counting), cellular products (proteins, DNA), enzyme activities, and organelle function (Table 35.1). bCSAs are also used to detect disruption of membrane integrity, induction of apoptosis, inhibition of proliferation, and oxidative stress.

Assays for *membrane integrity* use either detection of intracellular enzymes (e.g., lactate dehydrogenase, adenylate kinase) in the supernatant of cultured cells or the uptake of cell-impermeable dyes into the cells. For dye uptake, the fluorescent dyes propidium iodide, ethidium

TABLE 35.1
Detection Principles for Most Commonly Used Basal Cytotoxicity Assays

Basic Parameters	
Cell number	Coulter counter, CASY Technology, xCELLigence®
Protein content	Sulforhodamine B staining, leucine incorporation
DNA content	Nuclear dyes, especially PicoGreen ^a
Metabolism	ATP content
Enzyme activity	Dehydrogenase activity (formazan bioreduction), esterase activity
Organelle function	Neutral Red uptake
Membrane Integrity	
Dye exclusion	Lactate dehydrogenase, adenylate kinase
Dye uptake	Propidium iodide, ethidium homodimer-1, 7 Z-AAD
Apoptosis	
Membrane changes	Phosphatidylserine exposure: Annexin V-binding, increase in membrane permeability: Yo-PRO-1 uptake
Mitochondrial changes	Mitochondrial membrane potential, cytochrome C translocation
Caspase activation	Caspase 3/7 activation
Cytokeratin changes	Cytokeratin 18 fragmentation
DNA changes	Reparation: Detection of poly(ADP-ribose)polymerase activity or protein, condensation and degradation: terminal deoxynucleotidyl transferase-dUTP nick end labeling (TUNEL) assay
Proliferation	
Incorporation of labeled nucleotides	³ H-thymidine, immunocytochemical detection of BrdU
Production of Reactive Oxygen and Oxidative Cell Damage	
Cellular oxidative stress	Glutathione, catalase, superoxide dismutase, hemoxygenase-1 expression
Reactive oxygen detection	Rhodamine 123, lucigenin, dihydrodichlorofluorescein, dihydroethidium, cytochrome C
Detection of oxidation products	Lipid peroxidation (malondialdehyde and 4-hydroxynonenal), DNA (8-hydroxy deoxyguanine)

^a There are many other nuclear dyes, e.g., Hoechst, SYTO and TOTO dyes to stain nuclei but PicoGreen has the advantage of binding only to double-strand DNA and not to single-strand DNA and RNA and therefore detects only the nuclear volume.

homodimer-1 (Figure 35.3), 7-AAD, TO-PRO-3, TOTO-3, SYTOX dyes, all binding to DNA, are used. Alternatively, simple color detection with trypan blue and eosin can be performed.

Apoptosis can be identified in many different ways. On the one hand, morphological changes can be used (e.g., cell shrinkage, chromatin condensation, membrane blebbing, cell fragmentation, formation of apoptotic bodies, lysis or phagocytosis of apoptotic bodies). On the other hand, biochemical changes can quantify changes in the mitochondrial membrane, caspase activation, and plasma membrane permeability, or detect DNA strand breaks and cytoskeleton breakdown. Usually, more than one assay is performed because apoptotic events do not occur continuously, and one specific assay at a certain time point may not detect the total apoptotic effect: for example, at different time points increased caspase activity indicating apoptosis can be noted at varying levels (Figure 35.4a). Almost all phases of apoptosis can be detected using cytokeratin 18 fragmentation where signals are present over a longer period (Figure 35.4b).

Proliferation is evaluated by incorporating either fluorescent or radioactive labeled nucleotides. Radioactive thymidine uptake is still regarded as the gold standard to assess cell proliferation and

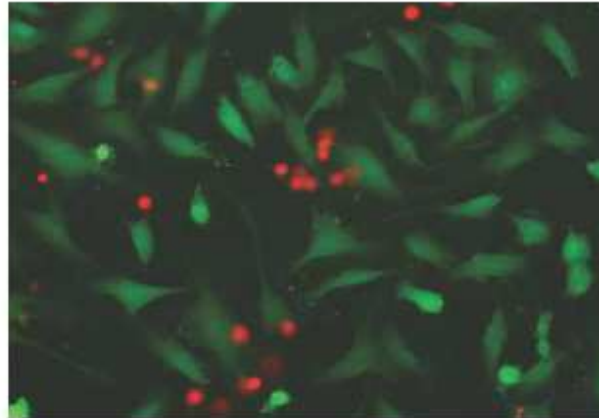


FIGURE 35.3 Detection of living and dead cells according to metabolization of calcein acetoxymethyl ester (green) for vitality and ethidium homodimer-1 (red) uptake for loss of membrane integrity. Upon exposure to 20 nm carboxyl polystyrene particles, several cells (red) show loss of membrane integrity.

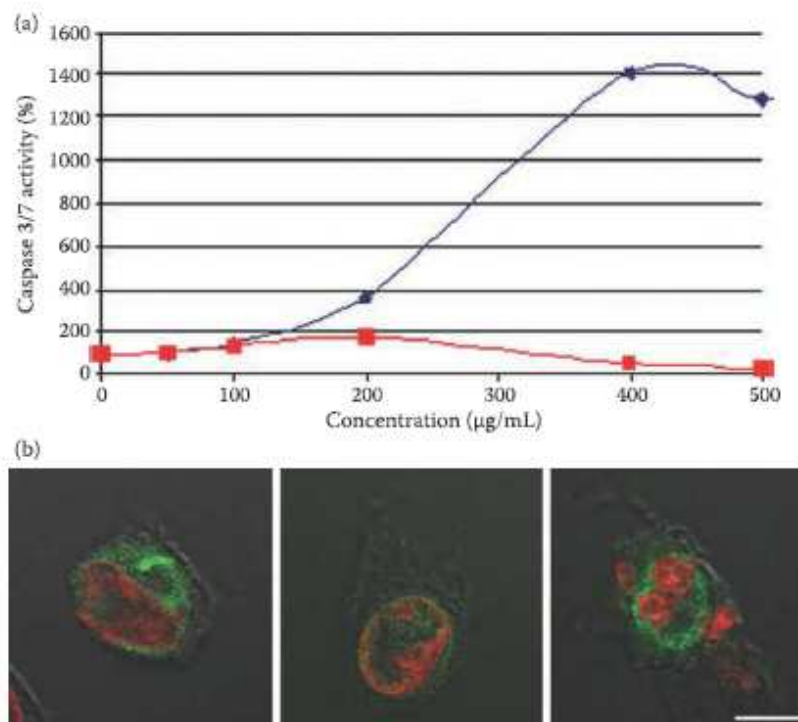


FIGURE 35.4 Assessment of apoptosis by caspase 3/7 activation (a) and by cytokine fragmentation (b). (a) Caspase 3/7 activation after 4 h (blue curve) is much higher than after 24 h (red curve) in the presence of 20 nm carboxyl polystyrene particles. The different shapes of the two curves show the time dependency of apoptotic events. (b) Immunocytochemical detection of cytokine fragmentation by M30 antibody (green) identifies cells in various phases of apoptosis. The staining is present at the early phase of apoptosis when only a few nuclear changes are seen (left); at the stage where nuclear condensation has occurred (middle); and at the late stage, when fragmentation of the nucleus is present (right). Nuclei are stained with propidium iodide (red). Scale bar: 10 μ m

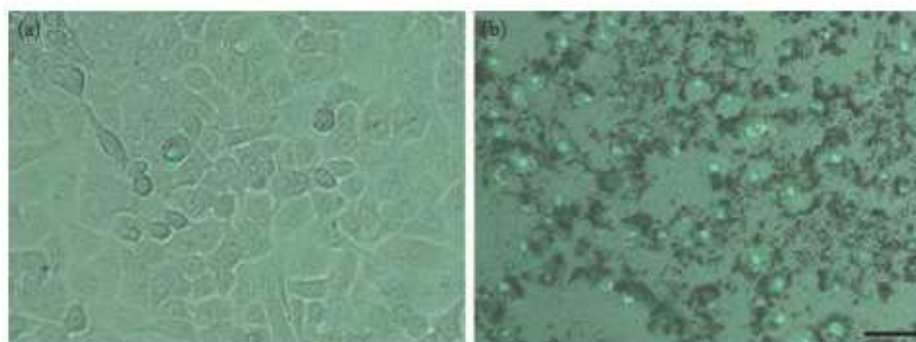


FIGURE 35.5 Detection of oxidative stress by DCF (green) in A549 cells exposed to high concentrations of quartz particles (500 $\mu\text{g}/\text{mL}$). Pictures of fluorescence and bright field are merged. Oxidative stress seen as green fluorescent cells in untreated cultures (a) is rare. Upon exposure to quartz particles (b), oxidative stress in cells is markedly increased. Quantification of the fluorescent signal using fluorescent readers is complicated by fluorescence quenching caused by the particles.

also the more sensitive technique, but fluorescent detection of BrdU by antibodies is used frequently because it avoids the need for radioactive material.

Oxidative stress, one of the key modes of action of NPs, can be studied by (1) detecting intracellular radicals, mainly superoxides; (2) converting substrates such as dichlorodihydrofluorescein, dihydroethidium, cytochrome *C*, lucigenin, and luminal; (3) molecules involved in the oxidative stress reaction (glutathione, superoxide dismutase, catalase, hemoxigenase-1); and (4) detecting cellular oxidation products (malondialdehyde, 4-hydroxynonenal and 8-hydroxy deoxyguanine). However, in all oxidative stress assays, quantification in the presence of high NP concentrations can be difficult (Figure 35.5).

To assess cytotoxicity of NPs, adherent cells are usually preferred to cells growing in suspension, mainly because NPs are most often designed for cancer cell treatment and regenerative medicine where epithelial cells and fibroblasts, both adherently growing, are the most relevant cell types. Many NPs stick to these cells and influence the readout, for instance, by color absorption. A major advantage during NP cytotoxicity testing is that adherent cells can be washed and NPs can be removed. Generally, a 96-well plate format with 4- and 24-h exposure is adequate for testing. In addition to the usual controls (blank, growth control, solvent control), wells should be reserved to test for NP interference with assay compounds and readout (NPs in the absence of cells) but also for NP interference by cell adherence (cells and NPs in the absence of assay compounds). For interference control, NPs instead of conventional drug compounds are used as positive and negative controls. In contrast to conventional drug compounds, NPs may cause problems in bCSAs by interfering with color, chemical reactivity, light scattering, and physical absorption of assay compounds. Carbon nanotubes and mesoporous silica particles are especially known to produce false positive or false negative results in most bCSAs (Casey et al. 2008; Fisichella et al. 2009; Monteiro-Riviere et al. 2009; Worle-Knirsch et al. 2006).

The MTT assay, a frequently used screening assay based on the intracellular reduction of 3-(4,5-dimethylthiazol-2-yl)-2,5-diphenyltetrazolium bromide to a colored product, is especially affected by NP interference (Worle-Knirsch et al. 2006). Other assays based on esterase activity such as calcein acetoxymethyl ester (AM) metabolization can be combined with membrane integrity assessment (Figure 35.3) to obtain additional information from a single experiment.

SPECIFIC CYTOTOXICITY SCREENING

Some NPs impair cell function at concentrations that do not decrease viability (Fröhlich et al. 2010). Specific cytotoxicity screening assays (sCSAs) address the effects of NPs on specific cell functions.

Potential specific cytotoxicity assays for brain cells are summarized in Table 35.2. In the brain, NPs can have cytotoxic effects on brain-specific cell types. For *neurons*, synthesis of transmitters and specific proteins (neuron-specific enolase, S-100) as well as neurite formation are relevant parameters. *Astrocytes* play an important role in brain structure (forming the BBB) and brain metabolism (creating the optimal milieu for neuron and oligodendrocyte function) and in the repair of brain lesions (glial scars). They produce a variety of peptides such as calcitonin gene related peptide, brain-derived neurotrophic factor (BDNF), somatostatin, and vasoactive intestinal peptide. Upon activation, astrocytes increase expression of their main intermediary filament, glial fibrillary acidic protein (GFAP), which can serve as a toxicity parameter. *Oligodendrocytes* produce myelin for electrical isolation of axons in the brain. Production of myelin basic protein serves as an indicator of oligodendrocyte damage *in vivo* (Follett et al. 2004). The main functions of microglial cells include production of cytokines (mainly IFN- γ , TNF- α , IL-8, IL-1 α and IL-1 β) and chemokines (MCP-1), phagocytosis, and oxidative burst (H₂O₂ and NO secretion). Because NPs may induce inflammation and inflammatory processes in the brain by microglia activation and may promote neurodegenerative diseases associated with microglia degeneration (such as prion disease, schizophrenia, and Alzheimer's disease), assessing microglia activation is of primary importance.

Certain cell lines can be used for specific neurotoxicity screening; these cell lines include: glioma C6 cells for oligodendrocyte function (myelination); PC-12 (pheochromocytoma cells) for neurotransmitter synthesis and release; NSC34 (hybrid murine neuronal cell line) for axonal transport, neurofilament organization, and action potential generation; and N1E115 (murine neuroblastoma cells) for differentiation (Harry et al. 1998). As markers for astrocyte function, GFAP and BDNF production of U251 (human glioma) cells can be studied (Kashima et al. 1993). Myelin basic protein expression as an indicator for oligodendrocyte function is lost in many cell lines but expressed upon differentiation in the MO3.13 (human oligodendroglial) cell line (Buntinx et al. 2003). Screening for microglia activation during inflammation is often performed in the murine microglial cell line BV2, which is a good model for microglial cells in mice but may be less representative for human microglia (Henn et al. 2009). Screening for inflammatory effects using a human, non-microglial cell line, is another option to assess activation of microglia. For brain-targeted NPs, increased cytokine secretion (IL-1b) and ROS levels in microglial cells exposed to silica particles can also be relevant (Choi et al. 2010).

Specific changes in cell function and cell damage have also been reported after exposure to NPs *in vivo*, for instance, astrocyte swelling and neuronal degeneration after administration of silver NPs (Tang et al. 2009) or depletion of antioxidant capacity in addition to changes in neurotransmitter release pattern after intraperitoneal application of TiO₂ NPs to mice (Ma et al. 2010). Intraperitoneal injection of Al₂O₃ particles caused glia cell activation according to increased ED1 in microglia, nesting in progenitor cells, and GFAP staining in astrocytes (Li et al. 2009). These data suggest that assessing brain-targeted NPs has to include not only basal but also specific cytotoxicity assays.

NPs may also interfere with sCSAs: the secretion of protein can be underestimated because many NPs adsorb proteins. This could lead to an underestimation of the inflammatory response

TABLE 35.2
Cell Types Used in Specific Neurotoxicity Assays

Astrocytes	BDNF, GFAP expression (e.g., in U251 cells)
Oligodendrocytes	Major Basic Protein (e.g., MO3.13 cells)
Neurons	TH immunoreactivity (e.g., in PC-12 cells)
	Neurite outgrowth (e.g., in PC-12, SY-SY5Y cells)
	Axonal transport (e.g., in NSC-34 cells)
Microglia	IL-1 secretion, NO production, phagocytosis (e.g., in BV2, EOC-2 cells)

based on cytokine secretion. Interference of NPs with color, fluorescence, and light scattering of specific CSAs can similarly occur for basic CSAs.

IN VIVO TECHNIQUES

In vivo studies on pharmacokinetics (PK) and pharmacodynamics (PD) are a reliable source of information during drug development and toxicological studies and the last step before a clinical trial. Target tissue toxicity is difficult to predict accurately *in vitro* but is a special focus of *in vivo* studies in addition to the ability of NPs to cross the BBB (PK) and the tissue response to the presence of NPs (PD). Several noninvasive and invasive methods are available to evaluate PK and PD of NPs in the brain:

- Histopathology
- Imaging techniques: positron emission tomography (PET), MRI, and magnetic resonance spectroscopy (MRS)
- Microdialysis (MD) and open flow microperfusion (OFM)
- Behavioral tests

HISTOPATHOLOGY

Histopathology remains the gold standard of neurotoxicity testing. There is a constant search for better neuropathological techniques for *in vivo* studies. The first step after brain extraction is tissue fixation. In routine studies, immersion fixation, paraffin embedding, and staining with hematoxylin and eosin (H&E) are performed. Perfusion fixation has the benefit of faster distribution of fixation media but if perfusion pressure is too high, blood vessels can rupture and cause artifacts. Sections from different regions of the brain should be made because composition and cell types vary between gray and white matter, cerebrum, cerebellum, and brain stem. Regions around the third and fourth ventricles are of special interest because they are supplied by blood vessels with a higher permeability allowing a higher exchange rate between blood and brain. Specific regions of the brain are prepared in consecutive sections, a tricky task demanding a skilled operator. Metal templates or molds for slicing provide assistance in a standardized production of sections. After tissue sectioning, a number of staining and immunohistochemical methods can be applied: GFAP is used to detect glial cells in paraffin-embedded sections in rodents and humans. S100 protein is used to detect neuronal cells such as Schwann cells, glial cells, and neurons. The presence of cytokines such as IL-1 α , IL-1 β , IL-8, IFN- γ , and TNF- α mainly provides information on the inflammatory status of the tissue and therefore toxic reactions. These markers bridge the gap between *in vivo* and *in vitro* tests because they are used in both. Additionally, *in vivo* sections contain histological information on cell necrosis, apoptosis, reactive gliosis, and other possible reactions to NPs.

Histological analysis of brain tissue requires brain tissue extraction at the end of the experiment and therefore sacrificing the subject. Time-resolved experiments necessitate the sacrifice of several animals per time point, which results in high animal usage.

IMAGING TECHNIQUES

Positron Emission Tomography

Positron emission tomography is a noninvasive technique that can be used to measure NP-induced changes in the brain metabolism of humans and animals (Brooks et al. 1984; Jossierand et al. 2006). The subject with the incorporated marker is positioned in a detector that counts emission of gamma photons emitted by the tracer. A two-dimensional (2-D) or 3-D image of the brain can be generated in real time by applying computer-supported imaging techniques (Dingemans et al. 1988; Hilbert

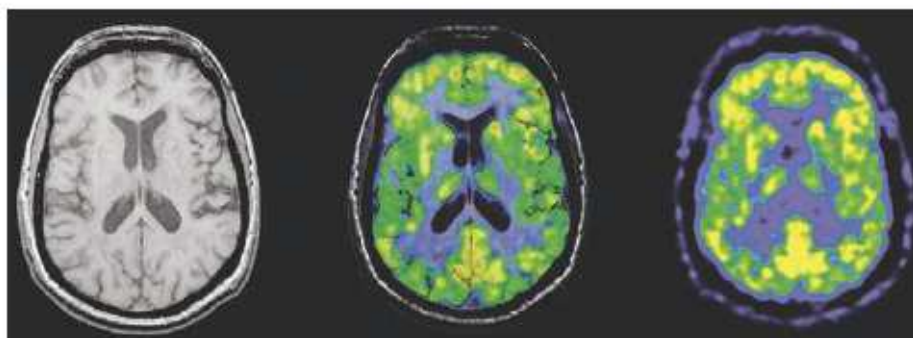


FIGURE 35.6 MR image (left) and PET image (right) and are merged to an image incorporating anatomical and metabolic information (center). Siemens Reference Number: somed200701-01.

and Battista 1991). Altered glucose metabolism, for instance, can be recorded by (18F)fluoro-deoxy-glucose. PET provides high sensitivity and exact time resolution; in addition, pharmacological compartment modeling can be used to assess PK. PET scans are increasingly combined with other imaging techniques such as MRI or CT to acquire both anatomic and metabolic information (Figure 35.6). This combination has many potential applications for brain imaging. Limitations of PET arise from the high costs of cyclotrons necessary to produce short-lived radionuclides for PET scanning and the need for a specially adapted on-site chemical synthesis apparatus to produce radiopharmaceuticals. Because no distinction can be made between parent compound and metabolites, directly monitoring a toxicological reaction to NPs is limited.

MRI and MRS

MRI is a sensitive, noninvasive technique to monitor a range of clinical pathologies such as multiple sclerosis, stroke, and brain tumors (Ewing et al. 2003; Patlak et al. 1983). Contrast agents improve identifying changes in blood perfusion and morphology. MRS can differentiate a wide range of chemical substances within the body but has the disadvantage of poor spatial resolution compared to MRI. A combination of both technologies can provide information about the distribution of NPs as well as information about PD during toxicological analyses. Similar to PET scans, MRI and MRS are very cost-intensive methods, which limit their applicability as screening methods.

ANALYTICAL TECHNIQUES

Microdialysis

Intracerebral MD is an invasive technique to continuously measure toxicity markers in extracellular tissue space. A cylindrical, semipermeable membrane is implanted into the target area in the brain and perfused with a physiological solution, the perfusate (Elmqvist and Sawchuk 1997). The perfusate is ideally closely matched to the ionic composition and the pH value of the extracellular fluid (ECF) of the brain to avoid changes in brain physiology that could lead to interference with the BBB (de Lange et al. 2000). The membrane allows substance exchange between ECF and perfusate according to concentration gradients and diffusion parameters. The perfusate inside the membrane is continuously exchanged—the standard setup consists of an active inflow, driven by a syringe pump; the outflow is passive and the perfusate (enriched with components from ECF) is collected into a vial, which is replaced periodically. A constant perfusate flow through the membrane allows continuous, parallel measurement of several markers and metabolites and a differentiation between parent compounds and metabolites. Toxicity markers such as the above-mentioned S100B and the cytokines are accessible by MD. Continuous measurement reduces the number of animals used and statistical problems such as intersubject variability. MD allows simultaneous and time-resolved

determination of cerebral ECF and plasma levels, which enables kinetic and dynamic monitoring of substances. To investigate a specific brain region, the MD probe can be implanted stereotactically with high local accuracy; several probes can be implanted.

A drawback in the MD application is that implantation of the MD probe damages cerebral capillaries and consequently affects BBB function. Different time spans (hours up to days) until the BBB is reestablished have been reported (de Lange et al. 1997; Groothuis et al. 1998; Westergren et al. 1995). A short time span between probe implantation and start of measurement may result in decreased local blood flow (Benveniste et al. 1987). Moreover, the membrane is the limiting factor in the exchange between tissue and perfusate because substances larger than the pore size of the membrane and lipophilic substances cannot pass the membrane and are subsequently excluded from the analysis (Rosenbloom et al. 2005). Finally, accurately determining the relationship between concentrations of the drug of interest in the solution that exits the dialysis probe and concentrations in the tissue (recovery) can be difficult. Pinpointing recovery *in vitro* is inaccurate because *in vitro* results usually exceed *in vivo* measurements. In particular, two methods are applied to overcome the recovery problem: no-net flux, which delivers a reliable outcome but is very time consuming, and retro dialysis, where a substance with similar diffusion behavior is added to the perfusate and the loss to the tissue of this substance is detected.

Open Flow Microperfusion

OFM is a recently developed method with a working principle similar to MD (Bodenlenz et al. 2005; Schaupp et al. 1999). It offers the possibility of continuous measurement in healed tissue with an intact BBB. The main difference is that OFM incorporates no membrane but rather an exchange area with macroscopic perforations 100 μm or larger (Figure 35.7) that allows sampling substances from tissues without limitations due to molecular size, protein binding, charge, or lipophilicity (Ellmerer et al. 2000; Ikeoka et al. 2010; Pachler et al. 2007). Many CNS active substances are lipophilic because the BBB allows transcellular diffusion of small lipophilic substances. Therefore, the possibility to sample lipophilic substances by OFM offers many benefits over MD. OFM requires two pumps operated at the same flow rate, for injection and withdrawal of the perfusate, since

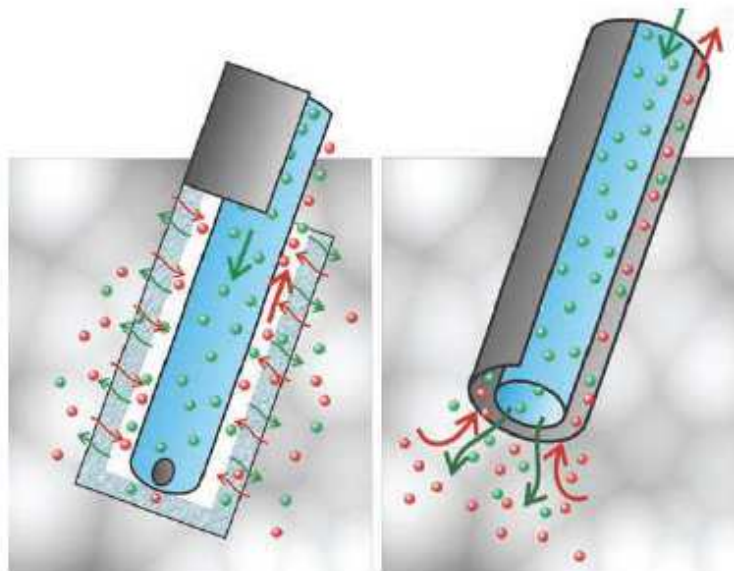


FIGURE 35.7 Working principle of MD (left) and OFM (right): MD uses a membrane as tissue interface. OFM provides a direct contact to the cerebral tissue.

the open structure provides less protection for internal microfluids compared to the MD membrane. OFM overcomes the limitation of MD membrane occlusion and pore narrowing as a result of membrane exposure to protein (Rosenbloom et al. 2006) and shows no relevant formation of a trauma layer, gliosis, and scar tissue formation around the probe, which has been observed in MD (Benveniste 1989). The absence of these limitations in application time in OFM allows a long healing period between OFM implantation and measurement start; therefore, full BBB recovery can be expected. Moreover, repeated measurements can be performed over several days without change in measurement performance, thereby promoting OFM use in long-term toxicity testing. The OFM probe can also be used to introduce NPs directly into the brain, bypassing the BBB, and allowing separate testing of transport across the BBB and nanotoxicity in brain tissue.

BEHAVIORAL TESTS

One aspect of brain toxicology is the change in the behavior of animals. Two types of behavioral tests can be distinguished: stimulus-oriented and internally generated behavior tests (Hodgson 2004). Stimulus-oriented behavior involves conditioned and unconditioned experimental setups in which the response to a particular stimulus is tracked. The conditioned test involves training to perform an action in order to receive a reward or avoid pain. Internally generated behavioral tests involve monitoring animal behavior in experimental situations such as social behavior, circadian behavior, and exploratory behavior. The performance of subjects treated with NPs is compared to that of a control group. Groups must be matched in terms of age, sex, species, and housing conditions. Combined with other techniques, behavioral variations represent an integrated whole organism response that is mostly nonspecific but sensitive and can increase our understanding of the toxicological effects of NPs in the CNS.

CONCLUSIONS

For a good assessment of the toxic effects of NPs in the brain, both *in vitro* and *in vivo* studies are needed. High-throughput testing in the early stage of pharmaceutical development demands *in vitro* methods for screening. Cytotoxicity screening methods can assess a large number of samples but they lack the complexity of *in vivo* systems. Preclinical *in vivo* testing is more time consuming and more expensive than *in vitro* methods but represents the distribution, metabolic, and elimination processes occurring in the body in a far better manner.

For *in vivo* assessment, histopathology is still the gold standard, but analytical methods such as MD and OFM offer the advantages of continuous measurement and monitoring of PK/PD in a single subject. OFM overcomes MD limitations of a narrow measurement spectrum and limited application time, which allows measurement of high molecular markers for cell damage, such as lactate dehydrogenase, and of cytokines for identifying the inflammatory response to NPs. Noninvasive imaging techniques are available and in development but their high costs impede their widespread use as preclinical tests.

In vivo models provide more reliable information than *in vitro* models and reflect an experimental situation closer to that in clinical trials. Detection of target organ toxicity is a question that is particularly difficult to answer accurately *in vitro*. Even for organs such as the liver, in which primary cells and tissue slices are commercially available, *in vitro* assays often cannot reliably predict *in vivo* dose-response effects (Kramer et al. 2007). A close consensus of *in vitro* and *in vivo* assessments is a prerequisite for efficient pharmaceutical development. *In vivo* models can be used to validate *in vitro* models and to verify outcomes of *in vitro* studies. In applying NPs to the brain, this means selecting brain-relevant cell lines such as astrocytes, brain endothelial cells, neurons, and microglia, and choosing adequate assays such as lactate dehydrogenase leakage, S100, BDNF, and cytokines, allowing a direct comparison of *in vitro* and *in vivo* results.

REFERENCES

- Au, C., Mutkus, L., Dobson, A. et al. 2007. Effects of nanoparticles on the adhesion and cell viability on astrocytes. *Biol Trace Elem Res* 120: 248–56.
- Belyanskaya, L., Weigel, S., Hirsch, C. et al. 2009. Effects of carbon nanotubes on primary neurons and glial cells. *Neurotoxicology* 30: 702–11.
- Benveniste, H. 1989. Brain microdialysis. *J Neurochem* 52: 1667–79.
- Benveniste, H., Drejer, J., Schousboe, A. et al. 1987. Regional cerebral glucose phosphorylation and blood flow after insertion of a microdialysis fiber through the dorsal hippocampus in the rat. *J Neurochem* 49: 729–34.
- Bhaskar, S., Tian, F., Stoeger, T. et al. 2010. Multifunctional nanocarriers for diagnostics, drug delivery and targeted treatment across blood–brain barrier: perspectives on tracking and neuroimaging. *Part Fibre Toxicol* 7: 3.
- Bodenlenz, M., Schaupp, L.A., Druml, T. et al. 2005. Measurement of interstitial insulin in human adipose and muscle tissue under moderate hyperinsulinemia by means of direct interstitial access. *Am J Physiol Endocrinol Metab* 289: E296–300.
- Brooks, D.J., Beancy, R.P., Lammertsma, A.A. et al. 1984. Quantitative measurement of blood–brain barrier permeability using rubidium-82 and positron emission tomography. *J Cereb Blood Flow Metab* 4: 535–45.
- Buntinx, M., Vanderlocht, J., Hellings, N. et al. 2003. Characterization of three human oligodendroglial cell lines as a model to study oligodendrocyte injury: morphology and oligodendrocyte-specific gene expression. *J Neurocytol* 32: 25–38.
- Casey, A., Herzog, E., Lyng, F.M. et al. 2008. Single walled carbon nanotubes induce indirect cytotoxicity by medium depletion in A549 lung cells. *Toxicol Lett* 179: 78–84.
- Choi, J., Zheng, Q., Katz, H.E. et al. 2010. Silica-based nanoparticle uptake and cellular response by primary microglia. *Environ Health Perspect* 118: 589–95.
- de Lange, E.C., Danhof, M., de Boer, A.G. et al. 1997. Methodological considerations of intracerebral microdialysis in pharmacokinetic studies on drug transport across the blood–brain barrier. *Brain Res Brain Res Rev* 25: 27–49.
- de Lange, E.C., de Boer, A.G., and Breimer, D.D. 2000. Methodological issues in microdialysis sampling for pharmacokinetic studies. *Adv Drug Deliv Rev* 45: 125–48.
- Dingemans, J., Sollie, F.A., Breimer, D.D. et al. 1988. Pharmacokinetic modeling of the anticonvulsant response of oxazepam in rats using the pentylenetetrazol threshold concentration as pharmacodynamic measure. *J Pharmacokinet Biopharm* 16: 203–28.
- Ellmerer, M., Schaupp, L., Brunner, G.A. et al. 2000. Measurement of interstitial albumin in human skeletal muscle and adipose tissue by open-flow microperfusion. *Am J Physiol Endocrinol Metab* 278: E352–6.
- Elmqvist, W.F., and Sawchuk, R.J. 1997. Application of microdialysis in pharmacokinetic studies. *Pharm Res* 14: 267–88.
- Ewing, J.R., Knight, R.A., Nagaraja, T.N. et al. 2003. Patlak plots of Gd-DTPA MRI data yield blood–brain transfer constants concordant with those of ¹⁴C-sucrose in areas of blood–brain opening. *Magn Reson Med* 50: 283–92.
- Fischella, M., Dabboue, H., Bhattacharyya, S. et al. 2009. Mesoporous silica nanoparticles enhance MTT formazan exocytosis in HeLa cells and astrocytes. *Toxicol In Vitro* 23: 697–703.
- Follett, P.L., Deng, W., Dai, W. et al. 2004. Glutamate receptor-mediated oligodendrocyte toxicity in periventricular leukomalacia: a protective role for topiramate. *J Neurosci* 24: 4412–20.
- Fröhlich, E., Kueznik, T., Samberger, C. et al. 2010. Size-dependent effects of nanoparticles on the activity of cytochrome P450 isoenzymes. *Toxicol Appl Pharmacol* 242: 326–32.
- Fröhlich, E., Samberger, C., Kueznik, T. et al. 2009. Cytotoxicity of nanoparticles independent from oxidative stress. *J Toxicol Sci* 34: 363–75.
- Groothuis, D.R., Ward, S., Schlageter, K.E. et al. 1998. Changes in blood–brain barrier permeability associated with insertion of brain cannulas and microdialysis probes. *Brain Res* 803: 218–30.
- Harry, G.J., Billingsley, M., Bruinink, A. et al. 1998. In vitro techniques for the assessment of neurotoxicity. *Environ Health Perspect* 106 Suppl 1: 131–58.
- Henn, A., Lund, S., Hedtjarn, M. et al. 2009. The suitability of BV2 cells as alternative model system for primary microglia cultures or for animal experiments examining brain inflammation. *Altx* 26: 83–94.
- Hilbert, J.M., and Battista, D. 1991. Quazepam and flurazepam: differential pharmacokinetic and pharmacodynamic characteristics. *J Clin Psychiatry* 52 Suppl: 21–6.
- Hodgson, E. (editor). 2004. *Book A Textbook of Modern Toxicology*. Hoboken, NJ: John Wiley and Sons.

- Ikeoka, D., Pachler, C., Korsatko, S. et al. 2010. Interleukin-6 produced in subcutaneous adipose tissue is linked to blood pressure control in septic patients. *Cytokine* 50: 284–91.
- Josserand, V., Pelerin, H., de Bruin, B. et al. 2006. Evaluation of drug penetration into the brain: a double study by in vivo imaging with positron emission tomography and using an in vitro model of the human blood–brain barrier. *J Pharmacol Exp Ther* 316: 79–86.
- Kashima, T., Tiu, S.N., Merrill, J.E. et al. 1993. Expression of oligodendrocyte-associated genes in cell lines derived from human gliomas and neuroblastomas. *Cancer Res* 53: 170–5.
- Kramer, J.A., Sagartz, J.E., and Morris, D.L. 2007. The application of discovery toxicology and pathology towards the design of safer pharmaceutical lead candidates. *Nat Rev Drug Discov* 6: 636–49.
- Lai, J.C., Lai, M.B., Jandhyam, S. et al. 2008. Exposure to titanium dioxide and other metallic oxide nanoparticles induces cytotoxicity on human neural cells and fibroblasts. *Int J Nanomed* 3: 533–45.
- Li, X., Zheng, H., Zhang, Z. et al. 2009. Glia activation induced by peripheral administration of aluminum oxide nanoparticles in rat brains. *Nanomedicine* 5: 473–79.
- Liu, S., Xu, L., Zhang, T. et al. 2010. Oxidative stress and apoptosis induced by nanosized titanium dioxide in PC12 cells. *Toxicology* 267: 172–7.
- Ma, L., Liu, J., Li, N. et al. 2010. Oxidative stress in the brain of mice caused by translocated nanoparticulate TiO₂ delivered to the abdominal cavity. *Biomaterials* 31: 99–105.
- Miller, G. 2002. Drug targeting. Breaking down barriers. *Science* 297: 1116–8.
- Monteiro-Riviere, N.A., Inman, A.O., and Zhang, L.W. 2009. Limitations and relative utility of screening assays to assess engineered nanoparticle toxicity in a human cell line. *Toxicol Appl Pharmacol* 234: 222–35.
- Pachler, C., Ikeoka, D., Plank, J. et al. 2007. Subcutaneous adipose tissue exerts proinflammatory cytokines after minimal trauma in humans. *Am J Physiol Endocrinol Metab* 293: E690–6.
- Pardridge, W.M. 2005. The blood–brain barrier: bottleneck in brain drug development. *NeuroRx* 2: 3–14.
- Patlak, C.S., Blasberg, R.G., and Fenstermacher, J.D. 1983. Graphical evaluation of blood-to-brain transfer constants from multiple-time uptake data. *J Cereb Blood Flow Metab* 3: 1–7.
- Reese, T.S., and Karnovsky, M.J. 1967. Fine structural localization of a blood–brain barrier to exogenous peroxidase. *J Cell Biol* 34: 207–17.
- Rosenbloom, A.J., Ferris, R.L., Sipe, D.M. et al. 2006. In vitro and in vivo protein sampling by combined microdialysis and ultrafiltration. *J Immunol Methods* 309: 55–68.
- Rosenbloom, A.J., Sipe, D.M., and Weedn, V.W. 2005. Microdialysis of proteins: performance of the CMA/20 probe. *J Neurosci Methods* 148: 147–53.
- Schaupp, L., Ellmerer, M., Brunner, G.A. et al. 1999. Direct access to interstitial fluid in adipose tissue in humans by use of open-flow microperfusion. *Am J Physiol* 276: E401–8.
- Shrivastava, R., Delomenie, C., Chevalier, A. et al. 1992. Comparison of in vivo acute lethal potency and in vitro cytotoxicity of 48 chemicals. *Cell Biol Toxicol* 8: 157–70.
- Speckmann, E.-J., Hescheler, J., and Kohling, R. 2008. *Physiologie*. 5th ed. Munich: Urban & Fischer.
- Tang, J., Xiong, L., Wang, S. et al. 2009. Distribution, translocation and accumulation of silver nanoparticles in rats. *J Nanosci Nanotechnol* 9: 4924–32.
- Westergren, I., Nystrom, B., Hamberger, A. et al. 1995. Intracerebral dialysis and the blood–brain barrier. *J Neurochem* 64: 229–34.
- Worle-Knirsch, J.M., Pulskamp, K., and Krug, H.F. 2006. Oops they did it again! Carbon nanotubes hoax scientists in viability assays. *Nano Lett* 6: 1261–8.
- Wu, J., Sun, J., and Xue, Y. 2010. Involvement of JNK and P53 activation in G2/M cell cycle arrest and apoptosis induced by titanium dioxide nanoparticles in neuron cells. *Toxicol Lett*.
- Zhang, Y., Ali, S.F., Dervishi, E. et al. 2010. Cytotoxicity effects of graphene and single-wall carbon nanotubes in neural pheochromocytoma-derived PC12 cells. *ACS Nano* 4: 3181–6.

Birngruber T, Ghosh A, Perez-Yarza VA, Kroath T, Ratzner M, Pieber T, Sinner F

Cerebral open flow microperfusion - a new in vivo technique for continuous measurement of substance transport across the intact blood-brain barrier;

Journal: Clinical and Experimental Pharmacology and Physiology

In press
